REPUBLIQUE DU CAMEROUN
Paix-Travail-Patrie
****
UNIVERSITÉ DE YAOUNDÉ I
****
FACULTÉ DES SCIENCES
****
CENTRE DE RECHERCHE ET DE FORMATION DOCTORALE EN SCIENCES, TECHNOLOGIES ET GEOSCIENCES
UNITE DE RECHERCHE ET DE FORMATION DOCTORALE PHYSIQUE ET APPLICATIONS
BP.812 Yaoundé
Email: crftstg@uy1.uninet.cm

REPUBLIC OF CAMEROON
Peace-Work-Fatherland
****
UNIVERSITY OF YAOUNDE I
****
FACULTY OF SCIENCES
****
POSTGRADUATES SCHOOL OF SCIENCE, TECHNOLOGY AND GEOSCIENCES
RESEARCH UNIT FOR PHYSICS AND APPLICATIONS
P.O.BOX.812 Yaoundé
Email: crftstg@uy1.uninet.cm

DEPARTMENT OF PHYSICS
LABORATORY OF NUCLEAR, ATOMIC, MOLECULAR PHYSICS AND BIOPHYSICS

ENERGY LOCALIZATION IN MICROTUBULES WITH RADIAL DISLOCATION

Laboratory of Nuclear, Atomic, Molecular Physics and Biophysics

THESIS

Submitted and defended in fulfillment of the requirements for the

award of the

Degree of Doctorat/Ph.D. in Physics

Speciality: Atomic, Molecular Physics and Biophysics

By

TABAPSI KAMDEM ROSTAND
Registration number: 12W0443
Master of Science in Physics

Under the supervision of:

PR. KOFANÉ TIMOLÉON CRÉPIN

University of Yaoundé I

Year 2025

UNIVERSITÉ DE YAOUNDÉ I
THE UNIVERSITY OF YAOUNDE I

FACULTÉ DES SCIENCES
FACULTY OF SCIENCES

DÉPARTEMENT DE PHYSIQUE
DEPARTMENT OF PHYSICS

ATTESTATION DE CORRECTION DE LA THÈSE DE DOCTORAT/Ph.D

Nous, Professeur **BOUETOU BOUETOU Thomas** et Professeur **BEN-BOLIE Germain Hubert**, respectivement Examinateur et Président du jury de la Thèse de Doctorat/Ph.D. de Monsieur **TABAPSI KAMDEM ROSTAND**, Matricule **12W0443**, préparée sous la direction du Professeur **KOFANE Timoléon Crépin** Université de Yaoundé I, intitulée : « **ENERGY LOCALIZATION IN MICROTUBULES WITH RADIAL DISLOCATION** », soutenue le mercredi**, 07 Mai 2025**, en vue de l'obtention du grade de Docteur/Ph.D. en Physique, Spécialité **Physique des Rayonnements et Biophysique,** option **Physique Atomique, Moléculaire et Biophysique,** attestons que toutes les corrections demandées par le jury de soutenance ont été effectuées.

En foi de quoi, la présente attestation lui est délivrée pour servir et valoir ce que de droit.

Fait à Yaoundé, le

Examinateur	Le Président du jury	Le Chef de Département de Physique
Pr. BOUETOU BOUETOU Thomas	BEN-BOLIE Germain Hubert	Pr. NDJAKA Jean-Marie

UNIVERSITÉ DE YAOUNDÉ I **Faculté des Sciences** Division de la Programmation et du Suivi des Activités Académiques		THE UNIVERSITY OF YAOUNDE I **Faculty of Science** Division of Programming and Follow-up of Academic Affaires
LISTE DES ENSEIGNANTS PERMANENTS		**LIST OF PERMANENT TEACHING STAFF**

ANNÉE ACADEMIQUE 2024/2025

(Par Département et par Grade)

DATE D'ACTUALISATION 30 septembre 2024

ADMINISTRATION

1. **DOYEN :** OWONO OWONO Luc Calvin, *Professeur*
2. **VICE-DOYEN / DPSAA:** NDJIGUI Paul-Désiré, *Professeur*
3. **VICE-DOYEN / DSSE :** NYEGUE Maximilienne Ascension, *Professeur*
4. **VICE-DOYEN / DRC :** NOUNDJEU Pierre, *Maître de Conférences*
5. **Chef Division Administrative et Financière :** NDOYE FOE Florentine Marie Chantal, *Maître de Conférences*
6. **Chef Division des Affaires Académiques, de la Recherche et de la Scolarité DAARS :** AJEAGAH Gideon AGHAINDUM, *Professeur*

1- DÉPARTEMENT DE BIOCHIMIE (BC) (44)

N°	NOMS ET PRÉNOMS	GRADE	OBSERVATIONS
1.	BIGOGA DAIGA Jude	Professeur	En poste
2.	FEKAM BOYOM Fabrice	Professeur	En poste
3.	KANSCI Germain	Professeur	En poste
4.	MBACHAM FON Wilfred	Professeur	En poste
5.	MOUNDIPA FEWOU Paul	Professeur	*Chef de Département*
6.	NGUEFACK Julienne	Professeur	En poste
7.	NJAYOU Frédéric Nico	Professeur	En poste
8.	OBEN Julius ENYONG	Professeur	En poste
9.	ACHU Merci BIH	Maître de Conférences	En poste
10.	AKINDEH MBUH NJI	Maître de Conférences	En poste
11.	ATOGHO Barbara MMA	Maître de Conférences	En poste
12.	AZANTSA KINGUE GABIN BORIS	Maître de Conférences	En poste
13.	BELINGA née NDOYE FOE F. M. C.	Maître de Conférences	*Chef DAF / FS*
14.	DAKOLE DABOY Charles	Maître de Conférences	En poste
15.	DONGMO LEKAGNE Joseph Blaise	Maître de Conférences	En poste
16.	DJUIDJE NGOUNOUE Marceline	Maître de Conférences	En poste
17.	DJUIKWO NKONGA Ruth Viviane	Maître de Conférences	En poste
18.	EFFA ONOMO Pierre	Maître de Conférences	*VD/FS/Univ Ebwa*
19.	EWANE Cécile Annie	Maître de Conférences	En poste
20.	KENGNE NOUEMSI Anne Pascale	Maître de Conférences	En poste
21.	KOTUE TAPTUE Charles	Maître de Conférences	En poste
22.	LUNGA Paul KEILAH	Maître de Conférences	En poste
23.	MANANGA Marlyse Joséphine	Maître de Conférences	En poste
24.	MBONG ANGIE M. Mary Anne	Maître de Conférences	En poste
25.	MOFOR née TEUGWA Clotilde	Maître de Conférences	*Doyen FS / UDs*
26.	NANA Louise épouse WAKAM	Maître de Conférences	En poste
27.	NGONDI Judith Laure	Maître de Conférences	En poste
28.	Palmer MASUMBE NETONGO	Maître de Conférences	En poste
29.	PECHANGOU NSANGOU Sylvain	Maître de Conférences	En poste
30.	TCHANA KOUATCHOUA Angèle	Maître de Conférences	En poste
31.	BEBEE Fadimatou	Chargée de Cours	En poste
32.	BEBOY EDJENGUELE Sara N.	Chargé de Cours	En poste
33.	FONKOUA Martin	Chargé de Cours	En poste
34.	FOUPOUAPOUOGNIGNI Yacouba	Chargé de Cours	En poste
35.	KOUOH ELOMBO Ferdinand	Chargé de Cours	En poste
36.	MBOUCHE FANMOE Marceline J.	Chargé de Cours	En poste
37.	OWONA AYISSI Vincent Brice	Chargé de Cours	En poste
38.	WILFRED ANGIE ABIA	Chargé de Cours	En poste
39.	BAKWO BASSOGOG Christian Bernard	Assistant	En Poste
40.	ELLA Fils Armand	Assistant	En Poste

41.	EYENGA Eliane Flore	Assistant	En Poste
42.	MADIESSE KEMGNE Eugenie Aimée	Assistant	En Poste
43.	MANJIA NJIKAM Jacqueline	Assistant	En Poste
44.	WOGUIA Alice Louise	Assistant	En Poste

2- DÉPARTEMENT DE BIOLOGIE ET PHYSIOLOGIE ANIMALES (BPA) (50)

1.	AJEAGAH Gideon AGHAINDUM	Professeur	*DAARS/FS*
2.	DIMO Théophile	Professeur	En Poste
3.	DJIETO LORDON Champlain	Professeur	En Poste
4.	DZEUFIET DJOMENI Paul Désiré	Professeur	En Poste
5.	ESSOMBA née NTSAMA MBALA	Professeur	*CD et Vice Doyen/FMSB/UYI*
6.	KEKEUNOU Sévilor	Professeur	*Chef de Département*
7.	NJAMEN Dieudonné	Professeur	En poste
8.	NOLA Moïse	Professeur	En poste
9.	TAN Paul VERNYUY	Professeur	En poste
10.	TCHUEM TCHUENTE Louis Albert	Professeur	*Inspecteur de service / Coord.Progr./MINSANTE*
11.	ZEBAZE TOGOUET Serge Hubert	Professeur	En poste

12.	ALENE Désirée Chantal	Maître de Conférences	*Vice Doyen/ Uté Ebwa*
13.	ATSAMO Albert Donatien	Maître de Conférences	En poste
14.	BILANDA Danielle Claude	Maître de Conférences	En poste
15.	DJIOGUE Séfirin	Maître de Conférences	En poste
16.	GOUNOUE KAMKUMO Raceline épse FOTSING	Maître de Conférences	En poste
17.	JATSA BOUKENG Hermine épse MEGAPTCHE	Maître de Conférences	En Poste
18.	KANDEDA KAVAYE Antoine	Maître de Conférences	En poste
19.	LEKEUFACK FOLEFACK Guy B.	Maître de Conférences	En poste
20.	MAHOB Raymond Joseph	Maître de Conférences	En poste
21.	MBENOUN MASSE Paul Serge	Maître de Conférences	En poste
22.	MEGNEKOU Rosette	Maître de Conférences	En poste
23.	MOUNGANG Luciane Marlyse	Maître de Conférences	En poste
24.	NOAH EWOTI Olive Vivien	Maître de Conférences	En poste
25.	MONY Ruth épse NTONE	Maître de Conférences	En Poste
26.	MVEYO NDANKEU Yves Patrick	Maître de Conférences	En poste
27.	NGUEGUIM TSOFACK Florence	Maître de Conférences	En poste
28.	NGUEMBOCK	Maître de Conférences	En poste
29.	TAMSA ARFAO Antoine	Maître de Conférences	En poste
30.	TOMBI Jeannette	Maître de Conférences	En poste

31.	AMBADA NDZENGUE GEORGIA ELNA	Chargé de Cours	En poste
32.	BASSOCK BAYIHA Etienne Didier	Chargé de Cours	En poste
33.	ETEME ENAMA Serge	Chargé de Cours	En poste
34.	FEUGANG YOUMSSI François	Chargé de Cours	En poste
35.	FOKAM Alvine Christelle Epse KENGNE	Chargé de Cours	En poste
36.	FOSSI TANKOUA Olivia Epse DJEUTCHOUANG SAYANG	Chargé de Cours	En poste (transfert Uté de Dla)
37.	GONWOUO NONO Legrand	Chargé de Cours	En poste
38.	KOGA MANG DOBARA	Chargé de Cours	En poste

39.	LEME BANOCK Lucie	Chargé de Cours	En poste
40.	MAPON NSANGOU Indou	Chargé de Cours	En poste
41.	METCHI DONFACK MIREILLE FLAURE EPSE GHOUMO	Chargé de Cours	En poste
42.	NGOUATEU KENFACK Omer Bébé	Chargé de Cours	En poste
43.	NJUA Clarisse YAFI	Chargée de Cours	*Chef Div. Uté Bamenda*
44.	NWANE Philippe Bienvenu	Chargé de Cours	En poste
45.	TADU Zephyrin	Chargé de Cours	En poste
46.	YEDE	Chargé de Cours	En poste
47.	YOUNOUSSA LAME	Chargé de Cours	En poste

48.	KODJOM WANCHE Jacguy Joyce	Assistante	En poste
49.	NDENGUE Jean De Matha	Assistant	En poste
50.	ZEMO GAMO Franklin	Assistant	En poste

3- DÉPARTEMENT DE BIOLOGIE ET PHYSIOLOGIE VÉGÉTALES (BPV) (32)

1.	AMBANG Zachée	Professeur	*Chef de Département*
2.	DJOCGOUE Pierre François	Professeur	En poste
3.	MBOLO Marie	Professeur	En poste
4.	MOSSEBO Dominique Claude	Professeur	En poste
5.	NDONGO BEKOLO	Professeur	En poste
6.	ZAPFACK Louis	Professeur	En poste

7.	ANGONI Hyacinthe	Maître de Conférences	En poste
8.	BIYE Elvire Hortense	Maître de Conférences	En poste
9.	MAHBOU SOMO TOUKAM. Gabriel	Maître de Conférences	En poste
10.	MALA Armand William	Maître de Conférences	En poste
11.	MBARGA BINDZI Marie Alain	Maître de Conférences	*DAAC /UDla*
12.	NGALLE Hermine BILLE	Maître de Conférences	En poste
13.	NGONKEU MAGAPTCHE Eddy L.	Maître de Conférences	*CT / MINRESI*
14.	TONFACK Libert Brice	Maître de Conférences	En poste
15.	TSOATA Esaïe	Maître de Conférences	En poste
16.	ONANA JEAN MICHEL	Maître de Conférences	En poste

17.	DJEUANI Astride Carole	Chargé de Cours	En poste
18.	GONMADGE CHRISTELLE	Chargé de Cours	En poste
19.	MAFFO MAFFO Nicole Liliane	Chargé de Cours	En poste
20.	MANGA NDJAGA JUDE	Chargé de Cours	En poste
21.	NNANGA MEBENGA Ruth Laure	Chargé de Cours	En poste
22.	NOUKEU KOUAKAM Armelle	Chargé de Cours	En poste
23.	NSOM ZAMBO EPSE PIAL ANNIE CLAUDE	Chargé de Cours	*En détachement/UNESCO MALI*
24.	GODSWILL NTSOMBOH NTSEFONG	Chargé de Cours	En poste
25.	KABELONG BANAHO Louis-Paul-Roger	Chargé de Cours	En poste
26.	KONO Léon Dieudonné	Chargé de Cours	En poste
27.	LIBALAH Moses BAKONCK	Chargé de Cours	En poste
28.	LIKENG-LI-NGUE Benoit C	Chargé de Cours	En poste
29.	TAEDOUNG Evariste Hermann	Chargé de Cours	En poste
30.	TEMEGNE NONO Carine	Chargé de Cours	En poste
31.	DIDA LONTSI Sylvere Landry	Assistant	En poste
32.	METSEBING Blondo-Pascal	Assistant	En poste

4- DÉPARTEMENT DE CHIMIE INORGANIQUE (CI) (27)

1.	GHOGOMU Paul MINGO	Professeur	*Ministre Chargé de Mission PR*
2.	NANSEU NJIKI Charles Péguy	Professeur	En poste
3.	NDIFON Peter TEKE	Professeur	*CT MINRESI*
4.	NENWA Justin	Professeur	En poste
5.	NGOMO Horace MANGA	Professeur	*Vice Chancelor/UB*
6.	NJIOMOU C. épse DJANGANG	Professeur	En poste
7.	NJOYA Dayirou	Professeur	En poste

8.	ACAYANKA Elie	Maître de Conférences	En poste
9.	EMADAK Alphonse	Maître de Conférences	En poste
10.	KAMGANG YOUBI Georges	Maître de Conférences	En poste
11.	KEMMEGNE MBOUGUEM Jean C.	Maître de Conférences	En poste
12.	KENNE DEDZO GUSTAVE	Maître de Conférences	En poste
13.	MBEY Jean Aime	Maître de Conférences	En poste
14.	NDI NSAMI Julius	Maître de Conférences	*Chef de Département*
15.	NEBAH Née NDOSIRI Bridget NDOYE	Maître de Conférences	*Sénatrice/SENAT*
16.	NYAMEN Linda Dyorisse	Maître de Conférences	En poste
17.	PABOUDAM GBAMBIE AWAWOU	Maître de Conférences	En poste
18.	TCHAKOUTE KOUAMO Hervé	Maître de Conférences	En poste
19.	BELIBI BELIBI Placide Désiré	Maître de Conférences	*Chef Service/ ENS Bertoua*
20.	CHEUMANI YONA Arnaud M.	Maître de Conférences	En poste
21.	KOUOTOU DAOUDA	Maître de Conférences	En poste

22.	MAKON Thomas Beauregard	Chargé de Cours	En poste
23.	NCHIMI NONO KATIA	Chargée de Cours	En poste
24.	NJANKWA NJABONG N. Eric	Chargé de Cours	En poste
25.	PATOUOSSA ISSOFA	Chargé de Cours	En poste
26.	SIEWE Jean Mermoz	Chargé de Cours	En Poste
27.	BOYOM TATCHEMO Franck W.	Assistant	En Poste

6- DÉPARTEMENT DE CHIMIE ORGANIQUE (CO) (33)			
1.	Alex de Théodore ATCHADE	Professeur	*DEPE/Univ. Bertoua*
2.	DONGO Etienne	Professeur	*Vice-Doyen/FSE/UYI*
3.	NGOUELA Silvère Augustin	Professeur	*Chef de Département UDS*
4.	PEGNYEMB Dieudonné Emmanuel	Professeur	*Recteur UBertoua/ Chef de Département*
5.	MBAZOA née DJAMA Céline	Professeur	En poste
6.	MKOUNGA Pierre	Professeur	En poste
7.	AMBASSA Pantaléon	Maître de Conférences	En poste
8.	EYONG Kenneth OBEN	Maître de Conférences	En poste
9.	FOTSO WABO Ghislain	Maître de Conférences	En poste
10	KAMTO Eutrophe Le Doux	Maître de Conférences	En poste
11	KENMOGNE Marguerite	Maître de Conférences	En poste
12	MVOT AKAK CARINE	Maître de Conférences	En poste
13	NGO MBING Joséphine	Maître de Conférences	*Chef de Cellule MINRESI*
14	NGONO BIKOBO Dominique Serge	Maître de Conférences	*C.E.A/ MINESUP*
15	NOTE LOUGBOT Olivier Placide	Maître de Conférences	*Dir ENS/Uté Bertoua*
16	NOUNGOUE TCHAMO Diderot	Maître de Conférences	En poste
17	TABOPDA KUATE Turibio	Maître de Conférences	En poste
18	TAGATSING FOTSING Maurice	Maître de Conférences	En poste
19	OUAHOUO WACHE Blandine M.	Maître de Conférences	En poste
20	ZONDEGOUMBA Ernestine	Maître de Conférences	En poste
21.	MESSI Angélique Nicolas	Chargé de Cours	En poste
22.	MUNVERA MFIFEN Aristide	Chargé de Cours	En poste
23.	NGNINTEDO Dominique	Chargé de Cours	En poste
24.	NGOMO Orléans	Chargée de Cours	En poste
25.	NONO NONO Éric Carly	Chargé de Cours	En poste
26.	OUETE NANTCHOUANG Judith Laure	Chargée de Cours	En poste
27.	SIELINOU TEDJON Valérie	Chargé de Cours	En poste
28.	TCHAMGOUE Joseph	Chargé de Cours	En poste
29.	TSAFFACK Maurice	Chargé de Cours	En poste
30.	TSAMO TONTSA Armelle	Chargé de Cours	En poste
31.	TSEMEUGNE Joseph	Chargé de Cours	En poste
32.	NDOGO ETEME Olivier	Assistant	En poste
33.	NGUEMDJO CHIMEZE Valery Wilfried	Assistant	En poste

6- DEPARTEMENT DES ENERGIES RENOUVELABLES (ER) (1)			
1.	BODO Bertrand	Professeur	*Chef de Département*

7- DÉPARTEMENT D'INFORMATIQUE (IN) (22)

1.	ATSA ETOUNDI Roger	Professeur	*Chef de Division des SI/ MINESUP*
2.	FOUDA NDJODO Marcel Laurent	Professeur	*Inspecteur Général Académique/ MINESUP*

3.	NDOUNDAM Réné	Maître de Conférences	En poste
4.	TSOPZE Norbert	Maître de Conférences	En poste

5.	ABESSOLO ALO'O Gislain	Chargé de Cours	*Chef de Cellule MINFOPRA*
6.	AMINOU HALIDOU	Chargé de Cours	*Chef de Département*
7.	DJAM Xaviera YOUH - KIMBI	Chargé de Cours	En Poste
8.	DOMGA KOMGUEM Rodrigue	Chargé de Cours	En poste
9.	EBELE Serge Alain	Chargé de Cours	En poste
10.	EKODECK Stéphane Gaël Raymond	Chargé de Cours	En poste
11.	HAMZA Adamou	Chargé de Cours	En poste
12.	JIOMEKONG AZANZI Fidel	Chargé de Cours	En poste
13.	KOUOKAM KOUOKAM E. A.	Chargé de Cours	En poste
14.	MELATAGIA YONTA Paulin	Chargé de Cours	En poste
15.	MESSI NGUELE Thomas	Chargé de Cours	En poste
16.	MONTHE DJIADEU Valery M.	Chargé de Cours	En poste
17.	NZEKON NZEKO'O ARMEL JACQUES	Chargé de Cours	En poste
18.	OLLE OLLE Daniel Claude Georges Delort	Chargé de Cours	*Directeur Adjoint ENSET Ebolowa*
19.	TAPAMO Hyppolite	Chargé de Cours	En poste

20.	BAYEM Jacques Narcisse	Assistant	En poste
21.	MAKEMBE. S . Oswald	Assistant	*Directeur CUTI*
22.	NKONDOCK. MI. BAHANACK.N.	Assistant	En poste

8- DÉPARTEMENT DE MATHÉMATIQUES (MA) (34)

1.	AYISSI Raoult Domingo	Professeur	*Chef de Département*

2.	KIANPI Maurice	Maître de Conférences	En poste
3.	MBANG Joseph	Maître de Conférences	En poste
4.	MBEHOU Mohamed	Maître de Conférences	*Chef de Division/ENSPY*
5.	MBELE BIDIMA Martin Ledoux	Maître de Conférences	*Chef de Département de modélisation et applications industrielles/ENSPY*
6.	NOUNDJEU Pierre	Maître de Conférences	*VDRC/FS/UYI*
7.	TAKAM SOH Patrice	Maître de Conférences	En poste
8.	TCHAPNDA NJABO Sophonie B.	Maître de Conférences	*Directeur/AIMS Rwanda*
9.	TCHOUNDJA Edgar Landry	Maître de Conférences	En poste

10.	AGHOUKENG JIOFACK Jean Gérard	Chargé de Cours	*Chef Cellule MINEPAT*
11.	BOGSO ANTOINE Marie	Chargé de Cours	En poste
12.	BITYE MVONDO Esther	Chargé de Cours	En poste
13.	CHENDJOU Gilbert	Chargé de Cours	En poste
14.	DJIADEU NGAHA Michel	Chargé de Cours	En poste
15.	DOUANLA YONTA Herman	Chargé de Cours	En poste
16.	KIKI Maxime Armand	Chargé de Cours	En poste
17.	KOKOMO AYISSI Eric Brice	Chargé de Cours	En poste(transfert de l'université de Douala)
18.	LOUMNGAM KAMGA Victor	Chargé de Cours	En poste
19.	MBAKOP Guy Merlin	Chargé de Cours	En poste
20.	MBATAKOU Salomon Joseph	Chargé de Cours	En poste
21.	MENGUE MENGUE David Joël	Chargé de Cours	*Chef Dpt /ENS Université d'Ebolowa*
22.	MBIAKOP Hilaire George	Chargé de Cours	En poste
23.	NGUEFACK Bernard	Chargé de Cours	En poste
24.	NIMPA PEFOUKEU Romain	Chargée de Cours	En poste
25.	OGADOA AMASSAYOGA	Chargée de Cours	En poste
26.	POLA DOUNDOU Emmanuel	Chargé de Cours	*En stage*
27.	TENKEU JEUFACK Yannick Léa	Chargé de Cours	En poste
28.	TCHEUTIA Daniel Duviol	Chargé de Cours	En poste
29.	TETSADJIO TCHILEPECK M. Eric.	Chargé de Cours	En poste

30.	FOKAM Jean Marcel	Assistant	En poste
31.	GUIDZAVAI KOUCHERE Albert	Assistant	En poste
32.	MANN MANYOMBE Martin Luther	Assistant	En poste
33.	MEFENZA NOUNTU Thiery	Assistant	En poste
34.	NYOUMBI DLEUNA Christelle	Assistant	En poste

9- DÉPARTEMENT DE MICROBIOLOGIE (MIB) (24)

1.	ESSIA NGANG Jean Justin	Professeur	*Chef de Département*
2.	NYEGUE Maximilienne Ascension	Professeur	*Vice-Doyen / DSSE*
3.	SADO KAMDEM Sylvain Leroy	Professeur	En poste
4.	ASSAM ASSAM Jean Paul	Maître de Conférences	En poste
5.	BOUGNOM Blaise Pascal	Maître de Conférences	En poste
6.	KOUITCHEU MABEKU Epse KOUAM Laure Brigitte	Maître de Conférences	En poste
7.	MUNE MUNE Martin Alain	Maître de Conférences	En poste
8.	RIWOM Sara Honorine	Maître de Conférences	En poste
9.	NJIKI BIKOÏ Jacky	Maître de Conférences	En poste
10	TCHIKOUA Roger	Maître de Conférences	*Chef de Service de la Scolarité*
11	ESSONO Damien Marie	Chargé de Cours	En poste
12	LAMYE Glory MOH	Chargé de Cours	En poste
13	MEYIN A EBONG Solange	Chargé de Cours	En poste
14	MONI NDEDI Esther Del Florence	Chargé de Cours	En poste
15	NKOUDOU ZE Nardis	Chargé de Cours	En poste
16	NKOUE TONG Abraham	Chargé de Cours	En poste
17	TAMATCHO KWEYANG Blandine Pulchérie	Chargé de Cours	En poste
18	SAKE NGANE Carole Stéphanie	Chargé de Cours	En poste
19	TOBOLBAÏ Richard	Chargé de Cours	En poste
20	EZO'O MENGO Fabrice Télésfor	Assistant	En poste
21	EHETH Jean Samuel	Assistant	En poste
22	MAYI Marie Paule Audrey	Assistant	En poste
23	NGOUENAM Romial Joël	Assistant	En poste
24	NJAPNDOUNKE Bilkissou	Assistant	En poste

Dédicace

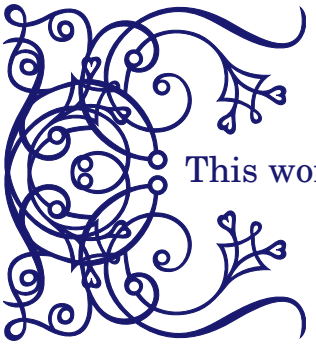

This work is dedicated to my dear parents.

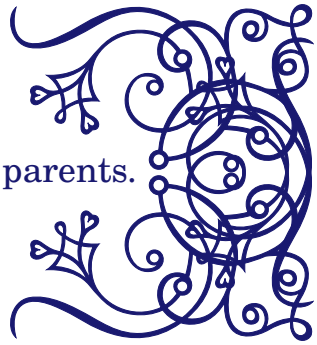

ACKNOWLEDGEMENTS

At the end of my doctoral studies, I am deeply grateful for the opportunity to have learned from and worked with so many brilliant teachers, collaborators and students. I would like to express my sincere gratitude to all those who, near and far, have accompanied me during these doctoral years and have contributed, directly or indirectly, to the completion of this document. Nevertheless, I will do my best to condense my thoughts.

- ☞ Above all, I thank the Almighty Creator for giving me the opportunity to carry out this work in favourable conditions and in good health.
- ☞ I would like to express my sincere gratitude to my supervisor, **Pr. KOFANÉ Timoléon Crépin**, despite his multiple academic, administrative and family commitments, accepted to supervise this thesis. I would like to thank him for all the teaching and advice he has given me.
- ☞ I am grateful to **Pr. OWONO OWONO Luc Calvin**, Dean of the Faculty of Science, for his teaching of atomic and molecular physics.
- ☞ I would like to thank **Pr. NDJAKA Jean-Marie**, Head of the Physics Department. I am very grateful for his administrative contribution and encouragement.
- ☞ I wish to express my deep gratitude to my professors in the Physics department for the richness and diversity of their teachings.
- ☞ I would like to express my sincere thanks to the honourable members of the jury — **Professors BEN-BOLIE Germain, KOFANÉ Timoléon Crépin, NANA ENGO Serge Guy, KENFACK SADEM Christian, and BOUETOU BOUETOU Thomas** — who kindly agreed to set aside their numerous obligations to evaluate this work. I express to them all my deepest respect.
- ☞ I wish to express my deep gratitude to **Pr. BEN-BOLIE Germain Hurbert**, Director of the Nuclear Physics Laboratory, for the high quality of his teaching, his kindness, his availability and his encouragement.
- ☞ I would like to express my gratitude to **Pr. EKOBENA FOUDA Henri Paul**, Director of the Laboratory of Biophysics and Special Measurements and Vice Rector of the University of Ngaoundéré, for his invaluable advice, constructive discussions and teaching.

☞ I would like to deeply thanks **Pr. TABI Conrad Bertrand** for his guidance and advice.

☞ I also wish to thank **Pr. SAÏDOU** for his teachings, constant encouragement, and insightful advice since my Master's program.

☞ I wish to express my deep gratitude to **Pr. MVOGO Alain** for his teachings and valuable advice provided in the laboratory.

☞ I would like to express my deep gratitude to **Dr. BELOBO BELOBO Didier** who, despite his many commitments, agreed to mentor this thesis. I thank him for our enriching exchanges, as well as for his support of learner autonomy. His invaluable academic, moral and social advice contributed greatly to my development. His perseverance and astute suggestions have played an essential role in the development of my intellectual abilities. I sincerely hope that he will find in this thesis all my gratitude.

☞ I would like to thank **Dr. DANG KOKO Adamou** for many fruitful discussions on different aspects of biology and nonlinear physics.

☞ I would like to express my gratitude to **Dr. BANSI KAMDEM Delphin Christel**, for her invaluable support, advice, encouragement, criticism and collaboration from my entry into the Masters programme to the completion of this thesis.

☞ I would like to thank **Dr. DOMGNO KUIPOU William**, **Dr. NDJAWA YOMI Pavel Arnold**, **Dr. DJEUFACK Leornard Boris** and **Dr. FOUEDJI Chenceline** for providing me with various critiques and support throughout this work.

☞ I am grateful to the **African Centre for Advanced Studies (ACAS)** for its various free workshops on the use of numerical methods and MATLAB software, which have better equipped me to carry out this work.

☞ I Would like to thank my mates who supported me with various actions throughout my academic carreer. I am thinking mainly of **Mrs. SIMO Danièle, Mr. NGWEM NGOM, Mr. MONEMPIMP Valdes, Mr. TAMKO Boris, Mrs. MOUAFO Sidoine, Mr. TABI Blaise, Mr. ESSAGA Billy, Mrs. DJOU MELI Yannela, Mrs. NGUEPI Vannelle, Mrs. ONANENA Capucine, Mrs. YANKAM Dorcasse** and others for their help, their intellectual contribution and their great solidarity, thanks to them, this thesis has been realized in a peaceful and harmonious social environement.

☞ I wish to thank my family, especially my brothers, **Dr. FOTSO KAMDEM Eddy, Dr. POLA Emmanuel, KAMGA KAMDEM Terrence**, and my sister, **METAGNE KAMGA Julienne Espe NKOLO**. I also thank the POLA Faustin family for their love and multifaceted support. Thank you all for your support and encouragement throughout my education, and for the unwavering belief you have in me.

☞ I wish to express my deep gratitude to the **TABAPSI André** Family for their invaluable support throughout the completion of this work. Their help and encouragement have been essential to the realization of this project.

☞ I would like to express my gratitude to the **SADO SADO Steven** family for their support throughout this thesis.

☞ I also want to thank **Mr. SIMADJI Christian, Mr. POUGOM Hermann, Mr. NGASSEU Gilles, Mr. MOUKAM Steve** for their support and encouragement during the completion of this work.

☞ A heartfelt thank you to all those, near and far, who have given me their moral, spiritual and intellectual support throughout this work. To those who may read these lines and search for their names without finding them, I offer my sincere apologies and thank you anonymously here: Thank you all.

CONTENTS

List of Figures

Page

List of abbreviations

MT(s)	Microtubule(s)
PF(s)	Protofilament(s)
GTP	Guanosine Tri-Phosphate
GDP	Guanosine Di-Phosphate
ATP	Adenosine Tri-Phosphate
γ**-TURC**	γ-Tubulin Ring Complex
γ**-TUSC**	γ-Tubulin Small Complex
MAP(s)	Microtubules Associated Proteins
MI	Modulational instability
BDKm	BOGNING-DJEUMEN-TCHAHO-KOFANÉ Method
MTOC	Microtubule Organizing Center
+TIPs	Tracking proteins plus end
KdV	Korteweg–de Vries
sG	sine-Gordon
RWA	Rotating Wave Approximation
HBM	Hirota Bilinear Method
CGL	Complex Ginzburg-Landau
NLS	Nonlinear Schrödinger
PDE(s)	Partial Differential Equations

ABSTRACT

The results presented in this study highlight the role of wave propagation in the dynamics of microtubules (MTs) within the cytosol. Initially, we examine MT behavior by incorporating cytosolic viscosity through a discrete angular dislocation model. By applying the semi-discrete approximation, we first convert the discrete model into its continuous counterpart, described by the complex cubic Ginzburg–Landau (CGL) equation. A linear stability analysis of plane waves reveals that cytosolic viscosity modifies the modulational instability of the system, enlarging unstable regions while reducing the growth rate of the instability. Motivated by biological processes in which MTs exhibit stationary behavior, we seek stationary-state solutions by first applying a direct method to the cubic CGL equation. We then return to the original discrete model and demonstrate that both bright and anti-dark soliton profiles serve as suitable candidates to describe certain biological mechanisms. Subsequently, we study the effect of viscosity on MT dynamics by modeling both longitudinal and angular displacements. Using the rotating wave approximation (RWA), we derive two decoupled CGL equations for these respective displacements. Two classes of analytical solitary wave solutions are constructed using the modified Hirota bilinear method (HBM). Our findings show that viscosity significantly reduces the amplitude of longitudinal displacements, whereas its effect on angular displacements is negligible. These analytical predictions are validated through numerical simulations using the constructed solutions as initial conditions, showing excellent agreement. The results offer promising perspectives for regulating cytosolic viscosity to control MT assembly, disassembly, and overall structural stability.

Keywords : *Microtubules, viscosity, angular model, Priya model, rotating wave approximation, complex Ginzburg-Landau equation, solitary waves, Hirota method.*

RÉSUMÉ

Les résultats exposés dans ce document mettent en lumière la propagation des ondes sur la dynamique des microtubules (MTs) dans le cytosol. Dans un premier temps, nous examinons cette dynamique en tenant compte de la viscosité du cytosol à l'aide d'un modèle de dislocation angulaire discret. En appliquant l'approximation semi-discrète, nous transformons d'abord le modèle discret en son équivalent continu, représenté par l'équation de Ginzburg–Landau cubique complexe (CGL). Une analyse de la stabilité linéaire des ondes planes démontre que la viscosité du cytosol altère l'instabilité modulationnelle du système, élargissant les zones instables tout en réduisant le taux de croissance de l'instabilité. Motivés par la présence de processus biologiques où les MTs affichent un comportement stationnaire, nous recherchons des solutions d'état stationnaire, en appliquant tout d'abord une méthode directe à l'équation cubique de CGL. Ensuite, nous revenons au modèle discret original pour montrer que les profils de solitons lumineux et anti-sombres sont des candidats appropriés pour expliquer certains mécanismes biologiques. Par la suite, nous étudions l'effet de la viscosité sur la dynamique des MTs en modélisant des déplacements longitudinaux et angulaires. À l'aide de l'approximation de l'onde tournante (RWA), nous dérivons deux équations de CGL découplées pour ces déplacements respectifs. Deux types de solutions analytiques d'ondes solitaires sont ainsi construites en utilisant la méthode bilinéaire modifiée de Hirota (HBM). Il en ressort que la viscosité atténue les déplacements longitudinaux des MTs en réduisant significativement l'amplitude des ondes longitudinales, tandis que son effet sur les déplacements angulaires est négligeable. Ce résultat est validé par nos prédictions analytiques obtenues par simulations numériques, en utilisant les solutions construites comme conditions initiales. Cette confirmation est observée avec une meilleure précision. Ces solutions offrent donc des perspectives prometteuses pour réguler la viscosité du cytosol afin de contrôler l'assemblage, le démontage et la stabilité des MTs.

Mots clés: *Microtubules, viscosité, modèle angulaire, modèle de Priya, approximation de l'onde rotative, équation de Ginzburg-Landau complexe, ondes solitaires, méthode d'Hirota.*

General Introduction

As early as 1903, Nikolai Koltsov's forward-thinking approach led to the revolutionary concept of a network of tubules acting as an internal support system, which gave the cell its distinctive shape and structure. This was named the cytoskeleton. This pioneering concept not only laid the conceptual foundations of modern cytoskeletal theory but also established an essential pillar in the burgeoning fields of cell biology and developmental biology.

The cytoskeleton, this essential protein polymer, gives cells their mechanical and architectural properties, enabling them to respond to the myriad stimuli of their organic environment in an adept manner. The cytoskeleton is organised like a framework, comprising three types of finely woven structures that extend throughout the cytoplasm: actin microfilaments, intermediate filaments, and MTs, which will be the focus of this study.

MTs, discovered in the 1940s through electron microscopy by the Belgian biologist Albert Claude, prove to be indispensable players within eukaryotic cells [1]. They form a superposed protein network in dimers, branching into three distinct categories: kinetochore MTs, non-kinetochore MTs (also known as interpolar), and astral MTs [2]. Kinetochore MTs, anchored at one end of the kinetochore, hold critical importance in chromosome signaling and positioning, potentially orchestrating their movement [3]. They stretch from the kinetochore to the centrosome, although the exact dynamics of their polymerization/depolymerization remain to be elucidated. Astral MTs, emanating from the spindle poles, contribute to spindle positioning, either by exerting pressure on the cell cortex, utilizing traction forces rooted in the cortex, or interacting with force generators in the cytoplasm, or combining these various processes [4–13]. The remaining MTs, neither kinetochore nor astral, are termed non-kinetochore MTs, forming the majority of MTs in the metaphase spindle of metazoans. Involved in multiple aspects of cell transport [14], they play a crucial role during cell division, acting as a dynamic structure that spatializes duplicated chromosomes [15]. Their ends possess distinct properties

and are subject to polymerization/depolymerization phenomena, influenced by various stimuli encountered by the cell depending on organismal needs, acting as a wave. Following early experimental research on MTs [1, 16, 17], numerous theoretical studies have been devoted to understanding MT transport properties. Among these properties, the physical mechanism of MT solitons (stable solitary waves propagating in a nonlinear medium) holds particular importance, especially in the context of anticancer treatments targeting MTs, where stability and control of dynamic processes, including waves, are crucial. Additionally, several applications in bio-nanotechnology also target MTs in their treatments [18, 19]. The generation and propagation of matter waves in MTs are now an active research domain at the confluence of atomic physics and biophysics, with notable advances both theoretically and experimentally, including dark solitons, bright solitons, and dark-bright solitons, to name a few.

A great deal of work has been done to study the properties of solitons in MTs. This has involved exploring temporal and/or spatial variations of cubic nonlinearities in confinement potentials of various shapes. One of the key questions surrounding solitons in MTs is how they are generated. Theoretically predicted, the generation of solitons in MTs through the activation of modulational instability (MI) falls within the framework of the cubic nonlinear Schrödinger equation (NLS), as well as that of the CGL equation. Due to its potential applications, this technique has attracted increasing interest and has been studied in various contexts, including active matter [20] and Bose-Einstein condensates [21].

In a broader context, all physical systems are considered to be open due to their interaction with the environment [22]. Studying the effect of cytoplasm viscosity on MTs opens new perspectives for understanding upcoming cellular processes. The cytosol, the environment in which cellular organelles operate, directly influences MT dynamics through its viscosity and shear resistance, closely linked to the concept of rheology, where temperature also plays a crucial role [23]. Previous research has examined the effect of viscosity on vibrations in MTs, highlighting the influence of electrical signals from yeast cells on MT oscillations [20]. Additionally, models have been developed to explain the nonlinear dynamics of MTs through kink solitons moving within these structures [15]. The impact of cytosol viscosity on MT polymerization and depolymerization mechanisms has also been explored, revealing substantial modifications in these processes depending on viscosity [24–27]. This viscosity variability also appears to affect MT formation and disassembly rates, suggesting significant implications for their stability and function, particularly in the context of cancer treatment [28, 29]. These

observations raise several major questions:

Questions

how does the viscosity of the cytosol affect the localization of energy within MTs? In other words, how can be used to control the dynamics of MTs? Finally, what are the resulting biological implications?

To our knowledge, the necessary information to answer these questions has not yet been provided. In other words, investigating these questions offers an opportunity to explore new directions in the dynamics of MTs. This opens the door to numerous possibilities for both analytical and numerical analyses. To this end, we propose to study the influence of cytosol viscosity on modulational instability. Using wave analysis, we construct new solitary wave solutions where viscosity acts through an angular model. Subsequently, we evaluate the effects of this viscosity on the interaction of dimers in the presence of an electric field. For this purpose, solitary wave solutions subjected to the influence of viscosity are generated through a two-dimensional model. In order to achieve these objectives, our work is organised as follows:

- ☞ Chapter 1 presents a literature review on MTs, addressing their composition, structure, dynamics, associated proteins, diseases related to their dysfunction, as well as the origin of the soliton concept with some examples.
- ☞ Chapter 2 proposes a conceptualization of existing models, with a discussion on the various considerations taken into account. We also outline the investigative methodology, including the analytical and numerical methods used for our work.
- ☞ In Chapter 3, Chapter 3 focuses on two main objectives: filling our knowledge gap regarding the influence of cytoplasm viscosity on modulation instability and developing new soliton solutions to explain MT dynamics in the presence of this viscosity. Next, we examine the impact of cytosol viscosity on dimer interaction in the presence of an electric field. Subsequently, we construct exact solutions that illuminate microtubule dynamics, considering this viscosity that influences MTs through a two-dimensional model.
- ☞ Finally, a general conclusion closes the thesis by proposing open problems and perspectives.

CHAPTER 1

LITERATURE REVIEW OF MICROTUBULES

Contents

1.1 Introduction

It is well established that MTs cannot be reduced to mere static pillars. While they are often associated with rigid support structures within cells, their nature is far more complex and dynamic. This complex dynamics sometimes even challenges our understanding, prompting some biologists to move beyond the simplistic mechanical view of these structures. By exploring their intrinsic dynamism, we discover that they cannot be simply categorized as mechanical components. Their nonlinear dynamics endow them with the properties of a complex system, including the ability to self-organize. This introductory paragraph on MTs is not intended to be an exhaustive presentation, given the complexity and controversy surrounding their dynamics. Consequently, we will concentrate on the most important aspects that are necessary for understanding the phenomena that will be discussed in the following text. We begin by examining the structure and composition of MTs, before moving on to explore their dynamics, which is a crucial aspect for understanding the models we are studying. We examine the elements with which they interact and explore their multiple roles and functions. Finally, we will discuss the diseases associated with their dysfunction and the preventive measures that can be taken to mitigate them. Finally, we will conclude by discussing the origin of the soliton concept and its various classes.

1.2 Localization and composition of microtubules

MTs are predominantly found in various regions of eukaryotic cells such as the cytoplasm, neurons, the mitotic spindle, cilia and flagella, centrosomes, cellular organelles, and during cell division. They result from the assembly of tubulin, a protein consisting of two subunits, α and β, each containing 450 amino acids. Each subunit possesses a nucleotide-binding site for GTP in its N-terminal region, where the β subunit can exchange between GTP and GDP, while the α subunit remains permanently bound to GTP. Crystallographic analysis of the heterodimer, achieved through self-assembly of MT sheets in the presence of zinc and stabilized by taxol [30], reveals structural simi-

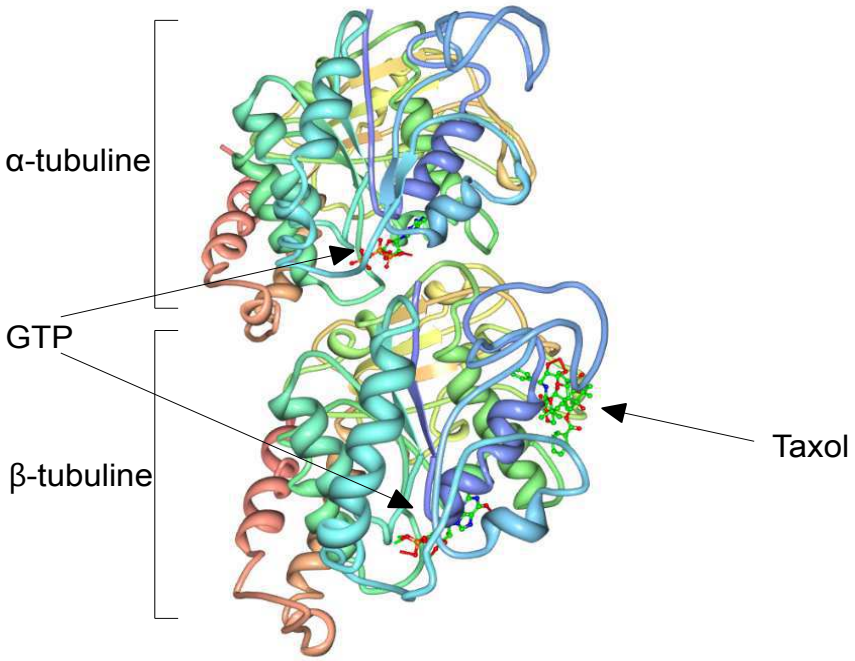

Figure 1.1: *Three-dimensional representation of the tubulin dimer structure. Each monomer has a GTP binding site, but the GTP of the α subunit is trapped and non-hydrolyzable. The β subunit has a taxol binding site (adapted from [30]).*

larity between the α and β subunits, with a composition comprising 39% α-helices and 18% β-sheets.

The tubulin dimer can be divided into three main parts: an N-terminal part containing the GTP or GDP binding site, an intermediate part with a binding site for taxol (a MT-stabilizing agent), and a C-terminal part exposed outside the dimer. The latter undergoes post-translational modifications that allow it to interact with other proteins [31].

1.3 GTP: protagonist of microtubule polymerisation

In addition to the α and β tubulin subunits, the GTP molecule plays a crucial role in MT polymerization. The GTP bound to α-tubulin is stable and cannot be exchanged or hydrolyzed, unlike the GTP attached to β-tubulin, which can be hydrolyzed into GDP or exchanged when the tubulin dimer is free in solution [32]. During polymerization, GTP-bound tubulin dimers are incorporated into MTs before the GTP on β-tubulin is hydrolyzed into GDP. This hydrolysis occurs after a delay, leaving the MT end covered by a GTP-tubulin «cap», also known as the «GTP-cap», which facilitates polymerization.

Once the GTP is hydrolyzed, a conformational change in the tubulin dimer is ob-

served [33, 34]. GTP-bound dimers have a straight conformation, while GDP-bound dimers adopt a curved shape [35, 36]. The main body of the MT, primarily made of GDP-tubulin dimers, is kept in a straight configuration by the presence of the GTP cap, which protects the MT from depolymerization by stabilizing its structure. The loss of this cap due to GTP hydrolysis rapidly induces MT depolymerization [37, 38], partly by releasing the constraints that hold the protofilaments together [36].

However, the GTP-cap model is not universally accepted. Recent research by O. Valiron showed that GDP-tubulin dimers can also incorporate into MTs during polymerization, thereby stabilizing the MT network [39]. These findings suggest a strong link between GTP hydrolysis and MT stabilization. Additionally, in 2008, A. Dimitrov generated an antibody that specifically recognizes GTP-tubulin. Using this antibody, they identified randomly localized points along the MTs, referred to as GTP-tubulin "islands," which may initiate MT polymerization [40].

1.4 Structure of microtubules

MTs stand out for their imposing size and multifunctional role among the various cellular filaments. Composed of tubulin polymers, these protein structures are present in virtually all eukaryotic cells, forming a complex network of proteins assembled as dimers.

MTs take the form of hollow cylinders with an outer diameter of about 25 nm and an inner diameter of about 15 nm, with variable lengths. They result from the association of heterodimeric units of α and β tubulin, capable of longitudinally self-assembling to form protofilaments (PFs). These PFs, typically composed of 13 [41], then spiral helically to form a complete MT.

The association of each tubulin dimer depends on the presence of GTP [42]. The α subunit binds non-exchangeable GTP, while the β subunit binds hydrolysable GTP. Hydrolysis of the GTP bound to the β subunit is necessary for MT extension, allowing the incorporation of new dimers at its end. PFs laterally associate to form a cylindrical, hollow structure, typically with 10 to 15 PFs per MT, depending on assembly conditions.

Due to the diversity of tubulin dimers and their arrangement, MTs exhibit polarity (see Fig. (1.3), with a (+) end exposing the β subunit and a (-) end exposing the α subunit [32, 43, 44]. This polarity induces different assembly kinetics between the two ends of the MT, with the (+) end being more dynamic than the (-) end.

Furthermore, in close proximity to the centrosome, + end of MTs requires the presence of γ-tubulin to initiate MT nucleation, thereby initiating the assembly of tubulin α

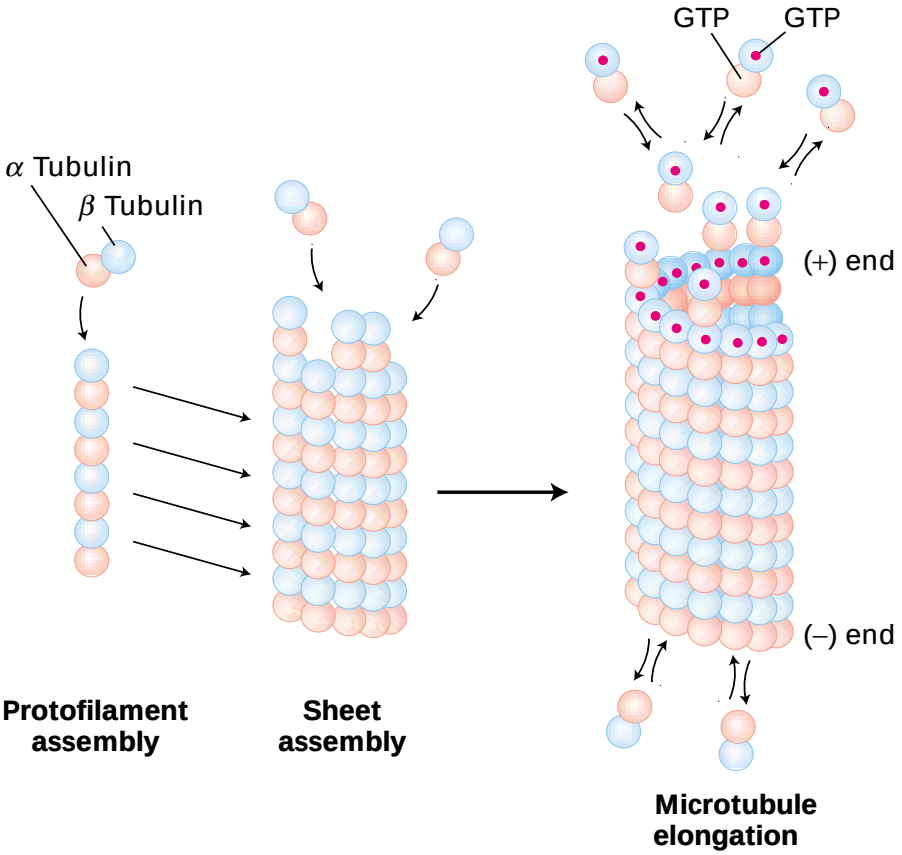

Figure 1.2: *Formation of MTs. Tubulin monomers α and β associated with each other to form a PF. The PFs then associate longitudinally and helically to form MTs [45].*

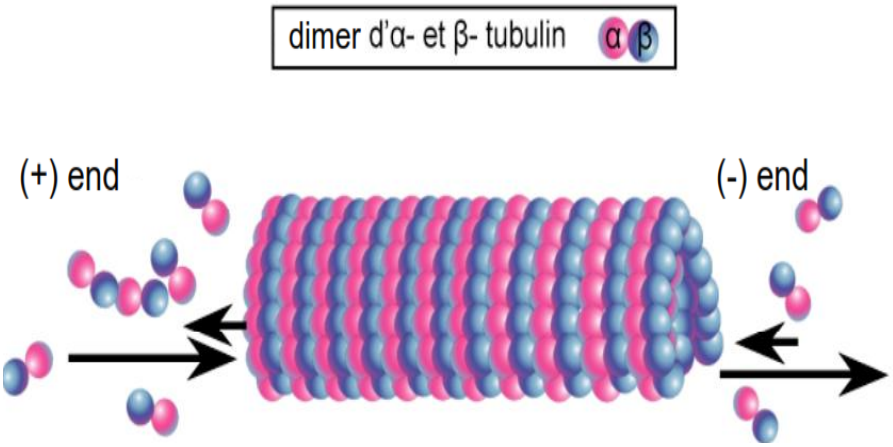

Figure 1.3: *Polarity of Microtubules [46].*

and β dimers and the polymer elongation process. However, γ-tubulin is also distributed in the cytoplasm, where it associates with a protein complex known as the γ-TuRC (γ-Tubulin Ring Complex). In this configuration, γ-tubulin acts as a platform for MT assembly, mimicking a minus end [47]. This polarity of MTs is essential for enabling attachment and movement along these structures by protein complexes.

1.5 Mechanics of microtubules

MTs are a fundamental component of cellular architecture, playing a key role in maintaining cell shape, motility, and intracellular transport. The rigidity of various cytoskeletal elements varies, and one way to measure it is through the persistence length, which represents the distance over which MTs can bend without breaking. This characteristic can be determined passively, by inducing MT curvature through thermal fluctuations, or actively, for example, by using mechanical flow to bend the structure [48].

Due to their structural role, MTs are the most rigid components of the cytoskeleton, formed by the assembly of tubulin dimers into tubular structures. However, despite this rigidity, MTs can adopt very curved conformations within the cell, bending over short distances. This ability to deform is crucial, particularly for the formation of MTs bundles. Indeed, when MTs are more flexible, they can better align when forming these bundles at large angles [49]. In plant cells, they can even coil to follow the plasma membrane.

The mechanical behavior of MTs is adjusted according to cellular needs [50, 51]. Various factors influence the rigidity of MTs, notably certain microtubule-associated proteins (MAPs). Among the most studied MAPs, the neuronal proteins Tau and MAP2 increase the rigidity of MTs [52–54]. Conversely, the MAP65 protein makes MTs more flexible [55].

MT flexibility also depends on the state of tubulin. In its GTP-bound form, tubulin stabilizes the protofilaments, making them more rigid. However, when GTP is hydrolyzed to GDP, the protofilaments become more curved, thus increasing the flexibility of the MT [56].

Other factors, such as temperature and certain chemicals, can also modulate MT rigidity. For instance, an increase in temperature enhances their flexibility, likely by accelerating GTP hydrolysis [57, 58]. Certain drugs also influence the mechanics of MTs: although taxol was initially perceived to increase their flexibility, it is now established that it actually strengthens their rigidity [52, 54, 59].However, this increased rigidity can interfere with the dynamic instability of MTs, potentially disrupting essential cellular processes such as mitosis.

Finally, the rate of polymerization and the length of MTs also play a role in their flexibility. Rapid polymerization leads to greater flexibility, possibly due to defects in the MT wall that decrease its rigidity [60]. Surprisingly, it has been observed that the longer a MT is, the more rigid it becomes, likely due to stronger longitudinal interactions between tubulin dimers compared to lateral interactions between protofilaments [61].

To meet the cell's needs, MTs can rapidly adjust their organization. These dynamically regulated properties within the cell are the origin of their numerous cellular functions as well as the observed changes in shape at the cellular level.

1.6 Dynamics of microtubules

1.6.1 Nucleation

In vitro, MT nucleation begins with an oligomerization step of tubulin, which is slow and energetically unfavorable. However, this process can be accelerated by the presence of nucleation centers, such as axonemes. Several factors influence MT nucleation and assembly [62], including the presence of GTP, Mg^{2+}, the absence of Ca^{2+} (which induces MT depolymerization), a temperature around 35°C, and a pH close to the physiological pH. In the absence of nucleation centers, MTs can nucleate spontaneously, but this is highly dependent on the concentration of tubulin-GTP. Once this concentration exceeds a critical threshold, MTs begin to self-assemble [63]. Two main theories have been proposed to explain the mechanism of MT self-assembly. The first model suggests that tubulin dimers align to form protofilaments, which then group together into sheets that act as nucleation cores. The lateral and longitudinal addition of tubulin dimers subsequently closes these sheets to form a MT (see Fig. (1.4-a)) [64]. The second model proposes that tubulin dimers first assemble laterally to form oligomers. These oligomers then associate longitudinally to create a sheet, which also closes to form an MT (see Fig. (1.4-b)) [63].

In cells, the concentration of tubulin is typically too low to allow spontaneous nucleation. MTs mostly polymerize from nucleation centers such as the centrosome, adopting a radial organization [17]. The centrosome concentrates a specific isoform of tubulin, γ-tubulin, which allows the cell to regulate MT nucleation and localization. γ-tubulin forms a large complex called the γ-tubulin ring complex (γ-TuRCs), which serves as a nucleation platform [66]. For a long time, it was thought that most MTs were formed from the centrosome (see Fig. (1.5)).

However, this radial organization is not ideal for all specialized cells. It has been dis-

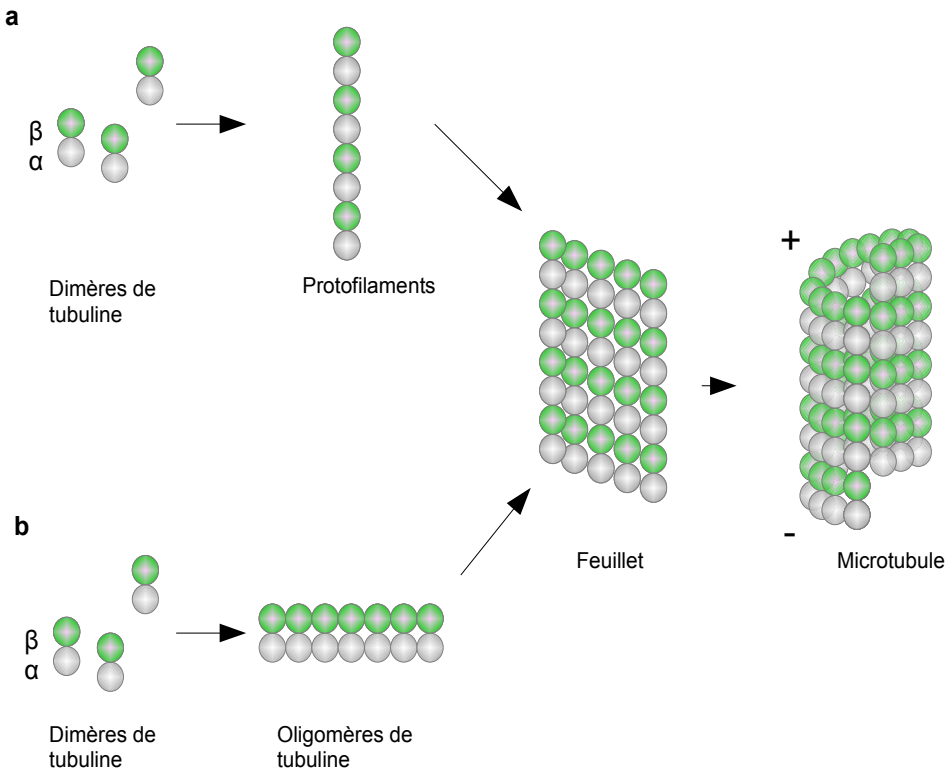

Figure 1.4: *a. Model of nucleation from a nucleating core in the form of protofilaments allowing the formation of a sheet. b. Model of nucleation in the form of tubulin oligomers formation of a leaflet. b. Model of nucleation in the form of tubulin oligomers obtained by lateral association of tubulin dimers [65].*

covered that other MTs can form from Golgi vesicles, directly linking the MT network with vesicular transport [68]. This nucleation mechanism has been observed in various cell types such as hepatocytes, epithelial cells, muscle cells, and neurons [68]. Golgi membranes contain anchoring proteins for γ-tubulin, allowing them to mimic the centrosome's function [69]. Without these proteins, fewer MTs form from the Golgi. Due to the low concentration of γ-tubulin in the Golgi, other proteins are required to stabilize and facilitate MT polymerization, such as the tubulin chaperone TBCE, which locally increases tubulin dimer concentration at Golgi "hot spots" [70], or plus-end binding proteins like CLASPs and EB1, which are also found in the Golgi to promote and regulate polymerization [71].

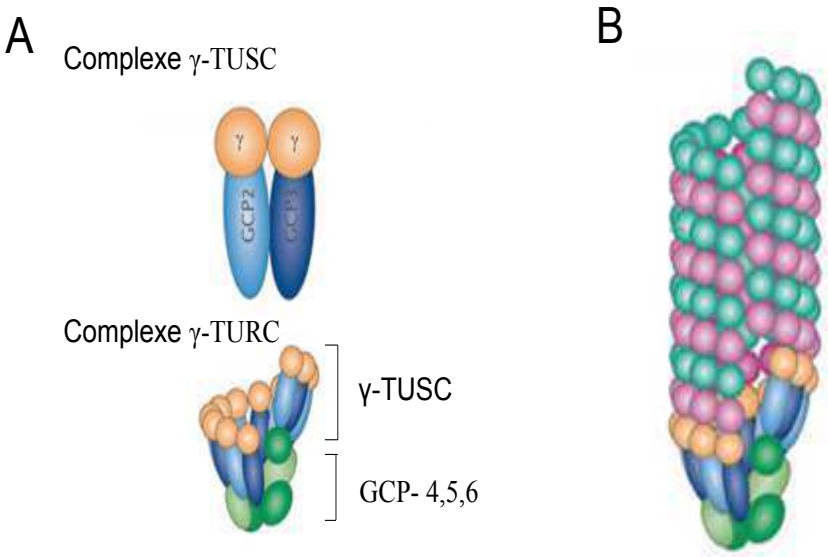

Figure 1.5: *Top: schematic representation of the gamma-TUSC complex made up of the GCP2 and 3 each associated with a gamma-tubulin. Bottom: assembly of the gamma-TURC complex, made up of the assembly of different complexes gamma-TUSC which will associate with the GCP 4,5 and 6 for form a structure circular structure allowing to serve as centre of nucleation at MTs at B [67].*

1.6.2 Elongation

Once the initial nucleation steps are completed, the newly formed MT seeds elongate by adding tubulin-GTP dimers to both ends (the + and - ends). Two models are proposed to explain this process: the first suggests that tubulin dimers are added helically at the MT end, while the second proposes that protofilaments extend by forming a sheet that eventually closes along the groove [72]. The second model is the most widely accepted, as electron microscopy studies have shown MT growth through sheet extension, both in cell extracts and in cells themselves [73]. This model involves two opposing forces: a longitudinal force that tends to curve the protofilaments outward, and a transverse force due to lateral interactions between protofilaments, which increases with the number of protofilaments, ultimately straightening and closing the sheet [74].

MT polymerization requires GTP on the β-tubulin subunit, which is hydrolyzed during assembly. Although this hydrolysis is not necessary for MT polymerization, it is crucial for destabilizing the MT wall and inducing its depolymerization [75]. Recent in vitro studies have shown that GDP-bound tubulin can also incorporate into MTs, altering their properties [39].

The two MT ends polymerize at different rates, with the (+) end growing approximately twice as fast as the (-) end. In vivo, the (-) end is typically stabilized by its

association with nucleation centers.

While MTs can grow simultaneously at both ends in in vitro systems, MT nucleation in mammalian cells generally occurs from the centrosome [76]. This process gives rise to complexes of different sizes, called γ-Tubulin Ring Complex (γ-TURC) and γ-Tubulin Small Complex (γ-TUSC) [77, 78]. These structures play an essential role in initiating MT polymerization and stabilizing their negative ends through a capping process [78]. Once formed, MTs are not static but rather dynamic, exhibiting various behaviors. The first observed phenomenon, described in [79, 80], is that of Treadmilling, also known as the treadmill effect. Subsequent in-depth cellular studies have revealed that MTs undergo cycles of polymerization and depolymerization, known as dynamic instabilities.

1.6.3 Treadmilling

The phenomenon of treadmilling (Fig. 1.6) refers to the simultaneous movement of polymerization and depolymerization at the ends of a filament, such as MTs, asymmetrically [81–84]. This dynamic process results in a net displacement of the filament in a specific direction without changing its total length. It is essential for regulating the size and stability of cellular structures, as well as for intracellular transport of organelles and proteins. MTs can behave differently in steady-state, with continuous growth at one end, and slow continuous depolymerization at the other. This treadmilling phenomenon leads to the movement of MTs within the cell when their negative ends are not anchored to a fixed structure. New tubulin subunits incorporated at the positive end are released by depolymerization at the negative end, allowing the MT to progress towards the cell periphery without net movement of tubulin subunits in the cytoplasm.

1.6.4 Dynamic instability

The ability of MTs to polymerize and depolymerize over time is crucial for the rapid reorganization of cellular networks to meet the changing needs of the cell. Their dynamic instability is primarily due to the behavior of their positive end, characterized by alternating phases of polymerization/depolymerization (see Fig. 1.7). During polymerization, there is hydrolysis of the GTP carried by tubulin, inducing a slight conformational change that stabilizes the polymer. However, if the PFs are not held together, a relaxation phenomenon occurs, leading to a catastrophe where the PFs dissociate from the MT. This alternation of growth and shortening phases of MTs is regulated by catastrophe and rescue events, where the positive end stops growing and starts depolymeriz-

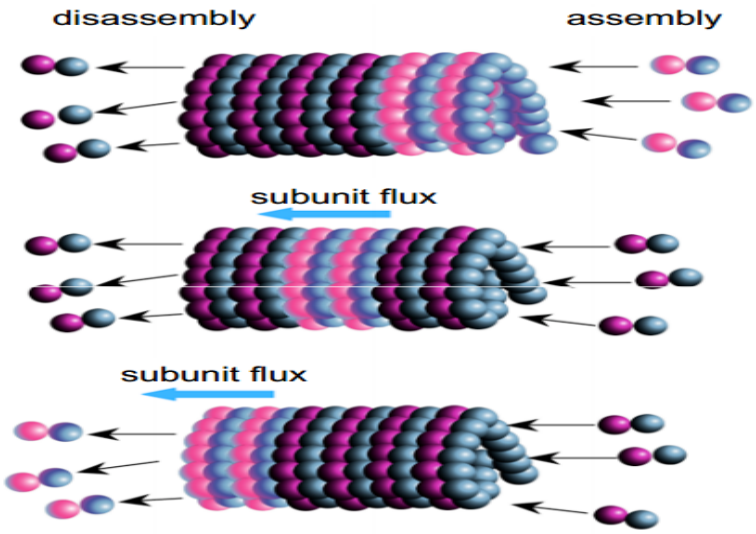

Figure 1.6: *Treadmilling phenomenon. It occurs during the assembly of tubulin at the plus end and the disassembly of tubulin at the minus end [85].*

ing during a catastrophe, while a depolymerizing MT can resume polymerization during a rescue event. Although these transition events have been observed for a long time, the mechanisms explaining their occurrence are not fully understood. Two working models described below help to better understand the mechanisms at play [42, 74, 86–88].

1.6.4.1 GTP cap

Dynamics of MTs are finely regulated by GTP hydrolysis, a process influenced by the proximity of tubulin dimers. This regulation leads to the formation of a GTP-tubulin cap at the plus end of the MT, protecting it from depolymerization [42].

Furthermore, as early as the 1980s, Mitchison and Kirschner suggested that the loss of this cap could trigger MT catastrophes [17, 92]. Subsequent research confirmed this hypothesis, demonstrating that while GTP hydrolysis is not required for polymerization, it is essential for destabilizing the MT wall and inducing its depolymerization [75, 93].

Moreover, when tubulin is in its GDP-bound form, it adopts a curved conformation, likely induced by GTP hydrolysis. This conformational change causes protofilaments to bend outward from the MT, destabilizing the lateral interactions between them [94].

The instability of the GTP cap is closely linked to the relative rates of polymerization and hydrolysis. If polymerization is rapid, the cap is maintained; however, if hydrolysis outpaces polymerization, the cap disappears, leading to a catastrophe. Additionally, observations have highlighted "rescue" events, where depolymerizing MTs switch back to polymerization. These phenomena may be associated with the presence of GTP-tubulin

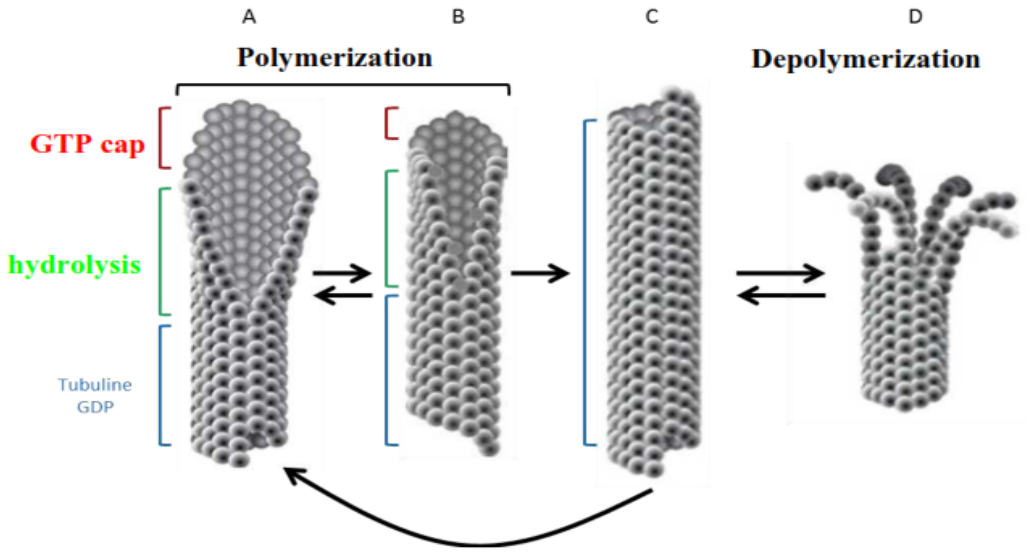

Figure 1.7: *Dynamic instability of MTs. (A) The polymerizing MT has a GTP-tubulin cap at its positive end and a sheet of PFs. (B) The GTP hydrolysis zone coincides with the closure of the PF sheet into a tube [89]. (C) When the PF sheet and GTP cap disappear, the MT no longer polymerizes. Polymerization can resume if a new sheet forms; otherwise, the mechanical energy contained in the tube can be released, causing a catastrophe and leading to depolymerization of the MT. (D) During depolymerization, the lateral bonds between PFs break, they bend outward, and the dimers become individualized [90, 91].*

islands resistant to depolymerization, formed due to incomplete hydrolysis during intense polymerization. These islands could also play a role in recruiting MAPs, thereby facilitating rescue events.

1.6.4.2 Conformational cap

The concept of conformational capping, elaborated in several studies [74, 86, 87], proposes an explanatory model for the dynamics of MTs by considering the internal forces of the MT. According to this model, the natural outward curvature of PFs in the MT is compensated for by lateral forces between adjacent PFs, resulting in their straightening and the stabilization of the MT. This straightening compensates for the energy accumulation caused by the curvature of PFs in the MT wall. The presence of a cap at the MT end allows the PFs to maintain their natural curvature stably, thereby contributing to MT stabilization [88]. The loss of this cap is associated with the onset of catastrophes, events where the MT undergoes rapid depolymerization. Another mechanism, consistent with this model, links the length of the cap, the energy accumulated in the MT wall, and the formation of defects during polymerization [95, 96]. When the cap is long enough, it can close by incorporating defects along the MT wall, such as abnormalities

in the number of PFs, interruptions in the MT structure, or abnormalities in the lattice. However, if the cap is too short, it cannot properly close over the defects, leading to a loss of conformational cap stability and MT depolymerization. The dynamics of MTs strongly depend on associated proteins, which regulate their formation, stability, and destabilization, thereby impacting their cellular functions.

The dynamic instability of MTs, observed early on, remains poorly understood in terms of the underlying mechanisms of stochastic changes at the positive end. Two hypotheses, GTP cap and conformational cap, provide perspectives to explain this instability, without mutually excluding each other. It is noteworthy that the apparent stability of the MT is mainly due to what happens at its end, rather than its centrally located, intrinsically unstable structure.

1.7 Microtubules-associated proteins

MTs form a supramolecular network extending from the centrosome to the cell periphery, where they interact with various cellular components and proteins. These proteins, designated as MAPs, have been identified as essential players in regulating the properties of MTs [97, 98]. Generally, two main types of MAPs are distinguished based on their function: structural MAPs, such as Type I MAPs (MAP1 family) and Type II MAPs (MAP2/MAP4/Tau family), and motor MAPs, such as dynein and kinesin, which move along MTs due to their motor activity. In this section, we will present some of these proteins.

1.7.1 Tau proteins

The tau proteins, [99, 100], are MAPs that play a key role in the nucleation and stabilization of MTs. These proteins have the ability to form MT aggregates and bind to their external and internal surfaces, as demonstrated by various studies [101–105].

To further understand the influence of tau protein on the spatial organization of MTs during axon formation, research has been conducted, notably using videomicroscopy, revealing that tau protein promotes MT stabilization in vitro. It accelerates their growth while reducing the frequency of destabilization events, known as catastrophes. Consistent with this stabilizing function, tau protein also decreases the disassembly rate of MTs and promotes rescue events [106–108].

Phosphorylation of tau proteins, primarily in the proline-rich region and their MT-binding domains, is a key regulatory mechanism. This post-translational modification,

studied by [106, 109, 110], influences the association of tau proteins with MTs, thus modulating their impact on MT dynamics.

1.7.2 Kinesin

First discovered by Vale et *al* [111], kinesins, such as kinesin-1, are tetrameric proteins composed of two light chains and two heavy chains. The heavy chains feature a globular head housing the motor domain and the MT-binding domain, as well as a tail serving as an attachment point for the cargo to be transported. The motor region and the MT-binding domain are generally conserved among different kinesins, unlike the tail, which confers specificity regarding the element to be moved.

These kinesins constitute a family of essential motor proteins present in cells, playing a crucial role in the intracellular transport of organelles, vesicles, and other cargo along MTs. By utilizing energy derived from ATP hydrolysis, they generate directional movement facilitating the displacement of various cellular structures. They are responsible for anterograde transport by undergoing an ATP hydrolysis cycle to ADP, thereby inducing a conformational change that propels the protein along the MT from the (-) end to the (+) end (see Fig.1.8) [112]. These proteins are indispensable for numerous cellular processes such as cell division, protein transport, and intracellular signaling. The movement of these kinesins along MTs can thus influence the length of the mitotic spindle and enable its shortening.

1.7.3 Dynein

Dyneins, much like kinesins, are complex assemblies of proteins comprising two heavy chains, two intermediate chains, and four light chains, as well as several other light chains. However, their function differs from that of kinesins in allowing movement in the reverse direction along MTs, from the plus (+) end to the minus (-) end [114]. The heavy chains contain MT-binding domains and other domains that, like kinesins, are involved in ATP exchange and hydrolysis to ADP, necessary for molecular movement. The intermediate chains and one of the light chains participate in interaction with the organelles to be transported. In neurons, dynein plays a crucial role in transporting organelles and vesicles along the axon, from the presynaptic compartment to the cell body [115–117]. Thus, the various kinesins and dyneins are involved in regulating and modulating the transport of vesicles and proteins along MTs.

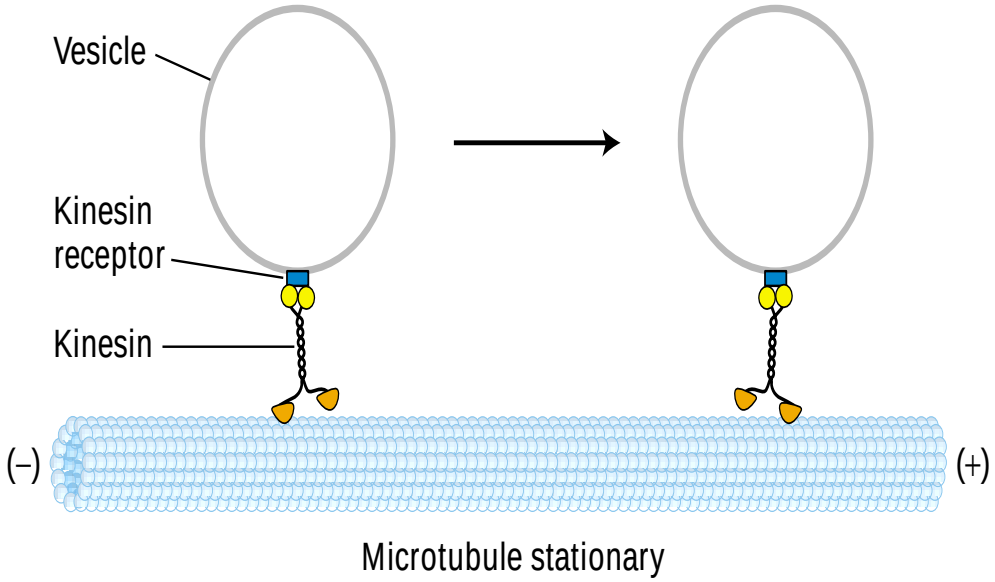

Figure 1.8: *Model of kinesin-catalyzed vesicule transport. Kinesin molecules, attached to unidentified receptors on the vesicule surface, transport the vesicules from the (-) end to the (+) end of a stationary MTs. ATP is required for movement (adapted from [111, 113]).*

1.7.4 Tracking proteins plus end (+TIPs)

+TIPs are specific proteins associated with MTs (MAPs) that typically localize to the growing ends of MTs [118]. They play a crucial role in facilitating the attachment between the ends of MTs and cellular components. Although the term "+TIPs" implies exclusive localization to the plus end of growing MTs, these proteins can also be found at the minus end of these MTs.

The process of localizing "+TIPs" to the ends of MTs remains largely unknown. Several models have been proposed to explain this phenomenon. The first model suggests active transport of "+TIPs" to the plus (+) end of MTs by a molecular motor. The second model proposes an autostop mechanism, where a protein is directed to the end of the MT through another protein present at that end. Finally, the last model considers a "treadmill" process, where the protein interacts with a specific structure or polymerizes with free tubulin at the plus (+) end of the MT. Subsequently, as the MT continues to grow, the protein ends up on the MT wall, and detachment could be caused by a change in affinity with this wall compared to the end. Other hypotheses include detachment from the MT wall following phosphorylation. Understanding the role of MT-associated proteins is crucial for understanding the involvement of MTs in various cellular func-

tions.

1.8 Implications of microtubules in cellular functions

The MTs play a crucial role in the proper execution of cellular processes, participating in both mitosis and interphase functions. In the following paragraph, we will not list all the cellular activities of MTs, but we will focus on the key functions of this network that are essential for tumor growth and propagation.

1.8.1 Microtubules, masters of cell division

Mitosis is a key process of cell division where a mother cell gives rise to two daughter cells. This phenomenon relies on the mitotic spindle, an assembly of MTs. Contrary to popular belief, multiple MTs interact with each chromosome to facilitate the steps of mitosis by their ability to alternate between growth and shrinkage. Kinetochore fibers play a crucial role in the attachment of chromosomes, a mechanism known as "search-and-capture" [119, 120]. However, research suggests that this mechanism alone is not sufficient to align chromosomes during mitosis. An alternative model, the "self-assembly" model [121], proposes that MTs form independently near the chromosomes. It is possible that these two models work simultaneously in a cell. Finally, the separation of chromosomes is made possible by the depolymerization of kinetochore fibers and the action of motor proteins, including kinesin 13 [122, 123].

1.8.2 Roles of microtubules in cell migration

Cellular motility, or cell migration, involves the active movement of cells, whether spontaneous or in response to signals, randomly or directionally, individually or in groups.

Initially, cell migration was considered to be primarily dependent on actin, regulated by Rho GTPase family proteins. However, research by [124] revealed the role of MTs in cell migration in most cell types. Schematically, this process can be divided into three stages: cell polarization, protrusion formation at the front, and translocation of the cell body. MTs participate in cell polarization by orienting the MT organizing center (MTOC) towards the migration front. Additionally, they contribute to stabilizing the MT network through post-translational modifications such as detyrosination or acetylation. These stabilized MTs act as transport pathways for vesicles and intracellular proteins, facilitating the reorientation of the MTOC and the Golgi apparatus towards the migration front. Ultimately, MTs participate in the translocation of the cell body.

In the context of cancer pathologies, cell migration is crucial at two levels. Firstly, in angiogenesis, where tumor cells promote the formation of new blood vessels by secreting chemokines, particularly from the CXC chemokine family, to stimulate proliferation and migration of endothelial cells. This contributes to the supply of nutrients and oxygen for tumor growth. Secondly, cell migration is critical in the metastatic dissemination of tumor cells, although the exact mechanisms remain poorly understood. This process likely involves chemotactic phenomena and interactions between tumor cells and components of the tumor microenvironment, such as fibroblasts or macrophages. Recent studies have highlighted that organs with high levels of chemokines may be more susceptible to tumor invasion [125].

1.8.3 Microtubules as intracellular transport tracks

MTs play a crucial role in the intracellular trafficking of organelles, vesicles, RNA, and proteins, contributing to both intra- and extracellular signaling pathways. They facilitate the transport of mRNA to appropriate cellular sites for expression and regulate their expression through sequestration, which contributes to intracellular protein distribution and maintenance of cell polarity [126, 127]. By interacting with numerous cellular proteins, MTs act as a protein reservoir, sequestering various proteins that can be released in response to stimuli.

MTs are also crucial in different cellular signaling pathways, acting as tracks for intracellular transport of organelles such as the Golgi apparatus, secretory vesicles, endoplasmic reticulum, and mitochondria [46, 128]. This transport process, directed along MTs, is mainly carried out by kinesins and dyneins, acting as molecular motors [46].

Understanding the multiple functions of MTs in the cell highlights their crucial importance in many biological processes. However, any alteration in these functions can lead to cellular dysfunction and the emergence of various diseases.

1.9 Anomalies related to microtubule dysfunction

Exploring pathologies associated with MT dysfunction is not limited to specific cases. However, examining diseases related to MTs also involves studying those associated with MAPs.

1.9.1 Pathologies related to the tau protein

Some neurodegenerative diseases, such as Alzheimer's disease, are characterized by the presence of intracellular aggregations of the tau protein, which constitute

tauopathies. Initially, tau protein aggregation was considered a major factor in the development of these pathologies, particularly by disrupting the MT cytoskeleton.

More than twenty neurological diseases presenting dementia associated with tau pathology have been identified [129]. Among these are various parkinsonian syndromes, some frontotemporal dementias like Pick's disease with parkinsonian syndrome, as well as syndromes such as Down syndrome and myotonic dystrophies like Steinert's disease [130, 131].

Alzheimer's disease, the primary tauopathy responsible for the majority of dementia cases, was first identified in the early 20th century by Alois Alzheimer. It is an age-related neurodegenerative disease that gradually and irreversibly leads to loss of memory and cognitive functions. At the neuronal level, it is characterized by neurofibrillary tangles (NFTs) and extracellular amyloid deposits [132].

1.9.2 Pathologies related to kinesin

Diseases associated with kinesin dysfunction are diverse and can affect different biological systems. Kinesin is a motor protein involved in intracellular transport along MTs. Its dysfunction can disrupt the transport of various molecules and organelles inside cells, leading to pathological consequences.

Research has established links between kinesin dysfunction and various diseases, including neurodegenerative diseases such as Huntington's disease and Parkinson's disease. For example, studies have shown that mutations in genes encoding kinesin proteins can contribute to the pathogenesis of Huntington's disease [133]. Additionally, alterations in axonal transport associated with kinesin dysfunction have been observed in Parkinson's disease [134].

Apart from neurodegenerative diseases, kinesin dysfunction can also be involved in other disorders, such as rare genetic diseases like primary ciliary dyskinesia (PCDs). For instance, studies have suggested that mutations in kinesin genes may contribute to the pathogenesis of PCDs by disrupting ciliary transport [135].

Thus, kinesin dysfunction can have significant health implications and be involved in a diverse range of diseases, highlighting its crucial role in maintaining normal cellular function.

1.9.3 Diseases associated with dynein dysfunction

Dysfunction of dynein is associated with various pathologies, including neurodegenerative diseases and diabetes. Dynein plays a crucial role in the transport of mitochondria,

and mitochondrial dysfunction is linked to diseases such as amyotrophic lateral sclerosis, Alzheimer's disease, and Huntington's disease [136, 137]. Studies on mice with mutations in the dynein gene have shown abnormalities in the striatum and insulin resistance, linked to decreased mitochondrial respiration [136]. Furthermore, a genetic deficiency in dynein can cause primary ciliary dyskinesia, characterized by chronic bronchitis and sterility due to immotile spermatozoa [138].

1.10 Origin of the soliton concept

The concept of a soliton, a spatially localized solitary wave endowed with remarkable stability properties, has generated considerable interest since its first observation by the hydrodynamics engineer John Scott Russell in 1834 [139]. While conducting experiments to determine the most efficient design for canal boats, he made a remarkable discovery [139]. As he described it in his *Report on Waves*: «I was observing the motion of a boat being rapidly towed along a narrow canal by a pair of horses, when the boat suddenly stopped — but not the mass of water in the canal which it had set in motion; it accumulated around the prow of the vessel in a state of violent agitation, and then, leaving it suddenly behind, rolled forward with great velocity, taking the form of a large solitary elevation, a rounded, smooth, and well-defined heap of water, which continued its course along the canal apparently without change of form or diminution of speed. I followed it on horseback, and overtook it still rolling on at a rate of about eight or nine miles an hour, maintaining its original shape of about thirty feet long and a foot to a foot and a half high. Its height gradually diminished, and after a chase of one or two miles, I lost it in the windings of the canal. Such, in August 1834, was my first chance encounter with that singular and beautiful phenomenon which I have called *the Wave of Translation*. This event took place on the Union Canal at Hermiston, very close to the Riccarton campus of Heriot-Watt University, Edinburgh.»

Intrigued by this unexpected discovery, Russell devoted a decade to its study, despite pre-existing linearized theories suggesting the impossibility of such phenomena. The decline in interest in solitons persisted until 1895, when a theory [140], based on the Korteweg-de Vries equation, finally provided an explanation. This theory was confirmed by a numerical experiment conducted by Fermi, Pasta, and Ulam in 1953 [141], revealing surprising phenomena concerning one-dimensional networks of coupled particles. It wasn't until a decade later, in 1965, that Zabusky and Kruskal [142] provided a definitive explanation by introducing the term "soliton". The soliton, simultaneously a wave and a localized energy maximum, propagates with constant shape and speed, re-

sembling the characteristics of a particle. It is defined as a robust solitary wave whose shape and speed remain unchanged even after collision with another solitary wave. This duality between wave and quasi-particle exhibits similarities with quantum systems, extending to the observation of a tunneling effect for solitons [143].

The pioneering work of Zabusky and Kruskal [142] marked a turning point in the history of solitons, propelling them to the forefront of scientific research and giving rise to countless studies, both mathematically and physically. Soliton equations, as examples of completely integrable systems, have piqued the interest of mathematicians due to their infinite degrees of freedom. However, solitons are not solely the domain of mathematics; they play a crucial role in physics, providing an accurate description of various phenomena, from wave propagation in hydrodynamics to the dynamics of biological macromolecules such as DNA and proteins. Although these systems are only approximately described by soliton equations, these quasi-solitons exhibit remarkable stability against perturbations, making them a powerful tool for describing the physics of nonlinear systems. Instead of adopting a linearized approach followed by the inclusion of nonlinearities as perturbations, the initial description using a soliton equation can often be more effective, allowing for the integration of perturbative contributions if necessary.

1.10.1 Different classes of soliton

Solitons, those remarkable and intriguing solitary waves, manifest in various forms and structures, each offering unique characteristics and distinct implications across diverse scientific domains. Among these diverse classes of solitons, we encounter Korteweg-de Vries solitons, Schrödinger solitons, topological solitons, sine-Gordon solitons and many others. These varied categories of solitons, distinguished by their specific properties and dynamic behavior, play a pivotal role in modeling and comprehending complex physical and mathematical phenomena. There are two types of solitons: the non-topological soliton and the topological soliton.

1.10.1.1 Non-topological solitons

A soliton is considered non-topological when the medium in which it propagates returns to its initial state after the wave has passed. These solitons are commonly encountered in hydrodynamics, though they also appear in solid mechanics. In hydrodynamic contexts, non-topological solitons can be described by the Korteweg–de Vries (KdV) equa-

tion [144, 145]:

$$\frac{1}{c_0}\frac{\partial \eta}{\partial t} + \left(1 + \frac{3\eta}{2h}\right)\frac{\partial \eta}{\partial x} + \frac{h^2}{6}\frac{\partial^3 \eta}{\partial x^3} = 0, \tag{1.1}$$

where $c_0 = \sqrt{gh}$ represents the speed of linear wave propagation in the limit of large wavelengths, h is the depth of the liquid, and η is the height of the liquid surface relative to the equilibrium level.

The KdV equation has a soliton solution [144, 145]:

$$n = \eta_0 sech^2\left[\frac{1}{2h}\sqrt{\frac{3\eta_0}{h}}\left(x - c_0\left[1 + \frac{\eta_0}{2h}\right]t\right)\right]. \tag{1.2}$$

The KdV equation is a fundamental model in soliton theory due to its remarkable mathematical properties. Among the various types of non-topological solitons, we distinguish the following:

- Pulse soliton: this type of soliton presents itself as a single pulse or wave. It can be described as a localized disturbance in the medium to which a certain amount of energy is attributed. Pulse solitons are often observed in systems where energy is concentrated in a single temporal or spatial peak (see Fig. 1.9).

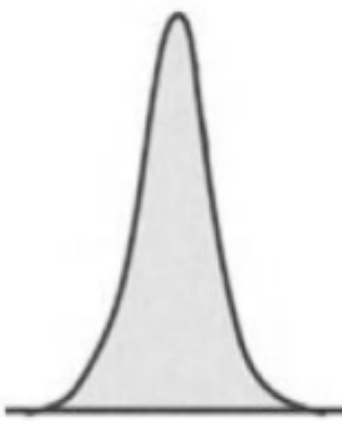

Figure 1.9: *Shape of a pulse soliton [146].*

- Envelope soliton: this structure forms from a set of smaller solitons. Unlike a pulse soliton, which is a single pulse, an envelope soliton is a casing that encompasses multiple individual solitons. It is characterized by a modulated amplitude that contains the individual solitons within its shape (see Fig. 1.10).

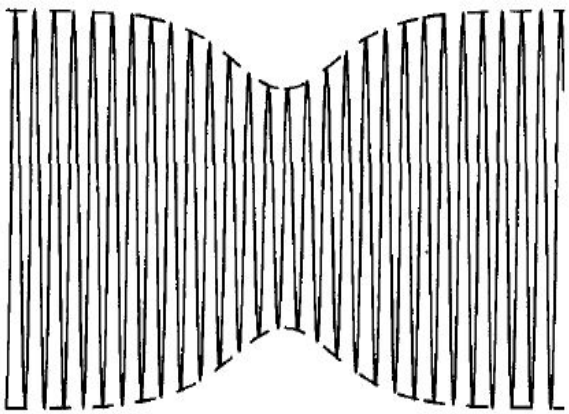

Figure 1.11: *Shape of a hole soliton [146].*

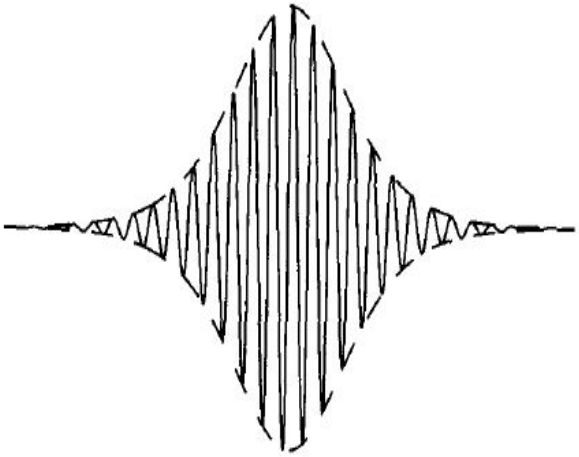

Figure 1.10: *Shape of a envelope soliton [146].*

- Dark soliton, also known as a dark hole, is a region where the amplitude of the wave is lower than that of the surrounding medium. Unlike pulse and envelope solitons, which represent regions of increased amplitude, the dark soliton is distinguished by a significant decrease in amplitude. It can be considered a negative perturbation in the medium (see Fig. 1.11).

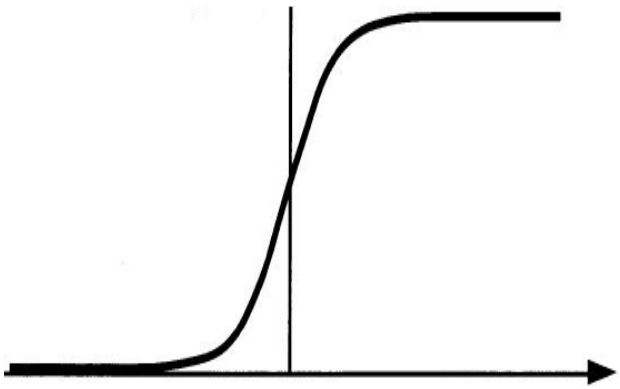

Figure 1.12: *Shape of a kink soliton [146].*

1.10.1.2 Topological Solitons

A soliton is topological when the propagation medium is in different states before and after the passing of the wave. The soliton can be described in this state by the sine-Gordon (sG) equation [145]. This sG equation, which is derived from a chain of pendulum of mass m and length l is given by

$$\frac{\partial^2\theta}{\partial t^2} - c_0^2\frac{\partial^2\theta}{\partial x^2} + \omega_0^2\sin(\theta) = 0; \tag{1.3}$$

where $\omega_0^2 = \frac{mgl}{I}$ is the frequency, $C_0^2 = \frac{c_0^2}{I}$ is the velocity and g is the gravity; I is the moment of inertial, C is the constant of torsion of the spring and a is the distance between the pendulum. As the KdV equation, this equation is completely integrale and admits exact soliton solutions. A soliton solution of this equation [144, 145]:

$$\theta(x,t)_{\pm} = 4arctan\left[\exp\left(\pm\frac{x-ct}{L}\right)\right] \tag{1.4}$$

where $L = \frac{c_0}{\omega_0}\sqrt{1-\frac{C^2}{c_0^2}}$ measures the spatial extension of the solution.

An example of a topological soliton is the kink soliton. A kink soliton, often simply referred to as a kink, is a specific type of soliton encountered in systems where a sharp transition or discontinuity occurs. It is characterized by a local deformation of the medium, often in the form of a region of high variation or rapid change in a physical quantity, such as density, phase, or field (see Fig. 1.12).

1.10.2 Some applications of solitons

The remarkable properties of solitons have been used to explain many unexplained phenomena, such as the Fermi-Pasta-Ulam paradox [147], and to develop new theories in various scientific and technological fields [145, 148, 149]. For example, in elastic tubes, solitons result from a balance between the nonlinearity caused by the hydrodynamics of blood flow and the dispersion related to the elasticity of the artery walls [150]. In neuroscience, a recently developed model suggests that signals in neurons propagate as pulsed solitons along the cell membrane [151, 152]. This model challenges the widely accepted Hodgkin-Huxley model [153], which describes signal transmission as action potentials. In hydrodynamics, tsunamis and rogue waves are well-known manifestations of solitons. Solitons also play a crucial role in telecommunications, particularly in data transmission. In 1998, a team from the Center for Research and Development at France Télécom successfully combined solitons of different wavelengths to achieve a transmission rate exceeding one terabyte per second.

1.11 Conclusion

In this chapter, we have explored the localization and composition of MTs, fundamental elements of the cellular cytoskeleton. We have examined their complex structure and dynamics, essential for numerous cellular processes. Additionally, we have discussed the proteins associated with MTs, which regulate their formation and function, emphasizing their importance in various cellular functions such as cell division, intracellular transport, and cell shape. By highlighting the implications of MTs in cellular functions, we underscored their crucial role in maintaining cellular integrity and proper cell function. Furthermore, we have explored abnormalities related to MT dysfunctions, which can lead to significant pathological consequences, particularly in neurodegenerative diseases and developmental disorders. In summary, a thorough understanding of MTs and their molecular regulation is essential for deciphering the underlying mechanisms of many normal and pathological cellular functions. This opens the door to new research avenues and potential therapeutic approaches for diseases associated with MT dysfunctions. As for solitons, they are fascinating phenomena occurring in various physical systems and have significant applications in many fields of science and technology. To address these questions rigorously, we will now turn to Chapter Two, where we will examine the various analytical and numerical approaches used to study MTs and their functional implications in cells.

CHAPTER 2

METHODOLOGY OF INVESTIGATIONS

Contents

2.1 Introduction

In the previous chapter, we explored the localization and composition of MTs, as well as the associated proteins that regulate their formation and function, highlighting their importance for various cellular processes. We also shed light on the implications of MTs in cellular functions and the dysfunctions associated with neurodegenerative diseases and developmental disorders. MTs provide an ideal environment for studying a range of biological, mechanical and architectural aspects, with a particular focus on exploring solitons, which are seen as key elements in many applications [153, 154]. The dynamic formation of solitonic structures within MTs is made possible by the phenomenon of modulation instability [24, 155–163]. The characteristics of solitons can be examined using exact analytical solutions of the complex Ginzburg-Landau equation. The search for such exact solutions is of paramount importance. The validation of these solutions by numerical integration further emphasises the value of an integrated approach combining analytical and numerical analyses to study the dynamic properties of MTs. This chapter provides a review of mathematical models of MTs, as well as analytical methods such as the RWA [164], the modulation instability phenomenon (MI) [164], the direct ansatz method and the bilinear Hirota method (HBM). Finally, the Runge-Kutta 4 method will be presented as a numerical approach to complete this study of MTs.

2.2 Several models in MTs

Essential components of the cellular cytoskeleton, MTs play a central role in numerous crucial biological processes, including cell division, intracellular transport, and cell motility. Their dynamic and complex structure has captured researchers' attention for many decades, giving rise to a vast and flourishing field of study aimed at elucidating their physical and biological properties. In this regard, several mathematical models have been developed to describe and predict the behavior of MTs. These models encompass a variety of approaches, levels of sophistication, and application domains, with some focusing on molecular dynamics and tubulin polymerization, while others delve into mechanical properties and the emergence of solitonic structures within these tubular polymers. In this section, we will briefly discuss some of the key mathematical models of MTs, highlighting their contribution to our current understanding of these vital structures in cell biology.

2.2.1 Sataric *et al.* model

The longitudinal model, introduced by Sataric et *al*. in 1993 [165], presents an innovative framework for understanding the nonlinear dynamics of MTs. In this model, Sataric et *al*. postulate the existence of a single degree of freedom, denoted by U_n, governing the movement of dimers within the PF. This model highlights the nonlinear dynamics of dimeric dipoles in a MT PF using the well-known double-well potential model. This approach has proven extremely useful in the physics of bistable molecular systems [166]. Its successes in other related areas, such as in describing dipolar excitations in ferroelectrics, are widely recognized [167]. The essential argument in favor of introducing the double-well model stems from the fact that the longitudinal projection of the dimer displacement interacts with the rest of the lattice through a mean-field force due to an anharmonic crystal potential. Here, U_n represents the projection of the dimer apex onto the direction of the PF. The model assumes that the inter-dimer bonds within the same PF are stronger than the bonds between neighboring PFs.

The kinetic energy associated with the longitudinal displacements of constituent dimers is given by the expression:

$$E_C = \frac{m}{2}\dot{U}_n^2, \tag{2.1}$$

where m represents the dimer's mass, and $\dot{U}_n$ is the first derivative with respect to time t of the longitudinal displacement. The potential energy of interaction between dimers belonging to the same PF is:

$$E_I = \frac{K}{2}(U_{n+1} - U_n)^2. \tag{2.2}$$

K denotes the intra-dimer stiffness parameter, and n signifies the position of the considered dimer within the PF. The overall effect of the surrounding dipoles on a chosen site n can be qualitatively described by the double-well quartic potential [165]

$$V(U_n) = -\frac{1}{2}A\,U_n^2 + \frac{1}{4}B\,U_n^4. \tag{2.3}$$

Thus, its representation is given by the Fig. (2.1). $B > 0$ is the model parameter that is independent of temperature, while A is generally a linear function of temperature that may change its sign at a temperature T_c, i.e., $A = \alpha(T - T_c)$, with $\alpha > 0$ below T_c. These values of A and B have been evaluated in [168]. Consequently, we assume that, together with the polarized water surrounding it, an MT generates a nearly uniform intrinsic electric field parallel to its axis. Therefore, the additional potential energy due to this electric field and associated with each dipole is

$$V_{el} = -C\,U_n, \text{ with } C = q\,E. \tag{2.4}$$

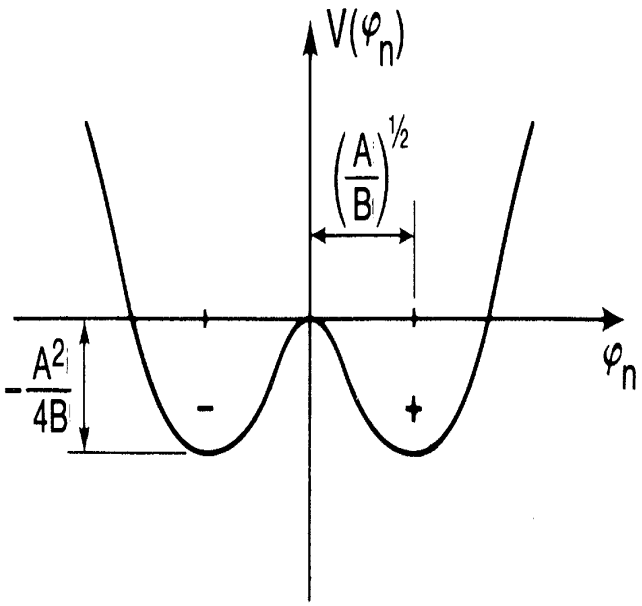

Figure 2.1: *Double-well potential located at the site defined by equation (2.3) [165].*

q denotes the effective mobile charge of a single dimer, and E is the magnitude of the intrinsic electric fields. The association of these different Eqs. (2.1)-(2.4) resulted in the following Hamiltonian:

$$H = \sum_n \left[\frac{m}{2} \dot{U}_n^2 + \frac{K}{2} (U_{n+1} - U_n)^2 - \frac{1}{2} A U_n^2 + \frac{1}{4} B U_n^4 - C U_n \right]. \tag{2.5}$$

This model showed that kink-type excitations occur as a result of GTP hydrolysis, and that an intrinsic electrical force can cause them to propagate along an MT [165, 169, 170].

2.2.2 U-Model

The longitudinal model of MTs, established in 1993 by Satarić and his colleagues [165], describes dimer movements in terms of angular oscillations, with a longitudinal coordinate U symbolizing the displacement of the dimer apex on the PF. Another similar model, named the Z model [171], also presupposes longitudinal dimer displacements. The main divergence between the two lies in their modeling methodology, with the Z model offering a broader perspective by including a variety of deformation and interaction modes. Although these models generate equivalent differential equations, only the analysis of the U model will be undertaken here.

A refined and generalized version of the original nonlinear model [165] is what we refer to as the U model [169], as elucidated in the following paragraphs. Both models assume that dimers act as electric dipoles and that the entire MT can be considered ferroelectric [165, 172]. This implies that the interaction between a single dimer and its environment can be modeled by a potential W [165, 167]. These assumptions lead to the development of the following Hamiltonian for the MT [165, 169, 173].

$$H_u = \sum_n \left[\frac{m}{2} \dot{U}_n^2 + \frac{K_u}{2} (U_{n+1} - U_n)^2 - \frac{1}{2} A U_n^2 + \frac{1}{4} B U_n^4 - Q E U_n \right]. \tag{2.6}$$

In Eq. (2.6), the dot denotes the first derivative with respect to time t, while the integer index n specifies the position of the considered dimer in the PF. The first term clearly corresponds to the kinetic energy of the dimer, having a mass m. Next, the second term describes the interaction between neighboring dimers belonging to the same PF in the nearest-neighbor approximation, with K_u representing an intra-dimer stiffness parameter. The next two terms describe the potential energy W mentioned earlier, with the parameters A and B requiring determination or estimation, assumed to be positive.

Finally, the last term takes into account that the dimer acts as an electric dipole within the field generated by all other dimers. Here, $Q > 0$ represents the dipole excess charge, and $E > 0$ corresponds to the internal electric field. The set of the last three terms can be interpreted as forming an asymmetric W potential. By introducing generalized coordinates q_n and p_n, defined as $q_n = U_n$ and $P_n = m\frac{dU_n}{dt}$, and applying the Hamilton-Jacobi formalism, the obtained discrete differential equation is as follows:

$$m\ddot{U}_n = K_u (U_{n+1} + U_{n-1} - 2U_n) + A U_n - B U_n^3 + Q E - \gamma \dot{U}_n. \tag{2.7}$$

The last term represents a viscosity force, where γ denotes the viscosity coefficient [165]. Thus, the nonlinear dynamics of MTs are described by Eq. (2.7). It is evident that the nonlinearity arises from the fourth-degree term in the W potential.

The Sataric model and the U-Model are two different approaches to studying MT dynamics, each with distinct assumptions and applications:

- The Sataric model focuses on the dynamics of MTs by using differential equations to describe the processes of polymerization and depolymerization. This model accounts for the interactions between tubulin dimers and the effects of MAPs. It is primarily used to understand the fundamental mechanisms of MT dynamics under specific biological conditions.

- The U-Model, on the other hand, is a more recent approach that incorporates nonlinear effects and complex interactions between MTs and their environment. This

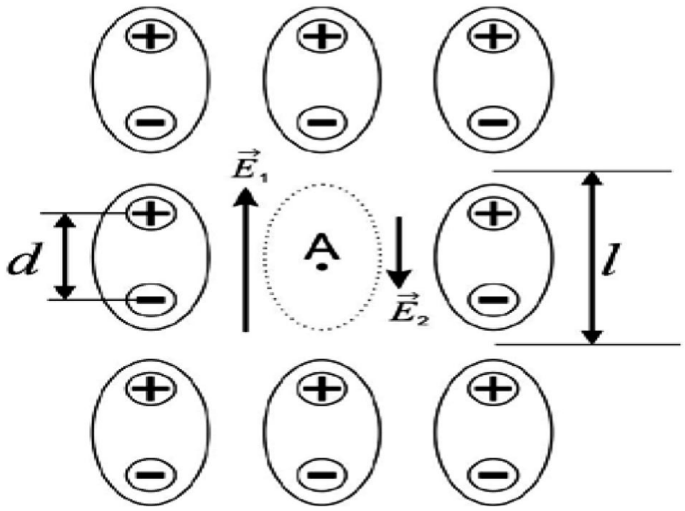

Figure 2.2: *Illustrative scheme of the radial model. A segment of three PFs (PF1, PF2, and PF3, from left to right) [15].*

model is often employed to study the effects of solvents and other external factors on MT dynamics. It provides insights into how MTs respond to varying conditions and how these responses influence their stability and function.

2.2.3 Radial model

Figure (2.2) provides a simplified representation, particularly relevant to the model examined in this study. The central dimer affiliated with PF2 is sensitive to electric fields emitted by neighboring dimers. Notably, the field $\overrightarrow{E_1}$ emanates from dimers within the same PF2, while $\overrightarrow{E_2}$ represents the longitudinal component of the field from dimers of adjacent PFs, namely PF1 and PF3. Detailed calculations of these fields are listed in Ref. [171]. It is noteworthy that the positions of PF1 and PF3 in Fig. 2.2 require adjustment upwards and downwards, respectively, to accurately reflect the real structure of the MT, including its intrinsic helicity. These adjustments induce an orthogonal component $\overrightarrow{E_{2p}}$ to $\overrightarrow{E_1}$. However, although present, this component $\overrightarrow{E_{2p}}$ is disregarded in the current model, deemed to have no effect on the degree of freedom in question. The tubulin dimers within the PFs can undergo conformational changes that propagate along individual PFs or small groups of PFs. The bending of PFs during MT disassembly stems from these cooperative conformations [174]. Studies have demonstrated that a maximal relative displacement of 32° between two neighboring dimers can be reached before disturbing the PF. Additionally, the angular displacements of monomers within a single dimer can reach 13° [175]. These observations prompted Zdravković *et al.* [15] to

limit their modeling to the angular conformations of dimers in the radial directions of the dipole electric field line, which is the sum of $\overrightarrow{E_1}$ and $\overrightarrow{E_2}$. Thus, they assume that the entire dimer undergoes rotation, noting the associated angular displacement φ. However, the exact reference around which this rotation occurs remains unknown at this stage.

The dipole potential energy of a single dimer is formulated as follows:

$$U(\varphi) = -\vec{p} \cdot \vec{E} = -q\, d\, E \cos\varphi. \tag{2.8}$$

In this formulation, q denotes the excess charge of the monomer in the dipole. They consider the conditions $p > 0$ and $E > 0$ to be met. Using the nearest-neighbor approximation, we obtain the expression of the Hamiltonian of a PF in a discrete version:

$$H = \sum_n \left[\frac{I}{2} \dot{\varphi}_n^2 + \frac{K}{2} \left(\varphi_{n+1} - \varphi_n\right)^2 - pE \cos\varphi_n \right], \tag{2.9}$$

which, after a series expansion of the cosine function, becomes

$$H = \sum_n \left[\frac{I}{2} \dot{\varphi}_n^2 + \frac{K}{2} \left(\varphi_{n+1} - \varphi_n\right)^2 - pE + pE \left(\frac{\varphi_n^2}{2} - \frac{\varphi_n^4}{24} \right) \right]. \tag{2.10}$$

The dot indicates a first derivative with respect to time t, I denotes the moment of inertia of the single dimer, and K represents the inter-dimer binding interaction within the same PF, provided by the link between corresponding protruding loops [15]. The integer n determines the position of the dimer in the PF. In Eqs. (2.9) and (2.10), the first term represents the kinetic energy of the dimer, while the second is a potential energy of the chemical interaction between dimers belonging to the same PF. Conversely, the chemical interaction between neighboring dimers belonging to different PFs is markedly less significant, and the corresponding energy is safely neglected here [31, 176]. This does not imply, however, that the influence of neighboring PFs is entirely disregarded, as the field $\overrightarrow{E_2}$ precisely originates from these PFs, as previously explained. This point is crucial as the magnitude of the electric moment $|\vec{p}|$ and the length of the MT result in a fairly high value for $\overrightarrow{E_1}$. Consequently, the field $\overrightarrow{E_2}$, directed opposite to $\overrightarrow{E_1}$, effectively reduces the value of the total intrinsic field $\vec{E}$. By using the generalized coordinates $q_n = \varphi_n$ and the angular momentum $p_n = I\dot{\varphi}_n$, and assuming the validity of a continuous approximation $\varphi_n(t) \to \varphi(x,t)$, the authors proceeded with a series expansion:

$$\varphi_{n\pm1} \to \varphi \pm \frac{\partial \varphi}{\partial x} l + \frac{1}{2} \frac{\partial^2 \varphi}{\partial x^2} l^2. \tag{2.11}$$

By cleverly introducing a viscosity moment $M_v = -\Gamma\dot{\varphi}$, where Γ denotes the viscosity coefficient, into the equation of motion, they arrived, according to the Hamilton-Jacobi

equations $\varphi = \dfrac{\partial H}{\partial P}, \dot{P} = -\dfrac{\partial H}{\partial \varphi}$, with $P = m\,\dot{\varphi}$, at the following equation:

$$I\,\frac{\partial^2 \varphi}{\partial t^2} - K\,l^2\,\frac{\partial^2 \varphi}{\partial x^2} + pE\,\varphi - \frac{pE}{6}\,\varphi^3 + \Gamma\,\frac{\partial \varphi}{\partial t} = 0. \tag{2.12}$$

It is widely recognized that an ordinary differential equation can be derived from Eq. (2.12) by introducing a unified coordinate ξ defined in the customary manner as:

$$\varphi(x,t) = \varphi(\xi) \equiv \varphi(k\,x - \omega t), \tag{2.13}$$

where k and ω are constants, representing the wave number and frequency respectively. Consequently, through the amalgamation of Eq. (2.13) with a suitable transformation

$$\varphi = \psi\,\sqrt{6}, \tag{2.14}$$

we readily convert Eq. (2.12) into the subsequent ODE

$$\alpha\,\frac{d^2\psi}{d\,\xi^2} - \rho\,\frac{d\,\psi}{d\,\xi} + \psi - \psi^3 = 0, \tag{2.15}$$

where the two dimensionless parameters α and ρ underscore the physics of the relevant model as delineated below

$$\alpha = \frac{I\,\omega^2 - K\,l^2\,k^2}{pE}, \rho = \frac{\omega\,\Lambda}{pE}. \tag{2.16}$$

The parameter α symbolizes the degree of interplay between the rotational kinetic energy of the tubulin dimer and its potential energy arising from associated chemical bonds, further moderated by the intensity of the intrinsic electric field $\vec{E}$. The pliability of chemical bonds and the notable surge in the dimer's kinetic energy [177], induced by the liberation of 0.25 eV of energy during GTP hydrolysis, necessitate that the parameter α be positive. This implies a dominance of kinetic energy, albeit the presence of additional dipolar potential suffices to forestall the disintegration of the PF when such excitation occurs distantly from MT ends. This observation underscores the pivotal role played by dipolar potential energy in stabilizing PFs and the MT structure itself, thereby sustaining polymerization. Subsequently, we presume ρ to be known, aiming to ascertain the critical parameter α.

2.2.4 Model by Priya *et al.* (2019)

In conceptualizing this model, Priya *et al.* [178] investigated neuronal MT networks, where protein pairs induce radial and longitudinal oscillations, thus creating a complexity of six degrees of freedom. In their various models, they chose to restrict each protein

pair to a single degree of freedom, based either on radial or longitudinal oscillations. To describe this phenomenon, they employed the following Hamiltonian:

$$H = \sum_n \left[\frac{m}{2}\dot{U}_n^2 + \frac{m}{2}\dot{\chi}_n^2 + \frac{K_1}{2}\left(U_{n+1} - U_n\right)^2 + \frac{K_2}{2}\left(\chi_{n+1} - \chi_n\right)^2 - \frac{A}{2}U_n^2 + \frac{B}{4}U_n^4 - pE\cos\chi_n \right]. \tag{2.17}$$

The above Hamiltonian results from the merger of the U and ϕ models. In this analysis, the first two terms describe the kinetic energy associated with longitudinal and radial displacements of the dimer with mass m. The "dot" denotes the first derivative with respect to time t. The next two terms arise from the restoring constraint forces between adjacent dimers in the PF. The inter-dimer stiffness parameters, K_1 and K_2, are assimilated into these terms for the U and ϕ models, respectively. As for the fifth and sixth terms, they depict the double-well potential of the U model. Finally, the last term describes the potential energy accumulated by the dimer in the presence of an intrinsic electric field E, aligned along the principal axis of a model in the neuronal MT system. In this expression, the symbol p represents the excess charge inside the dipole with $E, p > 0$. This demonstrates that the dimer acts as an electric dipole interacting with other present dipoles. The equations of motion can be formulated using the Hamilton-Jacobi formalism as follows:

$$\ddot{U}_n = \frac{K_1}{m}\left(U_{n+1} - 2U_n + U_{n-1}\right) + \frac{A}{m}U_n - \frac{B}{m}U_n^3, \tag{2.18a}$$

$$\ddot{\chi}_n = \frac{K_2}{m}\left(\chi_{n+1} - 2\chi_n + \chi_{n-1}\right) + \frac{pE}{m}\left(\frac{\chi_n^3}{6} - \chi_n\right). \tag{2.18b}$$

By applying the RWA, the obtained dynamical equation is:

$$i\dot{U}_n + \frac{B_1}{2}u_n + C_1|u_n|^2 u_n + A_1\left[u_{n+1} + u_{n-1} - 2u_n\right] = 0, \tag{2.19a}$$

$$i\dot{\chi}_n + \frac{B_2}{2}\chi_n + C_2|\chi_n|^2\chi_n + A_2\left[\chi_{n+1} + \chi_{n-1} - 2\chi_n\right] = 0, \tag{2.19b}$$

which is a discrete NLS equation describing the nonlinear dynamics of neuronal MTs, where the coefficients are defined as follows:

$$A_1 = \frac{K_1}{2\omega_1 m}, \quad B_1 = \frac{A}{\omega_1 m} + \omega_1, \quad C_1 = \frac{3B}{2\omega_1 m},$$
$$A_2 = \frac{K_2}{2\omega_2 m}, \quad B_2 = -\left[\frac{pE}{\omega_2 m} - \omega_2\right], \quad C_2 = \frac{pE}{4\omega_2 m}.$$

2.2.5 General model

Before introducing the general model, we briefly outline the existing U and φ models as seen in Sections (2.2.2) and (2.2.3), which describe the interactions among dimers

along the MTs. Longitudinal interactions along the MTs are significantly stronger than those between adjacent PFs, thus justifying the use of an individual PF Hamiltonian for MT dynamics. However, the influence of neighboring PFs is accounted for through the electric field. The U model exhibits a shortcoming with its final term in Eq. (2.6), where a dot product $-\vec{p}\cdot\vec{E} = -Q\,d\,E\cos\varphi$ would be more appropriate for potential energy, as in the φ model. The latter includes a potential W absent in the U model but introduces a sign problem in the terms ϕ_n^2 and ϕ_n^4. To address this, while retaining the potential W and the coordinate φ, we consider revising the U model, thus offering a more natural approach consistent with dimer radial oscillations. These considerations lead us to the following Hamiltonian:

$$H = \sum_n \left[\frac{I}{2}\dot{\varphi}_n + \frac{K}{2}\left(\varphi_{n+1} - \varphi_n\right)^2 - \frac{A}{2}\varphi_n^2 + \frac{B}{4}\varphi_n^4 - pE\ \cos\varphi_n \right], \tag{2.20}$$

where $A, B > 0$, and φ_n has the same meaning as in the φ_n model. By using the same process as in Section (2.2.3), we obtain

$$I\frac{\partial^2\varphi}{\partial t^2} - Kl^2\frac{\partial^2\varphi}{\partial t^2} - (A - pE)\varphi + \left(B - \frac{pE}{6}\right)\varphi^3 = 0. \tag{2.21}$$

2.3 Analytical and numerical methods

Methods for solving physical and mathematical problems can be classified into two main categories: analytical methods and numerical methods. Analytical methods seek exact solutions to equations using algebraic manipulations, integration, or differentiation techniques. They are often preferred when the equations are sufficiently simple or possess particular symmetries, allowing for explicit solutions. These methods provide highly accurate results but are limited to cases where the equation can be solved exactly.

In contrast, numerical methods are used when the equations are too complex for an analytical solution. They involve approximations and the use of algorithms to obtain an approximate solution. These methods are particularly useful for dealing with nonlinear systems or large-scale problems, where manual calculations become impractical. Computer simulations are often employed to implement these methods, enabling the handling of complex data and models in a short time.

2.3.1 Rotating wave approximation

The RWA, derived from the semi-discrete approximation, is a method employed in physics and applied mathematics to streamline the analysis of intricate dynamic sys-

tems [164, 179, 180]. This method focuses on truly effective interactions that is, those that transfer energy or information between systems. Rapidly oscillating terms are neglected because their average effect is zero; they do not contribute to the observable physical behavior of the system.

The merits of this method lie in its efficacy to simplify the analytical resolution of equations while retaining crucial aspects of the studied phenomenon. It facilitates the derivation of more accessible solutions, providing clearer insights into the system's behavior under specific conditions.

To illustrate the method, let's use network models as an example. One such model is the Klein-Gordon chain equation, which was studied by Kivshar et *al*. [164]. This equation is:

$$\ddot{U}_n = K(U_{n+1} - 2U_n + U_{n-1}) - \omega_0^2 U_n + \beta U_n^3. \tag{2.22}$$

In this context, K is emblematic of a consistent couple, ω_0 characterizes the frequency of subtle on-site vibrations within the potential landscape of the substrate, and β assumes the role of the anharmonicity parameter governing the potential dynamics. Through the application of a linear approximation to the chain, the introduction of the ansatz $U_n(t) = \propto \exp i(q\,n - \omega\,t)$ into Eq. (2.22) yields the linear dispersion relation:

$$\omega^2 = \omega_0^2 + 4K\sin^2(q/2). \tag{2.23}$$

In this context, where ω embodies the frequency and q represents the wave number, the grid spacing has been meticulously established at unity. As illuminated by Eq. (2.23), the linear spectrum not only reveals a conspicuous forbidden band denoted as ω_0, but also finds itself circumscribed by the cutoff frequency $\omega_{max}^2 = \omega_0^2 + 4K$, an outcome stemming from the inherent discretization.

In the pursuit of uncovering the gradual modulation of a carrier wave nestled within the linear frequency band, we substitute the trial solution into Eq. (2.22):

$$U_n(t) = \phi_n(t)e^{-i\,\omega_0\,t} + \phi_n(t)^* e^{i\,\omega_0\,t}. \tag{2.24}$$

In this scenario, where $\phi(n)$ is presumed to undergo a gradual variation over time with respect to the principal oscillation at the frequency ω_0, specifically, $\dot{\phi_n} \ll \omega_0\,\phi_n$, we retain only the terms proportional to $\exp(\pm\,i\,\omega_0\,t)$, resulting in the derivation of a discrete NLS-type equation for the intricate complex function $\phi_n(t)$:

$$2\,i\,\omega_0\,\dot{\phi}_n + K(\phi_{n+1} - 2\,\phi_n + \phi_{n-1}) + 3\,\beta\,|\phi_n|^2\phi_n = 0. \tag{2.25}$$

The assumption of the gradual variation in ϕ_n and the neglect of higher-order harmonics in deriving Eq. (2.25) presuppose that the frequency of the forbidden band, denoted

as ω_0, markedly surpasses other frequencies within the system manifested through $\omega_0^2 \gg 4K$ and $\omega_0^2 \gg \beta\phi_0^2$, where ϕ_0 represents the amplitude of the wave. The former condition holds true in a weakly dispersive system, wherein ω_{max} closely approximates ω_0, while the latter signifies a state of diminished nonlinearity. These prerequisites are conventional for deriving the NLS equation; however, within the lattice framework, the condition $\omega_0^2 \gg 4K$ further suggests the strong impact of discretization effects, highlighting the importance of the discrete version of the NLS equation over its continuous form.

2.3.2 Modulational instability phenomenon

Modulational instability is a phenomenon in which a periodic disturbance in a nonlinear dynamical system becomes unstable and evolves into more complex spatial or temporal structures. This instability occurs when nonlinear effects are strong enough to selectively amplify certain components of the periodic disturbance, leading to spatial or temporal modulation of the disturbance's amplitude or phase. Its presence is evident in various domains of physics, including plasma physics [181], nonlinear optics [182], nonlinear electrical transmission lines [183], and biological systems [184–188]. This instability serves as a vector through which localized patterns, such as solitons, are formed, which have been widely studied recently. Its activation leads to self-induced modulation, observable in both continuous and discrete contexts. For instance, in optical fibers, it induces the breakup of a continuous wave into ultrashort pulses, experimentally demonstrated [181, 189]. This modulation plays a crucial role in fluid dynamics [190, 191] and might even be involved in the formation of nonlinear excitations in discrete systems like hydrogen-bonded crystals or DNA molecules [192]. Understanding this phenomenon often requires an appropriate microscopic approach, such as the NLS equation, especially in coupled systems, to describe wave evolution.

2.3.2.1 Methodology of modulational instability phenomenon

To apply this method, we revisit Eq. (2.25) mentioned in reference [164], where n denotes different sites and t represents time in the moving frame, while U_n represents the wave envelope. This approach starts with the assumption that Eq. (2.25) admits a plane wave solution that can be expressed as follows:

$$\phi_n(t) = \phi_0\, e^{i\theta_n}, \text{where } \theta_n = q\, n - \Delta\omega\, t. \tag{2.26}$$

Here, q, ϕ_0, and $\Delta\omega$ represent the wave number, the actual amplitude of the considered wave, and the angular frequency, respectively. By substituting Eq. (2.26) into Eq. (2.25), we deduce a nonlinear dispersion relation in terms of q and $\Delta\omega$:

$$2\omega_0\Delta\omega = 4K\sin^2(q/2) - 3\beta\phi_0^2. \tag{2.27}$$

The linear stability analysis of solutions (2.26) and (2.27) can be undertaken by seeking a solution of the form:

$$\begin{aligned} F_n(t) &= (\phi_0 + b_n)e^{i\theta_n(t)+i\psi_n(t)} \\ &= (\phi_0 + b_n)(1+i\psi_n)e^{i\theta_n(t)} \\ &= (\phi_0 + i\phi_0\psi_n + b_n)e^{i\theta_n(t)}, \end{aligned} \tag{2.28}$$

where $|\psi_n(t)| \ll |\theta_n(t)|$. Here, $b_n = b_n(t)$ and $\psi_n = \psi_n(t)$ represent small perturbations in amplitude and phase, assumed to be negligible compared to the carrier wave parameters. Substituting Eq. (2.28) into Eq. (2.25), we obtain two linear equations describing the evolution of these two types of perturbations:

$$2\omega_0\dot{b}_n + K\left[(b_{n+1} - b_{n-1})\sin q + \phi_0\left(\psi_{n+1} + \psi_{n-1} - 2\psi_n\right)\cos q\right] = 0 \tag{2.29a}$$

$$\begin{aligned} &-2\omega_0\phi_0\dot{\psi}_n + K\left[(b_{n+1} + b_{n-1} - 2b_n)\cos q - \phi_0\left(\psi_{n+1} - \psi_{n-1}\right)\sin q\right] \\ &+ 6\beta\phi_0^2 b_n = 0. \end{aligned} \tag{2.29b}$$

The solutions of Eqs. (2.29) are assumed to take the following form:

$$\begin{bmatrix} b_n(t) \\ \psi_n(t) \end{bmatrix} = \begin{bmatrix} b_1 & b_1 \\ \psi_1 & \psi_1 \end{bmatrix} \begin{bmatrix} \exp(i(Q\,n + \Omega\,t)) \\ \exp(-i(Q\,n + \Omega^*\,t)) \end{bmatrix}, \tag{2.30}$$

where b_1 and ψ_1 are real constants, and Q and Ω represent the wave number and frequency of the perturbation, respectively. The asterisk (*) denotes the complex conjugate of a variable. By substituting Eq. (2.30) into Eq. (2.29) and linearizing around the perturbed plane waves, this leads to the dispersion relation:

$$\begin{aligned} (\omega_0\Omega - K\sin Q\sin q)^2 &= K\sin^2(Q/2)\cos q \\ &\times \left[4K\sin^2(Q/2)\cos q - 6\beta\phi_0^2\right] \end{aligned} \tag{2.31}$$

Equation (2.31) determines the stability condition of a plane wave with wave number q in the lattice. An instability region appears only if $\beta\cos q > 0$. For a given q, for instance, $q < \pi/2$, a plane wave will be unstable to any modulation provided that:

$$\phi_0^2 > \phi_{0,cr}^2 = 2K/3\beta, \tag{2.32}$$

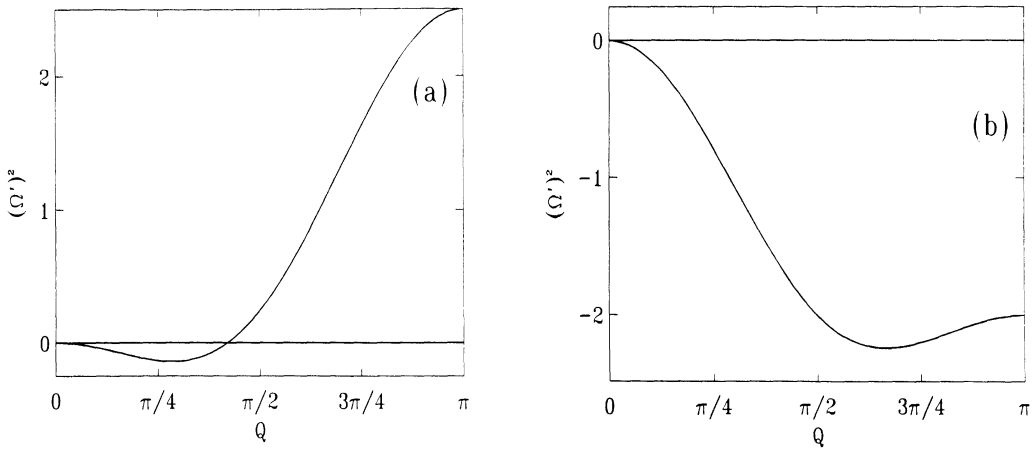

Figure 2.3: *Variation of Q as a function of $\Omega'^2 = (\omega_0\Omega - K\sin Q\sin q)^2$, for modulation waves, for $q = 0$ and $\beta > 0$, when the wave amplitude exceeds the critical value $\phi_{0,cr}$: (a) $\phi_0^2 < \phi_{0,cr}^2$ and (b) $\phi_0^2 > \phi_{0,cr}^2$ [164].*

where $\phi_{0,cr}$ represents the critical amplitude of the wave. Equation (2.32) directly follows from the fact that, in a lattice, the wave number is bounded by π. Fig. 2.3(a, b) illustrate the modulation instability regions in the case where $\beta > 0$. One of the main effects of MI is the creation of localized pulses. This is consistent with the results presented above, indicating that, for $\beta > 0$, the region of small q is unstable. Thus, nonlinearity can induce the formation of localized modes in the gap of the linear spectrum ($\omega^2 < \omega_0^2$). Such a localized mode can be obtained from discrete NLS Eq. (2.25) following the method of references [193–195].

2.3.3 Direct ansatz method

The variational method is a technique used primarily in theoretical physics and mathematics to find approximate solutions to complex equations, particularly when it is difficult to obtain exact solutions. It is based on the idea that certain physical quantities, such as the energy of a system, can be expressed in the form of functionals depending on unknown functions. These functions can be approximated by an ansatz (initial proposition) and optimized by minimizing this functional.

2.3.4 Principle of the direct ansatz method

The key idea is to formulate the problem in terms of a functional $F[\psi]$, a function of functions, which represents an important physical quantity, such as energy, that we

wish to minimize. We seek a function ψ that minimizes this functional. The method generally proceeds in several steps:

1. Definition of the ansatz: An approximate solution is proposed in the form of a function $\psi(x, \alpha)$, called the ansatz, which depends on one or more free parameters α. The ansatz is chosen based on the nature of the problem, often taking into account the symmetry or expected structure of the solution.

2. Substitution of the ansatz into the functional: The ansatz is then inserted into the functional $F[\psi]$ to obtain an expression that depends on the free parameters α. For example, if the functional is the energy, we express this energy as a function of α.

3. Minimization of the functional: We minimize the functional with respect to the parameters α. This amounts to solving the equation $\frac{F(\psi)}{d\alpha} = 0$, which gives the optimal values of the parameters α.

4. Obtaining the approximate solution: After finding the optimal parameters, they are reintroduced into the ansatz to obtain an approximate solution to the original equation.

2.3.4.1 Advantages of the direct ansatz method

- Applicability to complex systems: It allows dealing with problems where exact analytical solutions are impossible to obtain. Even for strongly nonlinear systems or quantum many-body systems, the variational method provides very useful approximate results.

- Flexibility of the ansatz: The ansatz can be adjusted according to prior knowledge of the system, such as symmetries or boundary behaviors. This allows capturing essential aspects of the system, even if the exact solution is unattainable.

- Physically significant results: By minimizing physical quantities such as energy, the method ensures that the solutions obtained have physical meaning, as they respect fundamental principles of dynamics or conservation.

2.3.4.2 Disadvantages of the direct ansatz method

- Dependence on the choice of ansatz: The accuracy of the solution heavily depends on the choice of ansatz. A poor ansatz can give results that are far from the exact solution. Thus, this method requires some physical or mathematical intuition to choose an appropriate ansatz.

- Approximations: The variational method provides approximate, not exact, solutions. These approximations may be insufficient in cases where high precision is required.
- Complexity of minimization: In some cases, minimizing the functional with respect to the parameters can become mathematically complicated, especially if the ansatz contains many parameters. There may also be multiple local minima that complicate the search for the global minimum.

The direct ansatz method is a powerful and flexible approach, ideal for obtaining approximate solutions in complex problems where analytical methods fail. It is particularly useful in theoretical physics, for example in quantum mechanics, in the study of many-body systems or nonlinear systems. However, it strongly relies on the judicious choice of the ansatz and requires optimization skills to efficiently minimize the functionals.

2.3.5 Hirota bilinear method (HBM)

The bilinear method by Hirota provides a compelling framework for determining localized structures propagating in nonlinear systems. Its principle relies on simplifying nonlinear systems using an appropriate transformation, favoring an algebraic rather than an analytical approach. This characteristic makes it a valuable tool in solving nonlinear equations, offering exact solutions with notable efficiency. It stands out with its innovative approach, using a specially tailored formulation to obtain exact solutions. Its ease of use and ability to generate new progressive wave solutions make it a unique method, combining precision, efficiency, and ease of application to solve complex problems in science and engineering.

The HBM offers an effective approach to identifying localized structures propagating in nonlinear systems. Its principles are based on the idea that any nonlinear system can be simplified through an appropriate transformation. Consider the model below to be solved:

$$G\left(U, \frac{\partial U}{\partial t}, \frac{\partial U}{\partial x}, \frac{\partial^2 U}{\partial x \partial t}, \frac{\partial^2 U}{\partial t^2}, \frac{\partial^2 U}{\partial x^2}, \frac{\partial^3 U}{\partial t^2 \partial x}, \frac{\partial^3 U}{\partial t \partial x^2}, \cdots\right) = 0. \tag{2.33}$$

The bilinearization of Eq. (2.33) requires representing $U(x,t)$ in a specific form, determined by the nature of the equation. For example, if Eq. (2.33) is the nonlinear Schrödinger equation, then $U(x,t)$) is defined as

$$U(x,t) = \frac{H(x,t)}{F^{1+i\delta_i}(x,t)}. \tag{2.34}$$

If Eq. (2.33) belongs to the KdV class, then $U(x,t) = \dfrac{\partial^2 F}{\partial x^2}$. In all cases, $H(x,t)$ is a complex function, while $F(x,t)$ and δ_i are real. For more details, the reader can refer to [196–203]. Once the correct form of $U(x,t)$ is determined and inserted into Eq. (2.33), the bilinear operators can be applied:

$$D^m_{x,\alpha} F(x)\cdot H(x) = \left(\frac{\partial}{\partial x_1} - \alpha\frac{\partial}{\partial x_2}\right)^m F(x_1)G(x_2)|_{x_1=x_2=x}, m \in \mathbb{N}, \tag{2.35}$$

can be applied. Then, Eq. (2.33) is factorized into a polynomial form, as follows:

$$P(D_t, D_x, D_x\cdot D_t, D_{xx}, \cdots)F\cdot F = 0. \tag{2.36}$$

Eq. (2.36) represents the generic class of bilinear equations derived from Eq. (2.33). The solutions to Eq. (2.36) are obtained by expanding the function $F(x,t)$ as follows:

$$F(x,t) = f_0 + \epsilon f_1(x,t) + \epsilon^2 f_2(x,t) + \epsilon^3 f_3(x,t) + \epsilon^4 f_4(x,t) + \cdots, \text{ where } f_0 = \text{ constant.} \tag{2.37}$$

The first-order solution of Eq. (2.36) is obtained by truncating the expansion of Eq. (2.37) at the first order. Thus, Eq. (2.36) becomes:

$$P(D_x, D_t, D_x\cdot D_t, D_x\ldots)\left[f_0\cdot f_0 + \epsilon(f_0\cdot f_1 + f_1\cdot f_0) + \epsilon^2(f_1\cdot f_1)\right] = 0 \tag{2.38}$$

Eq. (2.38) is solved recursively at each order of ϵ. The first and second orders of ϵ yield:

$$\epsilon : P\left(\frac{\partial}{\partial_t}, \frac{\partial}{\partial_x}, \frac{\partial^2}{\partial x \partial_t}, \frac{\partial^2}{\partial x^2}\cdots\right), \tag{2.39a}$$

$$\epsilon^2 : P(D_x, D_t, D_x\cdot D_t, D_{xx}\cdots)f_1\cdots f_1 = 0. \tag{2.39b}$$

Eq. (2.39) is linear, so its solutions can be expressed as follows:

$$f_1(x,t) = \exp(p\,x + q\,t + p_0). \tag{2.40}$$

The constants p, q, and p_0 are determined by inserting the solution of Eq. (2.40) into Eq. (2.39b), which allows for the construction of analytical solutions to Eq. (2.33). Consider the following equation, to which we will apply Hirota's method.

$$i\frac{\partial\psi}{\partial t} + \frac{\partial^2\psi}{\partial x^2} + |\psi|^2\psi = 0, \tag{2.41}$$

where $\psi = \psi(x,t)$ is a complex function representing the wave, and x, t are the position and time variables, respectively.

2. Hirota's Bilinear Transformation:

The first step in the bilinear method is to transform the complex wave function $\psi(x,t)$ into new functions through Hirota's bilinear transformation. We express $\psi(x,t)$ in the form:

$$\psi(x,t) = \frac{g(x,t)}{f(x,t)} \tag{2.42}$$

where $g(x,t)$ and $f(x,t)$ are functions to be determined.

1. Substitution into the Nonlinear Schrödinger Equation:
   Substitute $\psi(x,t)$ into the original equation:

$$i\frac{\partial}{\partial t}\left(\frac{g}{f}\right) + \frac{\partial^2}{\partial x^2}\left(\frac{g}{f}\right) + \left(\frac{|g|^2}{|f|^2}\right)\frac{g}{f} = 0 \tag{2.43}$$

   We use the product and quotient rules of differentiation to expand this equation.

2. Bilinear Equations:
   The objective is to convert this equation into bilinear forms (i.e., in terms of products of differential operators acting on the functions $g(x,t)$ and $f(x,t)$).

   We introduce Hirota's differential operators. The bilinear operator D for two functions $a(x,t)$ and $b(x,t)$ is defined as:

$$D_x^n D_t^m (a \cdot b) = \left(\frac{\partial}{\partial x} - \frac{\partial}{\partial x'}\right)^n \left(\frac{\partial}{\partial t} - \frac{\partial}{\partial t'}\right)^m a(x,t)b(x',t')\Big|_{x=x',t=t'} \tag{2.44}$$

   The nonlinear Schrödinger equation is rewritten in bilinear form after this transformation. The two main bilinear equations will take the form:

$$(D_t + D_x^2)g \cdot f = 0 \tag{2.45}$$

$$D_x^2 f \cdot f = 2g \cdot g^* \tag{2.46}$$

   where g^* represents the complex conjugate of g. These bilinear equations must be solved to determine the functions $g(x,t)$ and $f(x,t)$.

3. One-Soliton Solution (Basic Form):
   We seek a one-soliton solution. Let us try the following solution for $g(x,t)$ and $f(x,t)$:

$$g(x,t) = e^{\eta(x,t)} \tag{2.47}$$

$$f(x,t) = 1 + e^{\zeta(x,t)} \tag{2.48}$$

where $\eta(x,t)$ and $\zeta(x,t)$ are linear functions to be determined in terms of x and t. For a one-soliton solution, we assume:

$$\eta(x,t) = kx - \omega t + \eta_0 \tag{2.49}$$

$$\zeta(x,t) = 2(kx - \omega t) \tag{2.50}$$

with k and ω being the wave number and frequency, respectively, and η_0 a constant.

4. Substitution into the Bilinear Equations Substitute these expressions into the bilinear equations and find the values of k and ω by solving the resulting equations. After substitution and simplification, we find a relationship between k and ω, which describes the speed and shape of the soliton.

5. Final Solution: By reinserting the solutions $g(x,t)$ and $f(x,t)$ into the expression for $\psi(x,t)$, the one-soliton solution for the nonlinear Schrödinger equation takes the following form:

$$\psi(x,t) = \frac{e^{kx-\omega t}}{1 + e^{2(kx-\omega t)}} \tag{2.51}$$

This solution represents a soliton wave, stable and localized, which propagates without changing shape.

Hirota's bilinear method, after transforming the nonlinear Schrödinger equation, allows us to obtain exact solutions like the soliton. The details of the calculations involve deriving the bilinear equations and solving them with specific waveforms.

2.3.6 Fourth order Runge-Kutta method

Over the past six decades, scientific computation has emerged as the most versatile tool to complement theoretical frameworks and empirical studies. Numerical calculations have seamlessly integrated experimentation and theory, fundamentally transforming the nature of scientific inquiry. In this thesis, we have employed the fourth-order Runge-Kutta (RK4) method, a powerful numerical technique deeply rooted in Taylor expansion formulas. The RK methods, renowned for their efficacy in solving ordinary differential equations (ODEs), offer unparalleled precision and robustness. Specifically, the Runge-Kutta 4 method, our method of choice, boasts several undeniable advantages. It not only ensures superior accuracy compared to lower-order methods but also stands

out for its simplicity in implementation and understanding, making it widely embraced across various domains. Moreover, its robustness and stability shine through even in the face of complex problems with challenging initial conditions or highly nonlinear systems. Notably, it excels in handling stiff problems, delivering reliable performance even in scenarios with rapidly varying derivatives. Additionally, its versatility extends to a wide range of problem types, from ordinary to partial differential equations. The widespread availability of the Runge-Kutta 4 method in numerous software and numerical computing libraries further facilitates its seamless integration into research or engineering projects.

However, it is crucial to acknowledge the limitations inherent in the Runge-Kutta 4 method. Its increased complexity relative to lower-order methods may pose implementation challenges, requiring meticulous attention to detail. Furthermore, the computational overhead incurred by computing multiple derivatives at each step can significantly impact computation time, particularly for systems with numerous variables. This method may also exhibit reduced stability compared to alternative approaches, especially when confronted with stiff problems or challenging initial conditions. Sensitivity to rounding and approximation errors can further compound over extended periods, potentially leading to significant error accumulation. Moreover, the use of the Runge-Kutta 4 method may introduce spurious oscillations, particularly evident in highly nonlinear systems, and may not ensure the preservation of crucial physical quantities such as energy, introducing complexities in certain physical contexts. Nonetheless, despite these considerations, the RK4 method remains indispensable, providing a crucial intermediary step in the computation of y_{i+1}. To elucidate further, let us delve into the following definitions:

$$\frac{dy}{dt} = f(t,y), \quad y_{i+1} = y_i + \int_{t_i}^{t_{i+1}} f(t,y)dt. \tag{2.52}$$

To elucidate the philosophy behind RK methods, let's consider the second-order RK method. The initial approximation involves Taylor expanding $f(t,y)$ around the midpoint of the integration interval t_i to t_{i+1}, that is, at $t_{i+\frac{1}{2}}$, yielding:

$$\int_{t_i}^{t_{i+1}} f(t,y)dt \approx h f\left(t_{i+\frac{1}{2}}; y_{i+\frac{1}{2}}\right). \tag{2.53}$$

Consequently, we have:

$$y_{i+1} = y_i + h f\left(t_{i+\frac{1}{2}}; y_{i+\frac{1}{2}} + 0(h^3)\right). \tag{2.54}$$

However, the value of $y_{i+1/2}$ is unknown. Therefore, the next approximation involves using Euler's method to approximate $y_{i+1/2}$, resulting in:

$$y_{i+\frac{1}{2}} = y_i + \frac{h}{2}\frac{dy}{dt} = y(t_i) + \frac{h}{2}f(t_i, y_i). \tag{2.55}$$

The key distinction from previous one-step methods is the need for an intermediary step in our evaluation, specifically $t_i + \frac{1}{2} = t_{i+\frac{1}{2}}$, where we assess the derivatives f. While this entails more operations, the payoff is enhanced stability in the solution. The RK4 method, which we will employ in solving various differential equations below, follows the algorithm:

$$\begin{cases} k_1 = h\,f\,(t_i, y_i), \\ k_2 = h\,f\left(t_i + \dfrac{h}{2}, y_i + \dfrac{k_1}{2}\right), \\ k_3 = h\,f\left(t_i + \dfrac{h}{2}, y_i + \dfrac{k_2}{2}\right), \\ k_4 = h\,f\,(t_i + h, y_i + k_3), \end{cases} \tag{2.56}$$

with the final value:

$$y_{i+1} = y_i + \frac{1}{6}(k_1 + 2k_2 + 2k_3 + k_4). \tag{2.57}$$

Thus, the algorithm involves first computing k_1 with t_i, y_i, and f as inputs. Subsequently, we increment the step size by $h/2$ and calculate k_2, followed by k_3, and finally k_4. With this method, we can obtain the new value of the variable y.

2.4 Conclusion

This chapter has offered a detailed exploration of mathematical models and analytical methods. We have reviewed several specific mathematical models used in MTs, including the Sataric et *al*. model, the U-model, the radial model, the Priya et *al*. model, and the general model. Concerning analytical methods, we have explored approaches such as RWA, modulational instability phenomenon, direct ansatz method, and the HBM, all essential for developing new soliton profiles. Finally, we introduced the numerical method of Runge-Kutta 4 as an additional tool to validate analytical predictions. In the next chapter, titled Results and Discussions, we will analyze the outcomes derived

from the methods discussed here and engage in in-depth discussions regarding their implications and applications.

CHAPTER 3

RESULTS AND DISCUSSION

Contents

3.1 Introduction

This chapter builds upon our findings. While there is a wealth of research on MTs using the methods described in Chapter 2, our thesis specifically focuses on the impact of cytosol viscosity on soliton generation and localized structure formation through modulational instability processes. We also investigate the creation of new solutions capable of shedding light on the dynamics of MTs, whether in the presence or absence of cytosol viscosity.

3.2 Energy Localization in MTs with Radial Dislocation

In this section, we delve into the dynamics of MTs considering the influence of cytosol viscosity, using a model of discrete radial dislocations. Subsequently, we examine how this viscosity affects the modulational instability processes of MTs. Additionally, we develop new solution profiles to elucidate biological mechanisms involving stationary MTs.

The section is structured as follows: first, we introduce the model and derive the discrete nonlinear differential equation. Next, we analyze the influence of cytosol viscosity on the modulation instability processes of MTs. Utilizing the direct ansatz method, we search for new solution profiles and study their characteristics. We show that cytosol viscosity has no impact on the characteristics of the stationary solitonic waves obtained. Numerical simulations confirm the analytical results with a notable degree of accuracy.

3.2.1 The model

The theoretical methodology applied in this research is based on the model developed by Zdravković [15], as detailed in Section 2.2.3 of the previous chapter. In our study, the variable φ has been designated as χ_n. The Hamiltonian governing the evolutionary dynamics of a dimer within an MT-PF is expressed as follows:

$$H = \sum_n \left[\frac{I}{2} \dot{\chi_n}^2 + \frac{K}{2} \left(\chi_{n+1} - \chi_n\right)^2 + pE \left(\frac{\chi_n^2}{2} - \frac{\chi_n^4}{24} - 1 \right) \right]. \tag{3.1}$$

In Eq. (3.1), the symbol χ_n represents the angular displacement of a dimer located at position n relative to its equilibrium position. The notation $\dot{\chi_n}$ indicates a derivative with respect to time t. The moment of inertia is given by $I = \frac{1}{12} m L^2$ where the dimer's mass is $m = 1.8 \times 10^{-22}$ kg [204], and its length is $L = 8$ nm [15]. The intra-dimer stiffness parameter is denoted as $K = 0.1$ eV [24], while the electric dipole moment is represented

by $p = 337$ Debye $= 1.13 \times 10^{-27}$ Cm [205], with $pE = 0.25$ eV where E ($E = 4 \times 10^7$ V/m) denotes the intrinsic electric force. The orders of magnitude are specified in Refs. [206, 207] with $p, E > 0$.

The terms on the right-hand side of Eq. (3.1) have the following meanings:

- the first term represents kinetic energy,
- the second describes the chemical potential energy between two neighboring dimers belonging to the same PF,
- the last term corresponds to the dipole-dipole potential energy of the dimer χ_n.

Thus, the Hamiltonian (3.1) describes a conservative system. The effect of cytosol viscosity, which acts as a damping term, can be accounted for in the dynamics by introducing the viscosity torque $M_v = -\Gamma \dot{\chi_n}$, where Γ represents the viscosity coefficient [15]. Using the Hamilton-Jacobi formalism, the motion equation of the dimer can be derived as follows:

$$\ddot{\chi_n} + \varepsilon \dot{\chi_n} = \alpha \left(\chi_{n+1} - 2\chi_n + \chi_{n-1}\right) + \omega_g^2 (a \chi_n^3 - \chi_n), \tag{3.2}$$

with $\alpha = \frac{K}{I}, \omega_g^2 = \frac{pE}{I}, \varepsilon = \frac{\Gamma}{I}$, and $a = \frac{1}{6}$. Here,

- α quantifies the potential energy of chemical bonds during their rotation.
- ω_g represents the lowest cutoff frequency at which pE plays a crucial role in stabilizing PFs and the MT itself, imparting a crucial stabilizing effect to polymerization [15].

The understanding of MT dynamics in our study relies on analytical solutions of Eq. (3.2). To further explore this, we seek to solve Eq. (3.2). Our approach begins by assuming that χ_n represents a slowly modulated wave emerging from the initial nonlinear problem formulated in Eq. (3.1). This wave oscillates within the linear domain, allowing us to express it as follows:

$$\chi_n(t) = F_n(t) e^{-i\omega_g t} + F_n^*(t) e^{i\omega_g t}. \tag{3.3}$$

The functions $F_n(t)$ and $F_n(t)^*$ are considered as complex conjugates, whose temporal evolution is relatively slow compared to the main oscillation at frequency ω_g, as expressed by $\dot{\chi_n} \ll \omega_g \chi_n$ [164]. By substituting Eq. (3.3) into (3.2) and applying the RWA presented in Section 2.3.1, we derive the discrete cubic CGL equation governing the behavior of $F_n(t)$:

$$(\varepsilon - 2i\omega_g)\dot{F_n} - \alpha \left[F_{n+1} - 2F_n + F_{n-1}\right] - 3a\omega_g^2 |F_n|^2 F_n - i\varepsilon\omega_g F_n = 0, \tag{3.4}$$

which will be analyzed in the context of the MI phenomenon.

3.2.2 Modulational instability processes

The study of MT dynamics in Zdravković's radial model [15] is conducted using linear stability analysis. In this section, we focus on the MI phenomenon on the CGL Eq. (3.4), as we hypothesize its connection to Eq. (3.2). From this perspective, we first seek wave solutions to Eq. (3.4) of the form:

$$F_n(t) = \phi_0 \exp[i(q\,n - \omega_0\,t)], \tag{3.5}$$

were q, ω_0, and ϕ_0 denote an angle, angular frequency, and wave amplitude, respectively, with $\omega_0 = -\omega_g$. Substituting Eq. (3.5) into Eq. (3.4), we obtain the following nonlinear dispersion relation:

$$-\omega_0(2\,\omega_g + i\,\varepsilon) + 4\,\alpha\,\sin^2\left(\frac{q}{2}\right) - 3\,a\omega_g^2\,|\phi_0|^2 - i\,\omega_g\,\varepsilon = 0. \tag{3.6}$$

Eq. (3.6) holds if and only if $\phi_0^2 > 4$.

To assess the linear stability of the initial plane wave, we introduce small perturbations in both its amplitude and phase, assuming a solution of the form:

$$\begin{aligned} F_n(t) &= (\phi_0 + b_n)\,e^{i\,\theta_n(t) + i\,\psi_n(t)} \\ &\approx (\phi_0 + b_n)(1 + i\,\psi_n)\,e^{i\,\theta_n(t)} \\ &\approx (\phi_0 + i\,\phi_0\,\psi_n + b_n)\,e^{i\,\theta_n(t)}, \end{aligned} \tag{3.7}$$

where $\theta_n(t) = q\,n - \omega_0\,t$. Assuming that $|b_n(t)| \ll |\phi_0|$, and $|\psi_n(t)| \ll |\theta_n(t)|$ [164, 180], we substitute this expression into Eq. (3.4) and separate the real and imaginary parts, yielding:

$$\begin{aligned} \dot{b}_n &= N_1\,b_n + N_2(b_{n+1} - 2\,b_n + b_{n-1}) \\ &\quad + N_3(\psi_{n+1} - 2\,\psi_n + \psi_{n-1}) + N_4(b_{n+1} - b_{n-1}) \\ &\quad + N_5(\psi_{n+1} - \psi_{n-1}), \end{aligned} \tag{3.8a}$$

$$\begin{aligned} \dot{\psi}_n &= P_1\,b_n + P_2(b_{n+1} - 2\,b_n + b_{n-1}) \\ &\quad + P_3(\psi_{n+1} - 2\,\psi_n + \psi_{n-1}) + P_4(b_{n+1} - b_{n-1}) \\ &\quad + P_5(\psi_{n+1} - \psi_{n-1}). \end{aligned} \tag{3.8b}$$

The coefficients N_i and P_i (with $i = 1, \cdots, 8$) are expressed as follows:

$$
\begin{aligned}
N_1 &= \frac{6a\omega_g^2 \varepsilon \phi_0^2}{D},\ N_2 = \frac{\alpha \varepsilon \cos(q)}{D}, \\
N_3 &= -\frac{2\phi_0 \omega_g \alpha \cos(q)}{D},\ N_4 = -\frac{2\alpha \omega_g \sin(q)}{D}, \\
N_5 &= \frac{\alpha \varepsilon \sin(q)}{D},\ P_1 = \frac{12a\omega_g^3}{D}, \\
P_2 &= \frac{2\omega_g \alpha \cos(q)}{D\phi_0^2},\ P_3 = \frac{\alpha \varepsilon \phi_0 \cos(q)}{D\phi_0^2}, \\
P_4 &= \frac{\alpha \varepsilon \sin(q)}{D},\ P_5 = \frac{2\alpha \omega_g \sin(q)}{D\phi_0^2}.
\end{aligned} \tag{3.9}
$$

The solutions considered for Eq. (3.8) are assumed to take in the following form:

$$
\begin{bmatrix} b_n(t) \\ \psi_n(t) \end{bmatrix} = \begin{bmatrix} b_1 & b_1 \\ \psi_1 & \psi_1 \end{bmatrix} \begin{bmatrix} \exp(i(Q\,n + \Omega\,t)) \\ \exp(-i(Q\,n + \Omega^*\,t)) \end{bmatrix}, \tag{3.10}
$$

were b_1 and ψ_1 are real constants, while Q and Ω denote the wave number and the frequency of the perturbation, respectively. The asterisk (*) denotes the complex conjugate. Substituting Eq. (3.10) into Eq. (3.8) and linearizing around the perturbed plane waves lead to the following linear system:

$$
\begin{bmatrix} i\,\Omega + a_{11} & a_{12} \\ a_{21} & i\,\Omega + a_{22} \end{bmatrix} \begin{bmatrix} b_1 \\ \psi_1 \end{bmatrix} = \begin{bmatrix} 0 \\ 0 \end{bmatrix}. \tag{3.11}
$$

The coefficients are given by:

$$
\begin{aligned}
a_{11} &= 2\,i\,N_4 \sin(Q) - 4N_2 \sin^2(Q/2) + N_1, \\
a_{12} &= -4N_3 \sin^2(Q/2) + 2\,i\,N_5 \sin(Q), \\
a_{21} &= 2\,i\,P_4 \sin(Q) - 4P_2 \sin^2(Q/2) + P_1, \\
a_{22} &= -4P_3 \sin^2(Q/2) + 2\,i\,P_5 \sin(Q).
\end{aligned}
$$

For a non-trivial solution to exist, the determinant of the system (3.11) must vanish. This condition results in the formulation of a second-order polynomial dispersion relation:

$$
\Omega^2 + A_1\,\Omega + A_0 = 0. \tag{3.12}
$$

The coefficients A_1 and A_0 are given by:

$$\begin{aligned}
A_1 =& 4iN_2(\sin(Q/2))^2 + 4i(\sin(Q/2))^2 P_3 - iN_1 \\
&+ 2N_4 \sin(Q) + 2P_5 \sin(Q), \\
A_0 =& 8iN_2 \sin(Q)(\sin(Q/2))^2 P_5 - 16N_2(\sin(1/2Q))^4 P_3 \\
&- 8iN_3 \sin(Q)(\sin(Q/2))^2 P_4 + 16N_3(\sin(Q/2))^4 P2 \\
&+ 8iN_4 \sin(Q)(\sin(Q/2))^2 P_3 - 8iN_5 \sin(Q)(\sin(Q/2))^2 P_2 \\
&- 2iN_1 \sin(Q)P_5 + 4N_1(\sin(Q/2))^2 P_3 - 4N_3(\sin(Q/2))^2 P_1 \\
&+ 4N_4(\sin(Q))^2 P_5 + 2iN_5 \sin(Q)P_1 - 4N_5(\sin(Q))^2 P_4. \qquad (3.13)
\end{aligned}$$

Modulation instability arises when Ω is a complex number ($\Omega = \Omega_r + i, \Omega_i$), with a non-zero imaginary part. The system is considered unstable when $\Omega_i < 0$, and the instability growth rate is defined as $G = \text{Max}(-\Omega_i)$ ($i = 1, 2$). The modulation instability growth rate is plotted as a function of unstable wave numbers Q and the parameter ε (Fig. 3.1). In this representation, the width of the unstable mode regions increases along the axis of unstable wave numbers for low values of ε (ε being of the order of ω_g [206]). However, as ε increases, the amplitude of the instability growth rate gradually decreases until it eventually reaches zero. This suggests that while cytosol viscosity expands the range of unstable mode parameters for Q, at sufficiently high values, it suppresses instability. This finding aligns with the results of Molines et al. [27], who demonstrated that cytoplasmic viscosity plays a key role in regulating MT polymerization and depolymerization rates. Their study indicates that higher viscosity slows MT dynamics by increasing resistance to filament growth and shrinkage, which may explain the suppression of instability observed at large ε. These insights highlight the intricate interplay between mechanical constraints and biochemical regulation in shaping MT behavior within the cytoplasmic environment.

3.2.3 Analytical solutions

MI processes allow identifying parameter zones where solitary waves are likely to occur. However, certain essential characteristics of solitary waves, such as their shape, amplitude, and phase, when propagating through continuous media are not predicted by this analysis. To address this gap and obtain useful information about other types of waves that may propagate in these media, it is necessary to rely on analytical solutions. These solutions also allow for the validation of numerical results from models. Several powerful methods have been developed to solve nonlinear partial differential equations

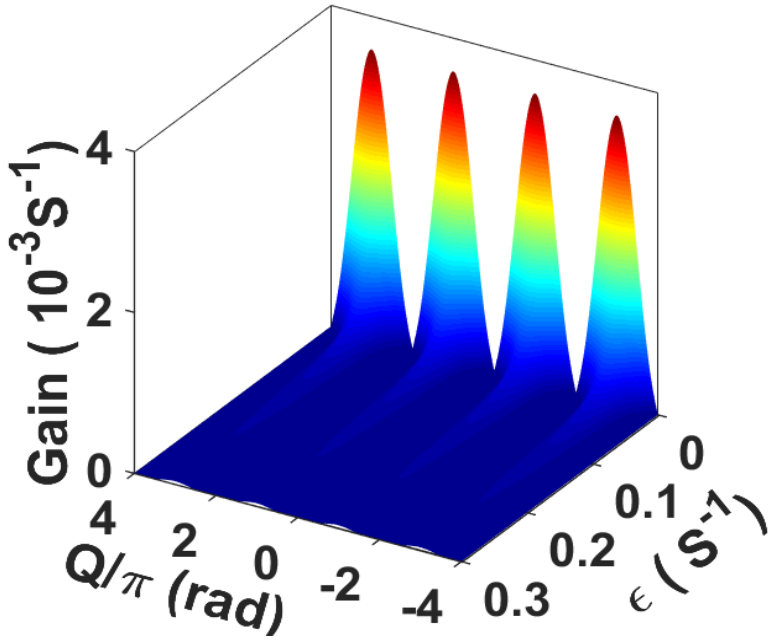

Figure 3.1: *MI growth rate versus unstable wavenumber* Q *and the* ε *parameter when* $q = 1.18$. *The presence of the cytosol viscosity stabilizes the system as it induces a decrease of the magnitude of the MI growth rate. However, by widening the unstable wavenumber region, the cytosol viscosity drives the system to instability. Parameters are:* $K = 0.1$ eV, $pE = 0.25$ eV and $\phi_0 = \sqrt{5}$.

similar to Eq. (3.2). Among these methods are the inverse scattering transform method [209], the tanh method [210], the exponential expansion method [211], the HBM [196, 199], the F-expansion method [212, 213], the (G'/G) expansion method [214], and the BDK method [215, 216]. In this study, we employ a direct approach to construct solitary wave solutions of Eq. (3.4). To achieve this, we reformulate solution (3.3) as follows:

$$h\,\chi_n(t) = h\,F_n(t)\,e^{-i\,\omega_g\,t} + h\,F_n^*(t)\,e^{i\,\omega_g\,t}, \tag{3.14}$$

with $0 \leq \chi_n(t) \leq \frac{\pi}{6}$, where h is a constant whose value will be determined later to satisfy experimental conditions [175]. We make the initial assumption that the function $F_n(t)$ and $F_n(t)^*$ vary slightly over time around the cutoff frequency. * represents the complex conjugate. This implies that $F_n(t)$ and $F_n(t)^*$ can be considered as continuous functions of space $x = n\,l$ (where $l = 80\,\text{Å}$ is the spacing between tubulin dimers [24]) and time t. These considerations suggest that the discrete functions present in Eq. (3.4) should be replaced by their continuous counterparts using appropriate Taylor series expansions. Then, the continuous form of the function $F_n(t)$ is denoted as $\varphi(x,t)$. After some algebraic manipulations, the continuous version of the discrete cubic CGL Eq. (3.4) is

obtained as follows:

$$i\,\varphi_t + P\varphi_{xx} + Q|\varphi|^2\varphi - i\,\gamma\varphi = 0. \tag{3.15}$$

The expressions for P, Q, and γ are as follows:

$$P = \begin{cases} P_r = \dfrac{2\,\alpha\, l^2\,\omega_g}{4\omega_g^2+\varepsilon^2}, \\ P_i = -\dfrac{\alpha\, l^2\,\varepsilon}{4\omega_g^2+\varepsilon^2}, \end{cases} \quad Q = \begin{cases} Q_r = \dfrac{6a_0\,\omega_g^3}{4\omega_g^2+\varepsilon^2}, \\ Q_i = -\dfrac{3a_0\,\omega_g^2\,\varepsilon}{4\omega_g^2+\varepsilon^2}, \end{cases}$$

$$\gamma = \begin{cases} \gamma_r = -\dfrac{2\,\omega_g^2\,\varepsilon}{4\omega_g^2+\varepsilon^2}, \\ \gamma_i = \dfrac{\omega_g\,\varepsilon^2}{4\omega_g^2+\varepsilon^2}, \text{ with } a_0 = a/h^2. \end{cases} \tag{3.16}$$

By applying the direct method explained in Section 2.3.3, we assume that the solution to Eq. (3.15) is:

$$\varphi(x,t) = \left[A\,sech(\beta x) + i\,B\,\tanh(\beta x)\right] e^{(i\,v^2\,t)}. \tag{3.17}$$

Subsequently inserting Eq. (3.17) into Eq. (3.15) and separating the real and imaginary parts, we obtain an overdetermined system of equations, the solutions of which are found using the symbolic computation software MAPLE 13 (see Appendix A):

$$A = \pm 2h\sqrt{2}, B = 0, v = \pm\sqrt{\omega_g}, \beta = \frac{\sqrt{2}\,\omega_g}{\sqrt{\alpha}\,l}. \tag{3.18}$$

From these results, we rewrite the solution (3.17) as:

$$\varphi(x,t) = \left[\pm 2h\sqrt{2}\,\frac{1}{\cosh(\beta x)}\right] \exp i\,(v^2\,t). \tag{3.19}$$

To retrieve the solution of the original discrete problem (3.2), we insert this solution into Eq. (3.3) with $x = n\,l$ to revert back to the discrete scenario. This corresponds to the solutions of Eq. (3.2) written as:

$$\chi_n(t) = \pm 2A\,sech(\beta n\,l). \tag{3.20}$$

The obtained solution satisfies the experimental condition stated in Eq. (3.14) provided that $h \leq \frac{\pi}{24\sqrt{2}}$. It is crucial to highlight that the solutions presented in Eq. (3.20) differ significantly from previously developed breathers solutions [15, 206, 208]. Stationary solutions, widely studied across various domains of physics [217–219], are particularly relevant in this context. Indeed, such solutions may offer valuable insights into biological processes in which MTs maintain long-term stability, such as cytoplasmic transport mediated by MAPs. This stability is essential for cellular organization since

MAPs regulate both the spatial and temporal distribution of cargo transport along MTs, ensuring efficient intracellular trafficking.

Furthermore, the width of the solution in Eq. (3.20), given by $(\beta l)^{-1} = \frac{1}{\sqrt{2}}\sqrt{\frac{K}{pE}}$, is directly influenced by the ratio between the rigidity and the electric energy of the dimer. An increase in the electric energy of the dimer leads to a decrease in the width of the solitary wave. This observation suggests that the electrical and chemical potential energies of neighboring dimers within the same PFs, along with their inertia, play a fundamental role in determining the spatial properties of solitary waves. Consequently, our solutions could serve as a theoretical framework for distinguishing MTs with varying masses and, by extension, different biophysical characteristics.

Moreover, the presence of two possible values for the parameter A leads to two distinct solution profiles: a bright solitary wave for $A > 0$ (see Fig. 3.2) and an anti-dark solitary wave for $A < 0$ (see Fig. 3.5). This variability offers a promising avenue for understanding and modeling MT behavior under different conditions. Bright solutions may correspond to localized energy transfer along MTs, potentially linked to intracellular signaling mechanisms, while anti-dark solutions might be associated with structural deformations occuring under mechanical or electrostatic stress. These finding further highlight the complex interplay between MT mechanical properties, electrical energy distribution, and biological function, shedding new light or their role in dynamic cellular processes.

3.2.4 Numerical analysis and discussions

It is commonly accepted that analytical solutions, whether exact or approximate, such as those expressed by Eq. (3.20) for nonlinear partial differential equations, may exhibit instability when applied to real physical experiments. Indeed, unstable solutions that do not manifest in these experiments are not considered tangible physical phenomena. To assess the stability of these analytical solutions in the context of a time-evolving partial differential equation, a common method involves first integrating them into the underlying equation, followed by numerically solving it. The stability of the numerical solution is confirmed if it evolves without disintegration over a sufficiently long period, matching the observation time of the phenomenon in the experiment.

In this context, we employ the fourth-order Runge-Kutta computational scheme, as outlined in Section 2.3.6, in conjunction with periodic boundary conditions [220]. A time step of $\Delta t = 10^{-10}$ s is chosen, and the spatial grid is set to range from -10 to 10 units, consistent with this numerical approach. The subsequent analysis will focus on evalu-

ating the numerical stability of the two types of solutions discussed earlier.

3.2.4.1 Bright solitary wave

We identify a stationary bright solitary wave with a positive amplitude from the solution to Eq. (3.2), defined by $\chi_n(t) = \frac{4\sqrt{2}}{\cosh(\beta nl)}$. Integrating this solution at the initial time $t = 0$ enables numerical analysis. The results, comparing the spatiotemporal evolution of the analytical (Fig. 3.3) and numerical (Fig. 3.4) solutions, show excellent agreement, with the solution remaining stable for ten times longer than those observed in previous studies [24, 206], indicating increased stability.

Stationary solutions, such as the one shown in Fig. (3.2), suggest the conservation of energy, enabling MTs to maintain a stable spatial configuration. This could facilitate the role of MAPs in intracellular transport, analogous to a railway track where MAPs transport essential cargo, providing insight into the biological function of MTs. Understanding the stationary states of MTs can shed light on biological phenomena, such as the presence of GTP or the conformation of the cap at the MT ends, both of which contribute to their stability and prevent catastrophic events. This ability to regulate MT stability is not only essential for cellular function but also presents therapeutic opportunities. One example is Epothilone D, a tubulin stabilizer that enhances MT stability and influences cellular dynamics. According to Kolman (2004) [221], it has proven effective in treating diseases associated with mitotic instability. Additionally, Wang et al. (2005) [222] demonstrated that Epothilone D helps overcome tumor cell resistance to other MT-targeting drugs, such as taxol, by stabilizing MTs and inducing irreversible structural changes. These findings highlight the importance of modulating MTs, both through stationary states and drug interventions, to regulate cellular stability and function, especially in oncology, where agents like Epothilone D and taxol disrupt MT instability to induce cell death in tumor cells [221, 222].

3.2.4.2 Anti-dark solitary wave

The initial configuration for the numerical integration of Eq. (3.2) is now specified as the anti-dark soliton wave, characterized by Eq. (3.20) with $\chi_n(t) = -4\sqrt{2}\ \mathrm{sech}(\beta nl)$. The spatiotemporal evolutions of the angular variation of dimers are detailed in panels (a) (analytical) and (b) (numerical) of Fig. (3.5), respectively. An important remark is that the numerical solution maintains the initial spatial distribution throughout the simulation until $t = 10^4\ ns$, which solidly confirms the stability of our anti-dark soliton wave. Furthermore, it is pertinent to emphasize that these anti-dark soliton wave solu-

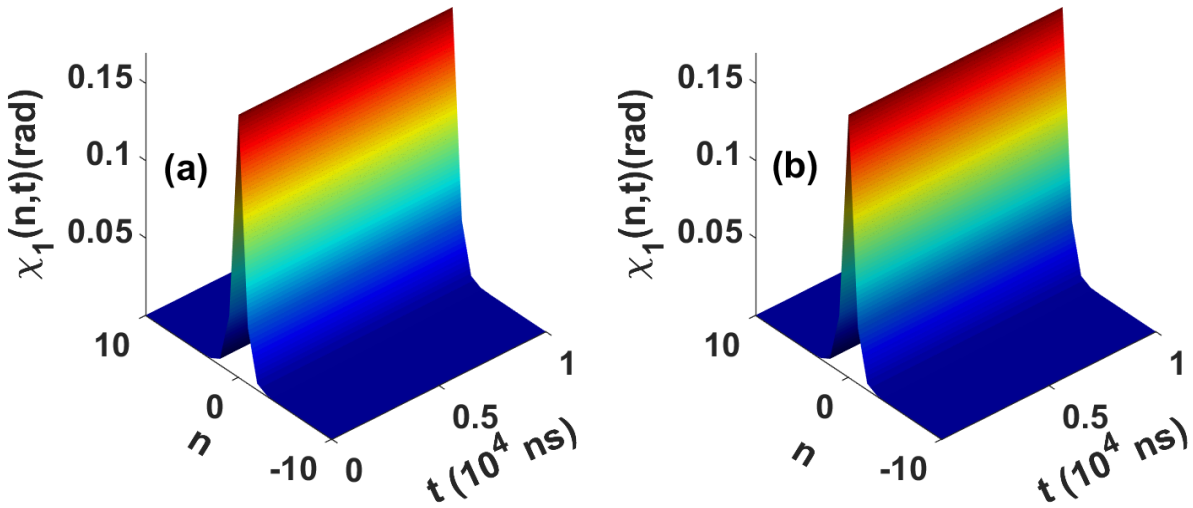

Figure 3.2: *Spatiotemporal evolutions of the bright solitary wave:* ***(a)*** *analytical,* ***(b)*** *numerical solutions. The numerical solution matches the analytical one with good accuracy.* $pE = 0.25$ eV, $K = 0.1$ eV, $l = 80$ Å, $\varepsilon = 1.1\omega_g$.

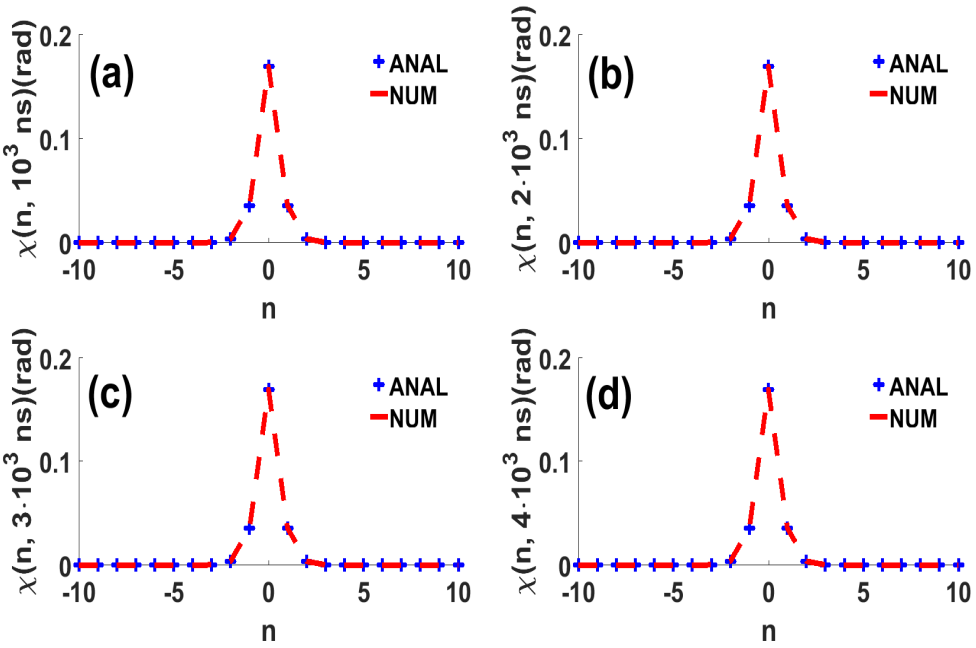

Figure 3.3: *Comparison between the numerical solution (represented by the red dotted line) and the analytical solution (represented by the blue dotted circles) of* $\chi_n(t)$ *at different time values, with* $\epsilon = 0$*: (a)* $t = 10^3$*, (b)* $t = 2.10^3$*, (c)* $t = 3.10^3$*, and (d)* $t = 4.10^3$.

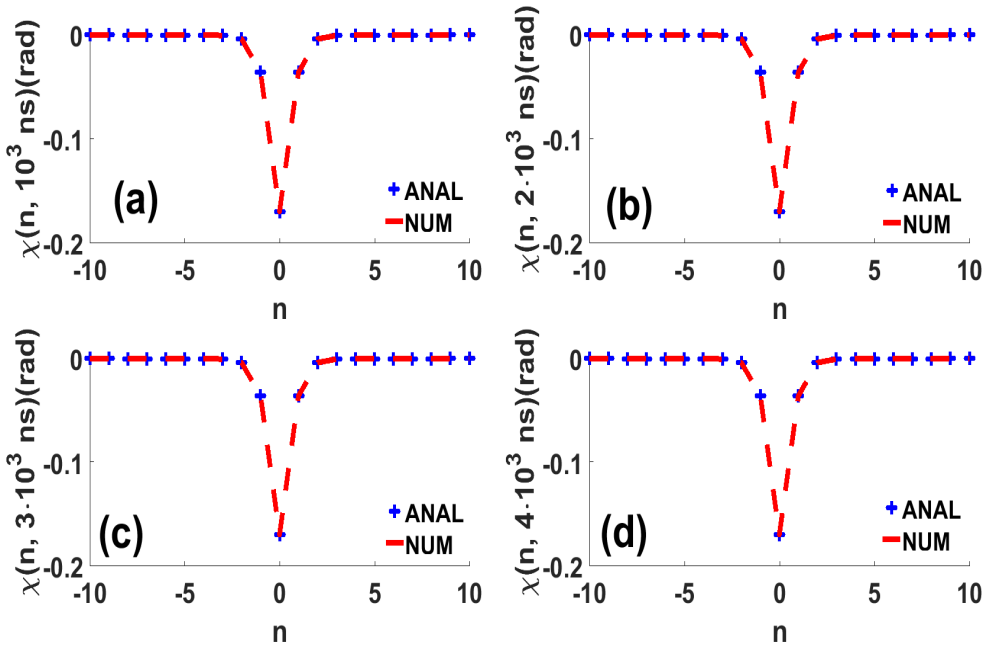

Figure 3.4: *Comparison between the numerical solution (represented by the red dotted line) and the analytical solution (represented by the blue dotted circles) of $\chi_n(t)$ at different time values, with $\epsilon = 0$: (a) $t = 10^3$, (b) $t = 2.10^3$, (c) $t = 3.10^3$, and (d) $t = 4.10^3$.*

tions hold particular interest in explaining the movements of MAPs along MTs, as well as in understanding the stable positions of MTs induced by the GTP cap. This observation enriches our understanding of biological processes involving MTs and opens new avenues for research in this field.

3.3 Nonlinear dynamics and the effect of cytosol viscosity on microtubules, with exact solutions

3.3.1 Model and equation of motion

In our analysis, we adopted the model by Priya et *al*. [178], extensively discussed in Section 2.2.4. This model is specifically applied to the study of neuronal MT networks, where protein pairs induce radial and longitudinal oscillations, thus generating a complexity of six degrees of freedom. Within this framework, the model considers two main degrees of freedom: longitudinal displacement following the U_n model [168, 169] and angular displacement following the φ_n model [15]. To keep the notation consistent, we assigned the variable χ_n to φ_n. We have chosen to introduce the moment of inertia, rather than simple mass, in the context of radial displacements. This consideration is based on the fact that it offers a more thorough characterisation of the behaviour of an

object subjected to rotational forces, while providing a more robust foundation for calculations and analysis in rotational dynamics. The resulting Hamiltonian is expressed as follows:

$$H = \sum_n \left[\frac{m}{2}\dot{U}_n^2 + \frac{I}{2}\dot{\chi}_n^2 + \frac{K_1}{2}(U_{n+1}-U_n)^2 + \frac{K_2}{2}(\chi_{n+1}-\chi_n)^2 - \frac{A}{2}U_n^2 + \frac{B}{4}U_n^4 - pE\cos(\chi_n)\right]. \tag{3.21}$$

In Eq. (2.5), the first couple of terms represents the kinetic energy related to the displacements U_n and χ_n , with m standing for the mass and $I = (m\,l^2)/12$, the moment of inertia of dimers, where $l = 8$ nm is the length of a single dimer. The dot implies the first derivative with respect to time t. The third and fourth terms emerge from the neighbouring dimers' restoring and deforming forces in the protofilament (PF), K_1 and K_2 account for inter-dimer stiffness parameters for the U_n and χ_n displacements, respectively. The fifth and sixth terms depict the double-potential well of U_n displacement [165, 169, 171], while the final term illustrates the dipole-dipole potential energy due to χ_n displacement. p denotes the electric dipole moment, and E is the intrinsic electric field of the dimers, whose order of magnitude is provided in Ref. [15, 207] making sure that $p, E > 0$. A and B are positive parameters of the double-potential well. The aforementioned Hamiltonian integrates both radial and longitudinal aspects of the dimers, which of course is a conservative system. In the context of eukaryotic cells, the cellular components are immersed in a fluid known as the cytosol, which is characterised by its viscosity. The viscosity of the cytosol acts as a dissipative term and may be incorporated into the dynamics using the following expressions: $F_v = -\gamma\dot{U}_n$ and $M_v = -\Gamma\dot{\chi}_n$. Here F_v and M_v denote the force and viscosity moment associated with longitudinal and angular displacements, respectively. The viscosity coefficients γ and Γ are related to be above specific displacements. Employing the Hamilton-Jacobi formalism, we derive the equations of motion that the dimer satisfies:

$$\ddot{U}_n + \varepsilon_1\dot{U}_n = \alpha_1(U_{n+1} - 2U_n + U_{n-1}) + \omega_{g_1}^2 U_n - \tau U_n^3, \tag{3.22a}$$

$$\ddot{\chi}_n + \varepsilon_2\dot{\chi}_n = \alpha_2(\chi_{n+1} - 2\chi_n + \chi_{n-1}) + \omega_{g_2}^2(a\,\chi_n^3 - \chi_n), \tag{3.22b}$$

where $\varepsilon_1 = \frac{\gamma}{m}$, $\alpha_1 = \frac{K_1}{m}$, $\alpha_2 = \frac{K_2}{I}$, $a = \frac{1}{6}$, $\omega_{g_2}^2 = \frac{pE}{I}$, $\tau = \frac{B}{m}$ and $\omega_{g_1}^2 = \frac{A}{m}$. The value of ε_2 varies proportianally with Γ, since I is a constant, according to the relationship $\varepsilon_2 = \frac{\Gamma}{I}$. Numerical values of the coefficients in Eqs. (3.22) are given in Tab. 3.1.

By exclusively considering the linear terms of Eq. (3.22), we scrutinize its solutions in the form of plane waves, expressed as $U_n(t) \propto \exp i(q_1 n - \omega_{g_1} t)$ and $\chi_n(t) \propto$

Table 3.1: Parameter network values

Parameters	values	References
γ	5.6×10^{-11} kg/s	[165, 169, 171]
A	1.8 eV	[223]
B	2.8 eV	[223]
K_1	0.5 N/m	[169]
K_2	0.1 eV	[24]
m	1.8×10^{-27} kg	[15, 171, 208]
Γ	43×10^{-30} Nms	[223]

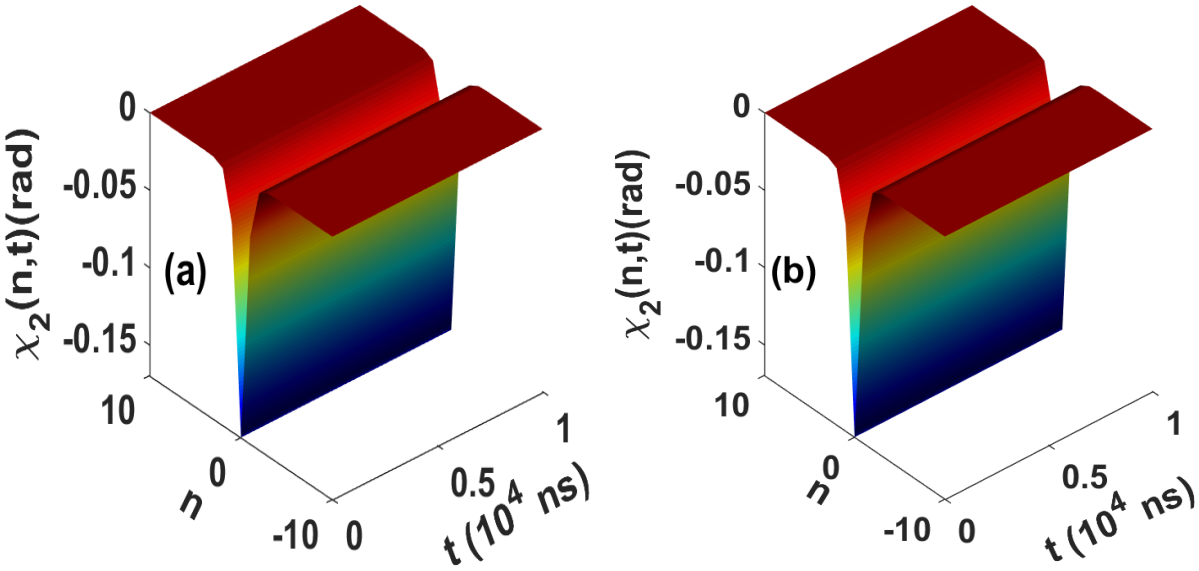

Figure 3.5: *Spatiotemporal evolutions of the anti-dark solitary wave:* ***(a)*** *analytical,* ***(b)*** *numerical solutions. The numerical solution recovers the analytical solution with high accuracy. Parameter values are:* $pE = 0.25$ eV, $K = 0.1$ eV, $l = 80$ Å, $\varepsilon = 1.1\omega_g$.

$\exp i(q_2 n - \omega_{g_2} t)$. Here, q_1, q_2 are the wave number and angle, while $\omega_{g_1}, \omega_{g_2}$ represent the longitudinal and angular frequencies, respectively. Inserting the above plane wave solutions into Eqs. (3.22) and neglecting frictionnal terms lead to the ensuing linear dispersion relations

After using these ansatze, we neglect the friction terms. By introducing these solutions into Eqs. (3.22), we derive the ensuing linear dispersion relations:

$$\omega_1^2 = -\omega_{g1}^2 + \frac{4K_1}{m}\sin^2\left(\frac{q_1}{2}\right), \text{ with } \omega_{g1}^2 < \frac{4K_1}{m}, \tag{3.23a}$$

$$\omega_2^2 = \omega_{g2} + \frac{4K_2}{I}\sin^2\left(\frac{q_2}{2}\right). \tag{3.23b}$$

By examining how a carrier wave with a frequency in the linear frequency range is

modulated, we can insert the test solution into Eq. (3.22), in the form:

$$U_n(t) = G_n(t)e^{-i\omega_{g_1}t} + G_n^*(t)e^{i\omega_{g_1}t}, \tag{3.24a}$$

$$\chi_n(t) = F_n(t)e^{-i\omega_{g_2}t} + F_n^*(t)e^{i\omega_{g_2}t}. \tag{3.24b}$$

First, we note that the functions $G_n(t), G_n^*(t), F_n(t), F_n^*(t)$ are complex functions that show slow variations over time compared to the main oscillations at frequencies $\omega_{g_1}, \omega_{g_2}$. This is expressed as $\dot{U}_n \ll \omega_{g_1} U_n, \dot{\chi}_n \ll \omega_{g_2}\chi_n$. Substituting Eqs. (3.24) into the Eqs. (3.22), and applying the RWA, i.e., keeping only terms proportional to $\exp(\pm i\omega_{g_1}t)$ and $\exp(\pm i\omega_{g_2}t)$, respectively, we derive the discrete CGL equations satisfied by $G_n(t)$,$F_n(t)$:

$$(\varepsilon_1 - 2i\omega_{g_1})\dot{G}_n - \alpha_1(G_{n+1} - 2G_n + G_{n-1}) - \omega_{g1}^2 G_n + 3\tau|G_n|^2 G_n - i\varepsilon_1\omega_{g_1}G_n = 0, \tag{3.25a}$$

$$(\varepsilon_2 - 2i\omega_{g_2})\dot{F}_n - \alpha_2(F_{n+1} - 2F_n + F_{n-1}) - 3a\omega_{g_2}^2|F_n|^2 F_n - i\varepsilon_2\omega_{g_2}F_n = 0. \tag{3.25b}$$

Also, we assume that the function $G_n(t), G_n^*(t), F_n(t), F_n^*(t)$ varies slightly with time in the vicinity of the cut-off frequency. This means that G and F can be viewed as continuous functions of both space $x = nl$ and time t. As a result, after an appropriate Taylor series expansion, the discrete functions $G_n(t)$ and $F_n(t)$ in Eqs (3.25) are replaced by their continuous counterparts $G(x,t)$ and $F(x,t)$, respectively, leading to

$$iG_t + P_1 G_{xx} + Q_1|G|^2 G - i\Lambda_1 G = 0, \tag{3.26a}$$

$$iF_t + P_2 F_{xx} + Q_2|F|^2 F - i\Lambda_2 F = 0. \tag{3.26b}$$

Eqs. (3.26) represents the continuous CGL equations, where P, Q, and Γ are defined as follow

$$P_1 = \begin{cases} P_{r_1} = \dfrac{\alpha_1 l^2 \varepsilon_1}{\varepsilon_1^2 + 4\omega_{g_1}^2} \\ \\ P_{c_1} = \dfrac{2\alpha_1 l^2 \omega_{g_1}}{\varepsilon_1^2 + 4\omega_{g_1}^2}, \end{cases} \quad Q_1 = \begin{cases} Q_{r_1} = \dfrac{3\tau\varepsilon_1}{\varepsilon_1^2 + 4\omega_{g_1}^2}, \\ \\ Q_{c_1} = \dfrac{6\tau\omega_{g_1}}{\varepsilon_1^2 + 4\omega_{g_1}^2}, \end{cases} \quad \Lambda_1 = \begin{cases} \Lambda_{r_1} = -\dfrac{3\omega_{g_1}\varepsilon_1}{\varepsilon_1^2 + 4\omega_{g_1}^2}, \\ \\ \Lambda_{c_1} = \dfrac{-2\omega_{g_1}^3 + \varepsilon_1^2\omega_{g_1}}{\varepsilon_1^2 + 4\omega_{g_1}^2}, \end{cases} \tag{3.27a}$$

$$P_2 = \begin{cases} P_{r_2} = \dfrac{2\alpha l^2 \omega_{g_2}}{4\omega_{g_2}^2 + \varepsilon_2^2}, \\ \\ P_{c_2} = -\dfrac{\alpha l^2 \varepsilon_2}{4\omega_{g_2}^2 + \varepsilon_2^2}, \end{cases} \quad Q_2 = \begin{cases} Q_{r_2} = \dfrac{6a\omega_{g_2}^3}{4\omega_{g_2}^2 + \varepsilon_2^2}, \\ \\ Q_{c_2} = -\dfrac{3a\omega_{g_2}^2\varepsilon_2}{4\omega_{g_2}^2 + \varepsilon^2}, \end{cases} \quad \Lambda_2 = \begin{cases} \Lambda_{r_2} = -\dfrac{2\omega_{g_2}^2\varepsilon_2}{4\omega_{g_2}^2 + \varepsilon_2^2}, \\ \\ \Lambda_{c_2} = \dfrac{\omega_{g_2}\varepsilon_2^2}{4\omega_{g_2}^2 + \varepsilon_2^2}. \end{cases} \tag{3.27b}$$

The next subsection is devoted to finding exact solutions of Eq.(3.26).

3.3.2 Exact solutions of cubic complex Ginzburg-Landau equation

Analytical solutions play a central role in exploring biological systems by providing precise details on their dynamic behaviors. Their exceptional accuracy allows for predicting and characterizing complex variations within these systems, thereby offering an in-depth understanding of biological processes. Furthermore, these solutions play a crucial role in validating numerical models, thus establishing a solid foundation for interpreting and predicting biological phenomena.

The modified HBM that we are using here stands out for its innovative approach in solving nonlinear equations. It employs a bilinear formulation specifically tailored to obtain exact solutions, thus demonstrating notable efficiency in addressing nonlinear evolutionary equations. Its user-friendliness and capacity to generate novel progressive wave solutions make it a distinctive method, combining precision, efficiency, and ease of implementation for solving complex problems in science and engineering.

A thorough study of CGL equations with third-order nonlinearity has been extensively investigated [198–202]. Among the various approaches to applying the modified HBM, the approach presented in [198] has particularly caught our attention. We define the modified Hirota operator [198, 199] as follows:

$$D^m_{\delta,t} D^n_{\delta,x} H \cdot T = \left(\frac{\partial}{\partial t'} - \delta \frac{\partial}{\partial t}\right)^m \left(\frac{\partial}{\partial x'} - \delta \frac{\partial}{\partial x}\right)^n H(x,t) T(x',t')|_{x'=x,t'=t}. \tag{3.28}$$

Setting

$$G(x,t) = \psi(x,t)\, e^{\Lambda_1 t}, \tag{3.29a}$$

$$F(x,t) = \phi(x,t)\, e^{\Lambda_2 t}, \tag{3.29b}$$

and substituting Eqs. (3.29) into Eqs. (3.26), we get:

$$i\,\psi_t + P_1\,\psi_{xx} + Q_1\,|\psi|^2\,\psi\, e^{\Lambda_1 t} = 0, \tag{3.30a}$$

$$i\,\phi_t + P_2\,\phi_{xx} + Q_2\,|\phi|^2\,\phi\, e^{\Lambda_2 t} = 0. \tag{3.30b}$$

The two solitary wave solutions of Eqs. (3.30) are looked for in the form:

$$\psi(x,t) = u_1(x,t) + u_2(x,t), \tag{3.31a}$$

$$\phi(x,t) = v_1(x,t) + v_2(x,t), \tag{3.31b}$$

where $u_1(x,t)u_2(x,t) = 0$ and $v_1(x,t)v_2(x,t) = 0$ correspond to one solitary wave. Insert-

ing Eqs. (3.31) into Eqs. (3.30), we get the system:

$$i\,u_{1t} + P_1\,u_{1xx} + Q_1\,|u_1|^2\,u_1\,e^{\Lambda_1 t} + Q_1\,e^{\Lambda_1 t}\left(2u_2\,|u_1|^2 + u_2^*\,u_1^2\right) = 0, \tag{3.32a}$$

$$i\,u_{2t} + P_1\,u_{2xx} + Q_1\,|u_2|^2\,u_2\,e^{\Lambda_2 t} + Q_1\,e^{\Lambda_2 t}\left(2u_1\,|u_2|^2 + u_1^*\,u_2^2\right) = 0, \tag{3.32b}$$

$$i\,v_{1t} + P_2\,v_{1xx} + Q_2\,|v_1|^2\,v_1\,e^{\Lambda_1 t} + Q_2\,e^{\Lambda_1 t}\left(2v_2\,|v_1|^2 + v_2^*\,v_1^2\right) = 0, \tag{3.32c}$$

$$i\,v_{2t} + P_2\,v_{2xx} + Q_2\,|v_2|^2\,v_2\,e^{\Lambda_2 t} + Q_2\,e^{\Lambda_2 t}\left(2v_1\,|v_2|^2 + v_1^*\,v_2^2\right) = 0, \tag{3.32d}$$

where the asterisk (*) denote the complex conjugate. We use the modified Hirota ansatz to construct solutions of Eqs. (3.32) as:

$$u_1(x,t) = H(x,t)\,T_1(x,t)^{-\delta_1},\; u_2(x,t) = L(x,t)\,T_1(x,t)^{-\delta_1}, \tag{3.33a}$$

$$v_1(x,t) = S(x,t)\,T_2(x,t)^{-\delta_2},\; v_2(x,t) = R(x,t)\,T(x,t)^{-\delta_2}. \tag{3.33b}$$

In Eqs. (3.33), H, L, S, and R are complex functions, and T_1 and T_2 are real functions. The complex constant $\delta_j = 1 + i\,\delta_{cj}$ (where $j = 1,2$) needs to be determined. Using Eq. (3.28) along with Eqs. (3.33) the bilinear form of Eqs. (3.32) are

$$\left(i\,D_{\delta_1,t} + P_1\,D_{\delta_1,x}^2\right) H \cdot T_1 = 0, \tag{3.34a}$$

$$\left(i\,D_{\delta_1,t} + P_1\,D_{\delta_1,x}^2\right) L \cdot T_1 = 0, \tag{3.34b}$$

$$D_x^2\,T_1 \cdot T_1 = \frac{2Q_1\,e^{2\Lambda_1 t}(|H|^2 + HL^* + 2LH^*)}{P_1\,\delta_1(\delta_1+1)\,T_1^{2\delta_1-2}}, \tag{3.34c}$$

$$D_x^2\,T_1 \cdot T_1 = \frac{2Q_1\,e^{2\Lambda_1 t}(|L|^2 + LH^* + 2HL^*)}{P_1\,\delta_1(\delta_1+1)\,T_1^{2\delta_1-2}}, \tag{3.34d}$$

$$\left(i\,D_{\delta_2,t} + P_2\,D_{\delta_2,x}^2\right) S \cdot T_2 = 0, \tag{3.34e}$$

$$\left(i\,D_{\delta_2,t} + P_2\,D_{\delta_2,x}^2\right) R \cdot T_2 = 0, \tag{3.34f}$$

$$D_x^2\,T_2 \cdot T_2 = \frac{2Q_2\,e^{2\Lambda_2 t}(|S|^2 + SR^* + 2RS^*)}{P_2\,\delta_2(\delta_2+1)T_2^{2\delta_2-2}}, \tag{3.34g}$$

$$D_x^2\,T_2 \cdot T_2 = \frac{2Q_2\,e^{2\Lambda_2 t}(|R|^2 + RS^* + 2SR^*)}{P_2\,\delta_2(\delta_2+1)T_2^{2\delta_2-2}}. \tag{3.34h}$$

Eqs. (3.34) are valid provided that the following conditions are satisfied $HL \neq 0, SR \neq$

$0,(H+L)(H^*-L^*)=0,(S+R)(S^*-R^*)=0,L=\epsilon H$ and $R=\epsilon S$, such that

$$\left(iD_{\delta_1,t}+P_1D^2_{\delta_1,x}\right)H\cdot T_1=0, \tag{3.35a}$$

$$\left(iD_{\delta_1,t}+P_1D^2_{\delta_1,x}\right)L\cdot T_1=0, \tag{3.35b}$$

$$D^2_xT_1\cdot T_1=\frac{2Q_1e^{2\Lambda_1t}(1+3\epsilon)}{P_1\delta_1(\delta_1+1)T_1^{2\delta_1-2}}|H|^2, \tag{3.35c}$$

$$D^2_xT_1\cdot T_1=\frac{2Q_1e^{2\Lambda_1t}(1+3\epsilon)}{P_1\delta_1(\delta_1+1)T_1^{2\delta_1-2}}|L|^2, \tag{3.35d}$$

$$\left(iD_{\delta,t}+P_2D^2_{\delta_2,x}\right)S\cdot T_2=0, \tag{3.35e}$$

$$\left(iD_{\delta,t}+P_2D^2_{\delta_2,x}\right)R\cdot T_2=0, \tag{3.35f}$$

$$D^2_xT_2\cdot T_2=\frac{2Q_2e^{2\Lambda_2t}(1+3\epsilon)}{P_2\delta_2(\delta_2+1)T_2^{2\delta_2-2}}|S|^2, \tag{3.35g}$$

$$D^2_xT_2\cdot T_2=\frac{2Q_2e^{2\Lambda_2t}(1+3\epsilon)}{P_2\delta_2(\delta_2+1)T_2^{2\delta_2-2}}|R|^2, \tag{3.35h}$$

with $\epsilon\in\{-1,0,1\}$. $\epsilon=0$ correspond to a one solitary wave. The left-hand sides of Eqs. (3.35c), (3.35d), (3.35f) and Eq. (3.35g) are real, so the right-hand sides must be as well. The latter requirements impose real solutions to the following equations:

$$\delta_{1c}=0,\ \delta_{2i}=0, \tag{3.36a}$$

$$(P_{1c}Q_{1r}-P_{1r}Q_{1c})=\tan(2\Lambda_{1c}t)\,(P_{1c}Q_{1c}+P_{1r}Q_{1r}), \tag{3.36b}$$

$$(P_{2c}Q_{2r}-P_{2r}Q_{2c})=\tan(2\Lambda_{2c}t)\,(P_{2c}Q_{2c}+P_{2r}Q_{2r}). \tag{3.36c}$$

Hence, Eqs. (3.35) can be rephrased as:

$$\left(iD_{\delta_1,t}+P_1D^2_{\delta_1,x}\right)H\cdot T_1=0,$$

$$\left(iD_{\delta_1,t}+P_1D^2_{\delta_1,x}\right)L\cdot T_1=0, \tag{3.37a}$$

$$D^2_xT_1\cdot T_1=\frac{(P_{1c}Q_{1c}+P_{1r}Q_{1r})\,e^{2\Lambda_{1r}t}(1+3\epsilon)}{\cos(2\Lambda_{1c}t)|P_1|^2}|H|^2,$$

$$D^2_xT_1\cdot T_1=\frac{(P_{1c}Q_{1c}+P_{1r}Q_{1r})\,e^{2\Lambda_{1r}t}(1+3\epsilon)}{\cos(2\Lambda_{1c}t)|P_1|^2}|L|^2, \tag{3.37b}$$

$$\left(iD_{\delta,t}+P_2D^2_{\delta_2,x}\right)S\cdot T_2=0,$$

$$\left(iD_{\delta,t}+P_2D^2_{\delta_2,x}\right)R\cdot T_2=0, \tag{3.37c}$$

$$D^2_xT_2\cdot T_2=\frac{(P_{2c}Q_{2c}+P_{2r}Q_{2r})\,e^{2\Lambda_{2r}t}(1+3\epsilon)}{\cos(2\Lambda_{2c}t)|P_2|^2}|S|^2,$$

$$D^2_xT_2\cdot T_2=\frac{(P_{2c}Q_{2c}+P_{2r}Q_{2r})\,e^{2\Lambda_{2r}t}(1+3\epsilon)}{\cos(2\Lambda_{2c}t)|P_2|^2}|R|^2. \tag{3.37d}$$

Once the bilinear conditions and forms are available, the next step is to find the solitary wave solutions. Multiple soliton solutions are accessible, such as impulsive, frontal, and dark solutions [200]. The modified bilinear operators (3.28) frequently utilize these solutions. The impulsive solutions are of significant interest to us because of their diverse applications in the signal processing and transportation of data in microtubular networks [155]. This is done by starting with an expansion written as:

$$H = e^{\theta_1}, T_1 = 1 + N_1(t)\, e^{\theta_1 + \theta_1^*}, \tag{3.38a}$$

$$\text{where, } \theta_1 = k_1 x + h_1(t).$$

$$S = e^{\theta_2}, T_2 = 1 + N_2(t)\, e^{\theta_2 + \theta_2^*}, \tag{3.38b}$$

$$\text{where, } \theta_2 = k_2 x + h_2(t), \text{ with } k_1, k_2 \in \mathbb{R}.$$

h_1, h_2, and N_1, N_2 are time-dependent complex an real functions, respectively. By inserting Eqs. (3.38) into Eqs. (3.37), we obtain:

$$\frac{dh_1}{dt} - iP_1 k_1^2 = 0, \tag{3.39a}$$

$$\frac{dh_2}{dt} - iP_2 k_2^2 = 0, \tag{3.39b}$$

$$\frac{1}{N_1(t)} \frac{dN_1}{dt} = 2P_{1c} k_1^2, \tag{3.39c}$$

$$\frac{1}{N_2(t)} \frac{dN_2}{dt} = 2P_{2c} k_1^2, \tag{3.39d}$$

$$N_1(t) = \frac{(P_{1c} Q_{1c} + P_{1r} Q_{1r})\, e^{2\Lambda_{1r} t}(1 + 3\epsilon)}{2k_1^2 |P_1|^2 \cos(2\Lambda_{1c} t)}, \tag{3.39e}$$

$$N_2(t) = \frac{(P_{2c} Q_{2c} + P_{2r} Q_{2r})\, e^{2\Lambda_{2r} t}(1 + 3\epsilon)}{2k_2^2 |P_2|^2 \cos(2\Lambda_{2c} t)}. \tag{3.39f}$$

After integration of Eqs. (3.39a - 3.39d), we have:

$$h_1(t) = iP_1 k_1^2 t, \tag{3.40a}$$

$$h_2(t) = iP_2 k_2^2 t, \tag{3.40b}$$

$$N_1(t) = N_{01} \exp\left(2k_1^2 P_{1c} t\right), \tag{3.40c}$$

$$N_2(t) = N_{02} \exp\left(2k_2^2 P_{2c} t\right). \tag{3.40d}$$

From Eqs. (3.39a), (3.39d) and Eqs. (3.40c), (3.40d), we obtain:

$$N_{01} = \frac{(P_{1c} Q_{1c} + P_{1r} Q_{1r})(1 + 3\epsilon)}{2k_1^2 |P_1|^2}, \tag{3.41a}$$

$$N_{02} = \frac{(P_{2c} Q_{2c} + P_{2r} Q_{2r})(1 + 3\epsilon)}{2k_2^2 |P_2|^2}. \tag{3.41b}$$

Inserting Eqs. (3.41) and Eqs. (3.40) into Eqs. (3.29) and using the transformations Eqs. (3.31), the soliton solution associated with Eqs. (3.26) can be expressed in the form:

$$G_1(x,t) = \frac{\exp\left(k_1 x + \left(\Lambda_{1r} + i\left(\Lambda_{1c} + P_1 k_1^2\right)\right) t\right)}{1 + N_{01}\exp(2k_1 x)}, \tag{3.42a}$$

$$G(x,t) = (1+\epsilon) G_1(x,t), \tag{3.42b}$$

$$F_1(x,t) = \frac{\exp\left(k_2 x + \left(\Lambda_{2r} + i\left(\Lambda_{2c} + P_2 k_2^2\right)\right) t\right)}{1 + N_{02}\exp(2k_2 x)}, \tag{3.42c}$$

$$F(x,t) = (1+\epsilon) F_1(x,t). \tag{3.42d}$$

Returning to the discrete system, Eqs. (3.42) transform as follows:

$$G_1(n,t) = \frac{\exp\left(k_1 n l + \left(\Lambda_{1r} + i\left(\Lambda_{1c} + P_1 k_1^2\right)\right) t\right)}{1 + N_{01}\exp(2k_1 n l)}, \tag{3.43a}$$

$$G(n,t) = (1+\epsilon) G_1(n,t), \tag{3.43b}$$

$$F_1(n,t) = \frac{\exp\left(k_2 n l + \left(\Lambda_{2r} + i\left(\Lambda_{2c} + P_2 k_2^2\right)\right) t\right)}{1 + N_{02}\exp(2k_2 n l)}, \tag{3.43c}$$

$$F(n,t) = (1+\epsilon) F_1(n,t). \tag{3.43d}$$

Employing Eqs. (3.33), (3.38), and (3.40) within the context of Eqs. (3.24) facilitates the derivation of spatio-temporal solutions characterizing the longitudinal displacement U_n and the angular displacement χ_n. These solutions serve to elucidate the dynamics of energy propagation within the MT network, as delineate by the formulation articulated in Eqs. (3.43). We obtain:

$$U_n(t) = 2(1+\epsilon)\frac{\exp\left(n l - V_{u_n} t\right)}{\exp(-k_1) + N_{01}\exp(k_1 n l)} \times \cos\{(k_1^2 P_{1r} + \Lambda_{1c} - \omega_{g_1}) t\}, \tag{3.44a}$$

$$\chi_n(t) = 2(1+\epsilon)\frac{\exp\left(n l - V_{\chi_n} t\right)}{\exp(-k_2) + N_{02}\exp(k_2 n l)} \times \cos\{(k_2^2 P_{2r} + \Lambda_{2c} - \omega_{g_2}) t\}, \tag{3.44b}$$

with

$$V_{U_n} = \frac{\omega_{g_1}\left(2l^2\alpha_1 {k_1}^2 + 3\varepsilon_1\right)}{\left({\varepsilon_1}^2 + 4{\omega_{g_1}}^2\right) k_1}, \tag{3.45a}$$

$$V_{\chi_n} = -\frac{2{\omega_{g_2}}^2 + \varepsilon_2\left(\alpha l^2 {k_2}^2\right)}{\left({\varepsilon_2}^2 + 4{\omega_{g_2}}^2\right) k_2}. \tag{3.45b}$$

Each solution of Eqs. (3.44) has a free parameter: k_1 for the longitudinal displacement and k_2 for the angular displacement. Eq. (3.44b) is valid for $0 < l\,\varepsilon_2\,\omega_{g_2}\,\alpha_2 < \frac{2\omega_{g_2}^2}{l^2 k_2^2}$. This implies that $k_2^2 \in \left[0, \frac{2\omega_{g_2}^2}{\alpha_2 l^2}\right]$, such that $k_2 \in [0, 1.6719]$, and $\chi_{(n,t)} \leq \frac{\pi}{6}$ [175]. This leads us

to choose the specific value $k_2 = 0.3$. The solution (3.44a) exists if $0 < l\,\varepsilon_1\,\omega_{g_1} - \frac{3\varepsilon_1}{2l^2k_1^2} < \alpha_1$ for $\alpha_1 = 4.5455 \times 10^{-6}$. This imperative led to our preference for $k_1 = 0.3$. It is important to note that the solitary wave solutions resulting from Eqs. (3.44) are solitary wave solutions that differ significantly from previously derived kinks, breathers [15, 224], and stationary bright solitary waves. When $\epsilon = 1$, $G(x,t) = 2G_1(x,t)$ and $F(x,t) = 2F_1(x,t)$ which correspond to the two solitary wave solutions. The two solitary wave solutions differ from one solitary wave solutions ($\epsilon = 0, G(x,t) = G_1(x,t)$ and $F(x,t) = F_1(x,t)$) by a factor of two and by the expressions of the parameters N_{01} and N_{02}, which directly influence the functions $G_1(x,t)$ and $F_1(x,t)$. In contrast to the bright stationary solutions presented in Section 3.2 which are independent of viscosity and remain constant over time, the solutions described here are dynamic and depend explicitly on both time and the viscosity of the cytosol. Finally, for $\epsilon = -1$, Eqs. (3.26) yields a null solution. One solitary wave is a well-established solution found in various domains of physics. This solution may explain the rolling carpet phenomena observed in the dynamics of MT, which often occurs during the transport of organelles within the cytoplasm. Unlike the solitary wave solutions usely found, we propose in this work two-soliton solutions to explain the dynamics of angular or longitudinal of MTs for the first time, to the best of our knowledge.

3.3.3 Numerical experiments

Analytical methodologies are used to solve systems of ordinary and partial differential equations. These methods provide analytical solutions, which are often approximate and may not accurately reflect the reality of the studied systems. In contrast, numerical methods offer more suitable solutions that better align with real-world scenarios. Due to the nonlinear nature and complexity of many biological models, analytical solutions are often difficult to obtain. As a result, researchers must carefully select appropriate numerical techniques to solve and compare the results versus analytical solutions. In this part of the work, our objective is to numerical solve Eqs. (3.22) and compared the results against the analytical prediction found above. The fourth-order Runge-Kutta method was employed to conduct numerical simulations of Eqs. (3.22). The computations were performed on a spatial grid with 10^5 equally spaced points spanning the interval $[-40, 40]$ with periodic boundary conditions. The initial conditions at time t = 0 were derived from the corresponding analytical solutions (Eqs. (3.44)). Simulations run up to $t_{fin} = 10^4$ ns with the time step of $dt = 0.1$ ns.

In the absence of viscosity (i.e., $\gamma = 0$ and $\varepsilon_2 = 0$), the analytical and numerical curves

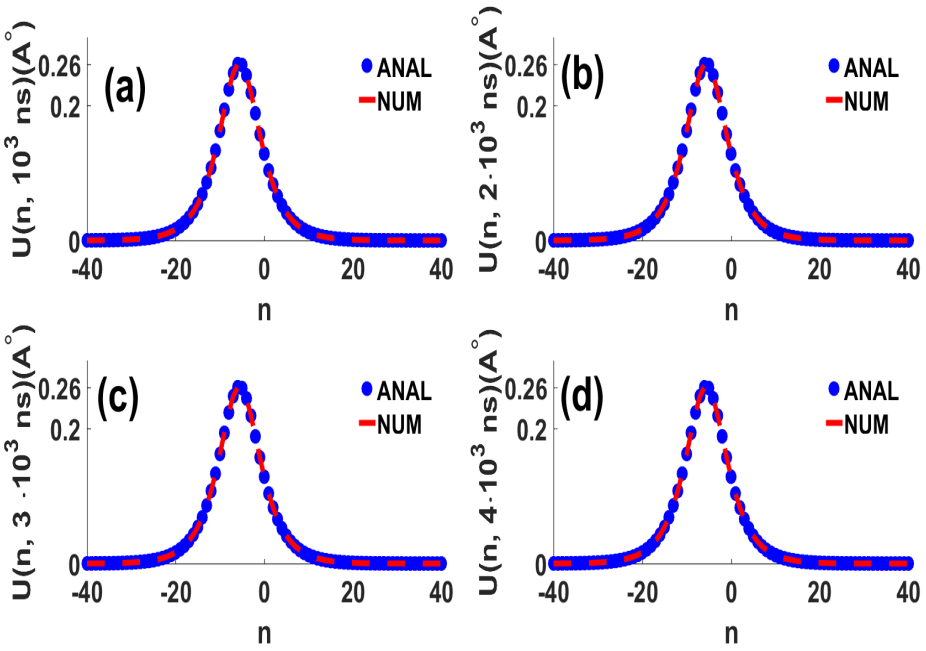

Figure 3.6: *Comparison between the numerical solution (red dotted line) and the analytical solution (blue dotted circles) of $U_n(t)$ at different time values: (a) $t = 10^3$, (b) $t = 2 \cdot 10^3$, (c) $t = 3 \cdot 10^3$, and (d) $t = 4 \cdot 10^3$, with $\gamma = 0$ and $\epsilon = 0$.*

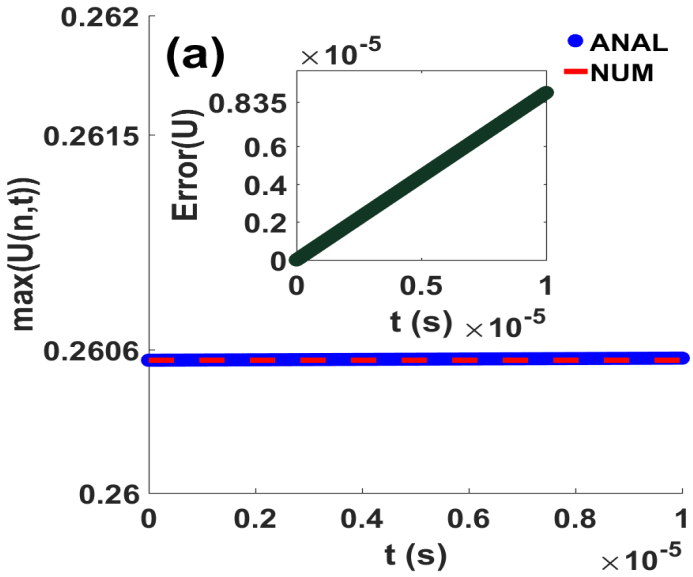

Figure 3.7: *Superposition of analytical and numerical maximum values: assessment of the absolute error for $\gamma = 0$, $\epsilon = 0$.*

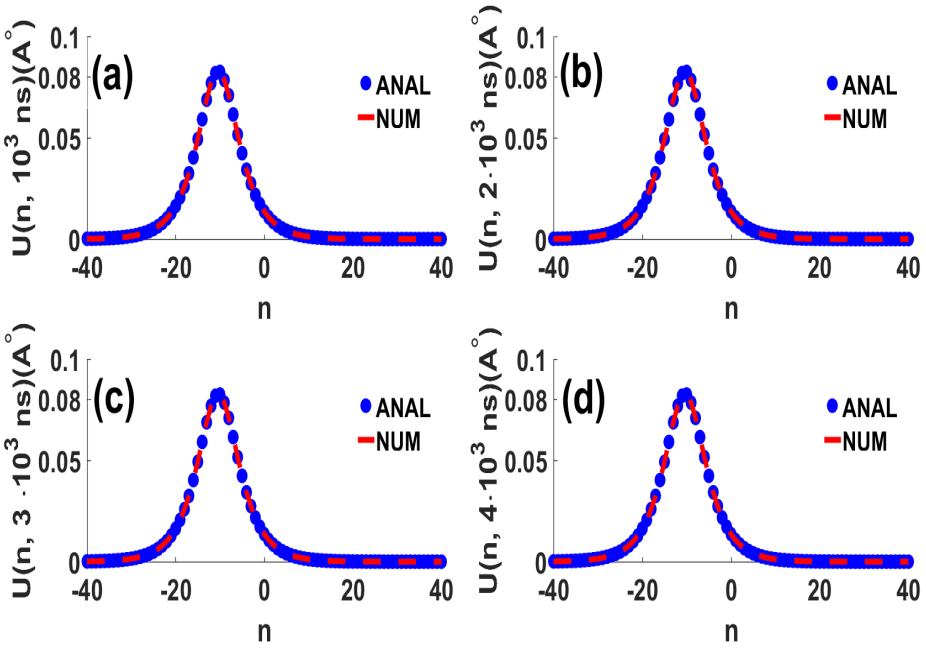

Figure 3.8: *Comparison between the numerical solution (red dotted line) and the analytical solution (blue dotted circles) of $U_n(t)$ at different time values, with $\epsilon = 0$: (a) $t = 10^3$, (b) $t = 2 \cdot 10^3$, (c) $t = 3 \cdot 10^3$, and (d) $t = 4 \cdot 10^3$, for $\gamma = 5.6 \times 10^{-11}$ kg/s.*

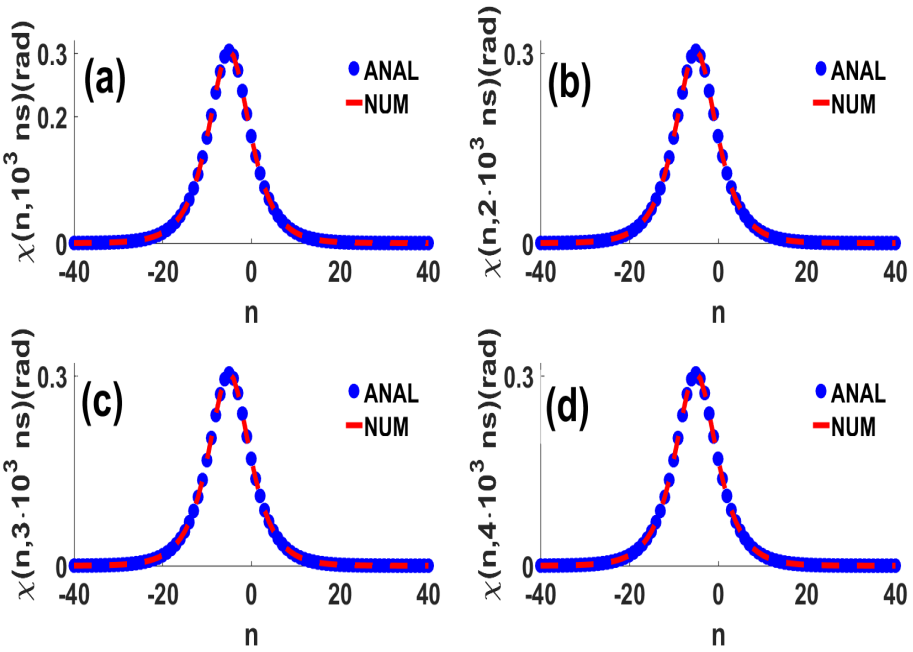

Figure 3.9: *Comparison between the numerical solution (red dotted line) and the analytical solution (blue dotted circles) of $\chi_n(t)$ at different time values, with $\epsilon = 0$: (a) $t = 10^3$, (b) $t = 2 \cdot 10^3$, (c) $t = 3 \cdot 10^3$, and (d) $t = 4 \cdot 10^3$, for $\varepsilon_2 = 0$.*

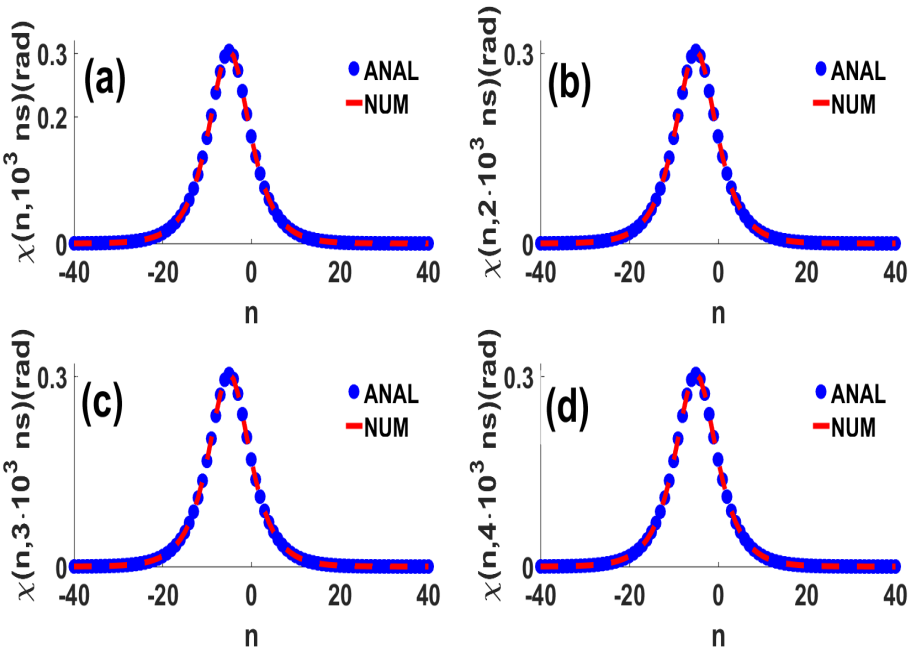

Figure 3.10: *Comparison between the numerical solution (represented by the red dotted line) and the analytical solution (represented by the blue dotted circles) of $\chi_n(t)$ at different time values, with $\epsilon = 0$: (a) $t = 10^3$, (b) $t = 2.10^3$, (c) $t = 3.10^3$, and (d) $t = 4.10^3$, for $\varepsilon = 1.1\omega_{g_2}$.*

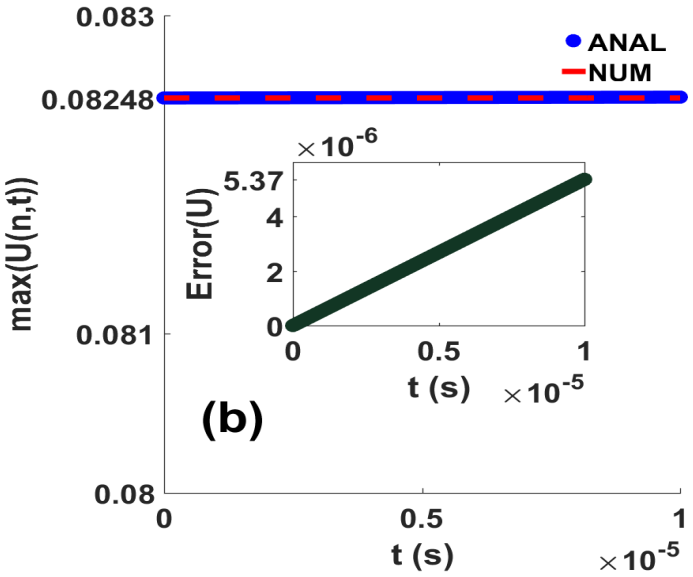

Figure 3.11: *Superposition of analytical and numerical maximum values: assessment of the absolute error for $\gamma = 5.6 \times 10^{-11}$ kg/s and $\epsilon = 0$.*

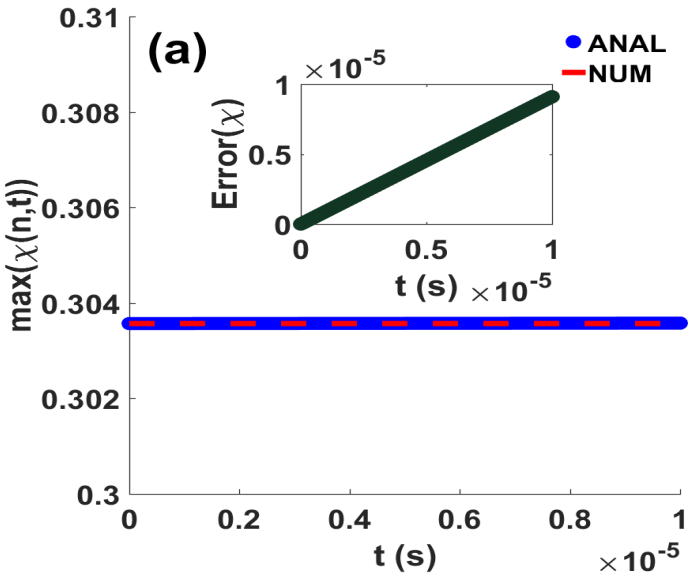

Figure 3.12: *Superposition of analytical and numerical maximum values: assessment of the absolute error for* $\varepsilon = 0$ *and* $\epsilon = 0$.

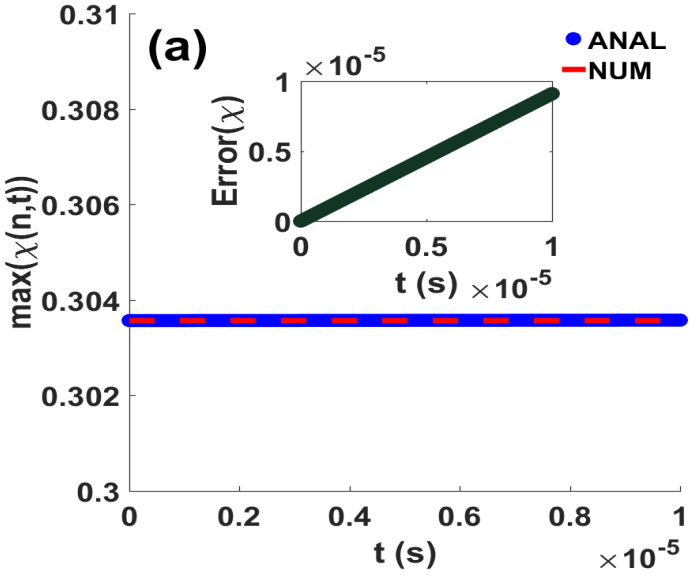

Figure 3.13: *Superposition of analytical and numerical maximum values: assessment of the absolute error for* $\varepsilon = 1.1\omega_{g_2}$ *and* $\epsilon = 0$.

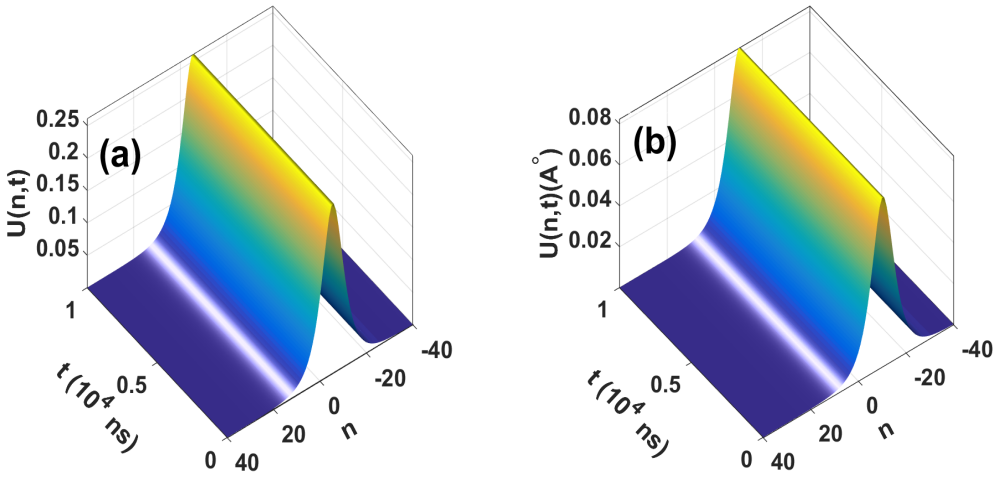

Figure 3.14: *Spatiotemporal evolution of the solitary pulse for the same parameters as in Fig. (3.6). Numerical solutions of* $U_n(t)$*: (a)* $\gamma = 0$*, (b)* $\gamma = 5.6 \times 10^{-11}$*,* $\epsilon = 0$*.*

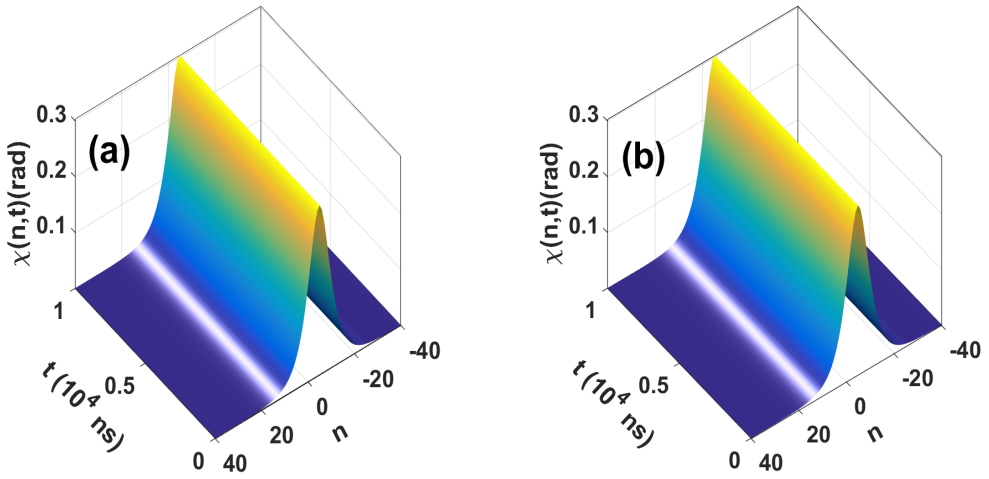

Figure 3.15: *Spatiotemporal evolution of the solitary pulse for the same parameter as in Fig.(3.9). Numerical solutions of* $\chi_n(t)$*: (a)* $\varepsilon_2 = 0$*, (b)* $\varepsilon_2 = 1.1\omega_{g_2}, \epsilon = 0$*.*

coincide perfectly at different time points, with constant maximum amplitudes of 0.26 Å in Fig. (3.6) for U_n and 0.3 rad in Fig. (3.9) for χ_n. These results correspond to the case $\epsilon = 0$. The error analysis reveals a slight discrepancy in Fig. (3.7) for U_n and in Fig. (3.12) for χ_n. For $\epsilon = 1$, the maximum amplitudes remain constant at 0.37 Å for U_n and at 0.303 rad for χ_n in Fig. (3.17.a). These observations are corroborated by the very minimal disrepancies (of the same order of magnitude) between the analytical and numerical solutions, as shown in Fig. (3.16.b) for U_n and in Fig. (3.17.b) for χ_n. The initial conditions in Figs. (3.14.a, 3.15.a, 3.16.a, 3.17.a) remain unchanged, reinforcing the reliability of our analytical predictions.

Viscosity has no effect on the angular dimer dynamics, as evidency by the numerical solution obtained for $\varepsilon_2 = 1.1\omega_{g_2}$, shown in Figs. (3.10), (3.9), (3.17.c) and (3.17.a), where $\varepsilon_2 = 0$ for both $\epsilon = 0$ and $\epsilon = 1$. In contrast, viscosity significantly affect the longitudinal displacement U_n, drastically reducing its maximum amplitude from 0.26 Å ($\gamma = 0$, see Fig. (3.6)) to 0.08 Å in Fig. (3.8) for $\epsilon = 0$. For $\epsilon = 1$, the maximum amplitude drops from 0.37 Å ($\gamma = 0$, see Fig. (3.16.a)) to 0.117 Å in Fig. (3.16.c). Our analytical solutions exhibit good agreement with the numerical one, achieving reasonable accuracy. The errors between the analytical and numerical solutions range between 5×10^{-6} and 10^{-5} for $\epsilon = 0$ and between 4×10^{-6} and 10^{-5} for $\epsilon = 1$. The obtained error values are nearly identical for $\epsilon \in \{0, 1\}$, further confirming the validity of our analytical solutions.

It is well known that the presence of viscosity in the medium influences the dynamics and functions of MTs in several ways. For instance, viscosity can affect the mobility of MTs by creating resistance to their movement, thus influencing the stability and processes of assembly and disassembly of MTs [28, 29]. Authors in [224, 225] suggested that an increase in viscosity acts as a damping factor for MT growth. Biologically, such a viscosity-induced resistance could be linked to an interaction between proteins associated with MTs, allowing the MT structure to remain stable. Regarding angular displacement, viscosity does not seem to influence the shape, amplitude, or propagation of the solution. This stability may be attributed to a stable configuration of MTs, including a curved conformation [89, 96] or the presence of a GTP cap at their ends [226]. This stability could also result from the interaction of MTs with associated proteins such as dynein and kinesin, all contributing to MT stability. The solutions obtained support potential important implications for regulating viscosity in the cytosol, the growth and division of cancer cells, as well as understanding and treating dysfunctions related to MTs. A better understanding of the correlation between cytosol viscosity and MTs could improve certain treatment modalities such as targeted therapies for specific pathologies,

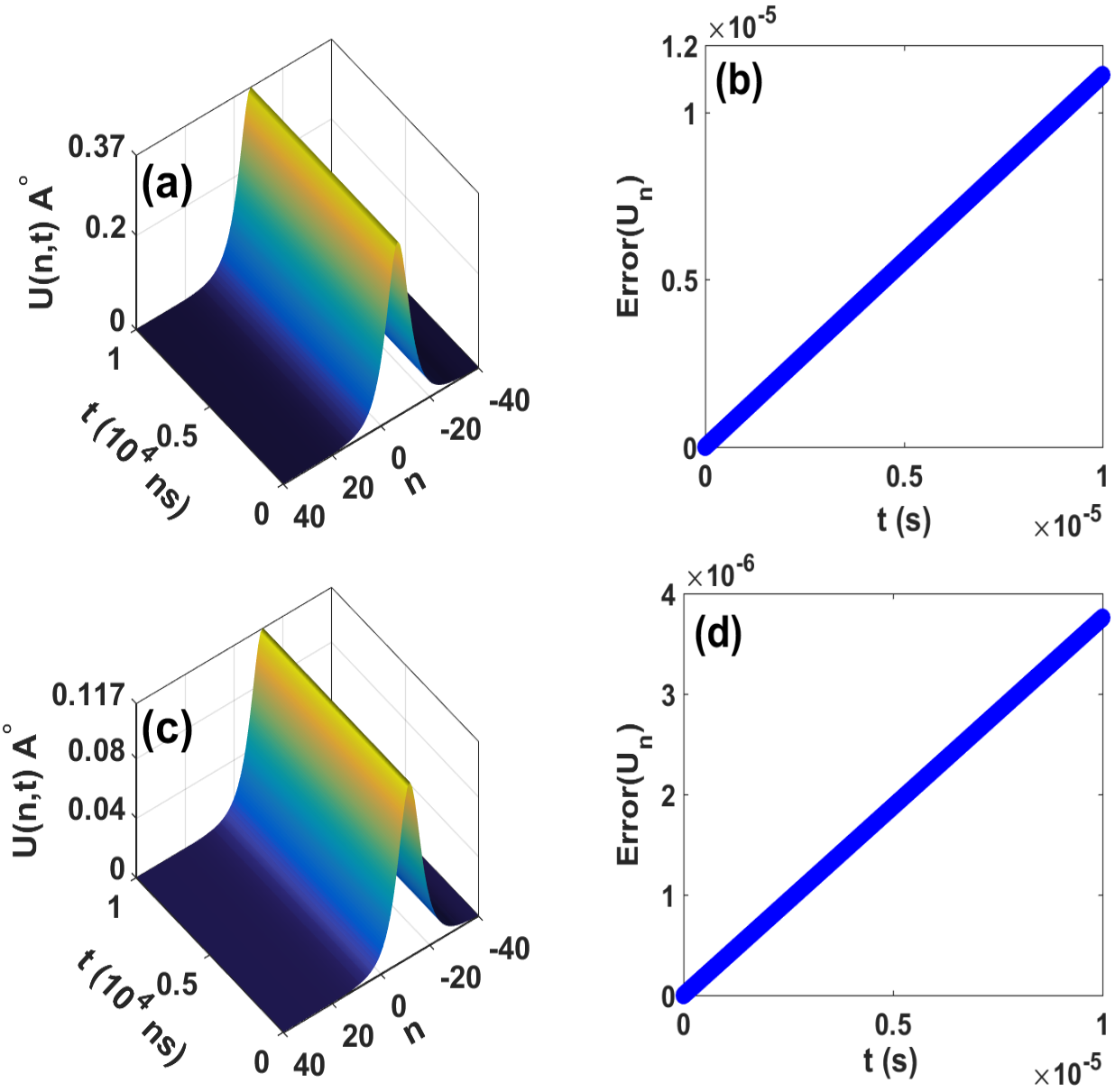

Figure 3.16: *Numerical spatiotemporal evolution of longitudinal displacement* $\epsilon = 1$. *For* $\gamma = 0$, *a) bright solitary wave, b) maximum of absolute error. For* $\gamma = 5.6 \times 10^{-11}$, *c) bright solitary wave, d) maximum of absolute error*.

including cancer and neurodegenerative diseases [89, 227].

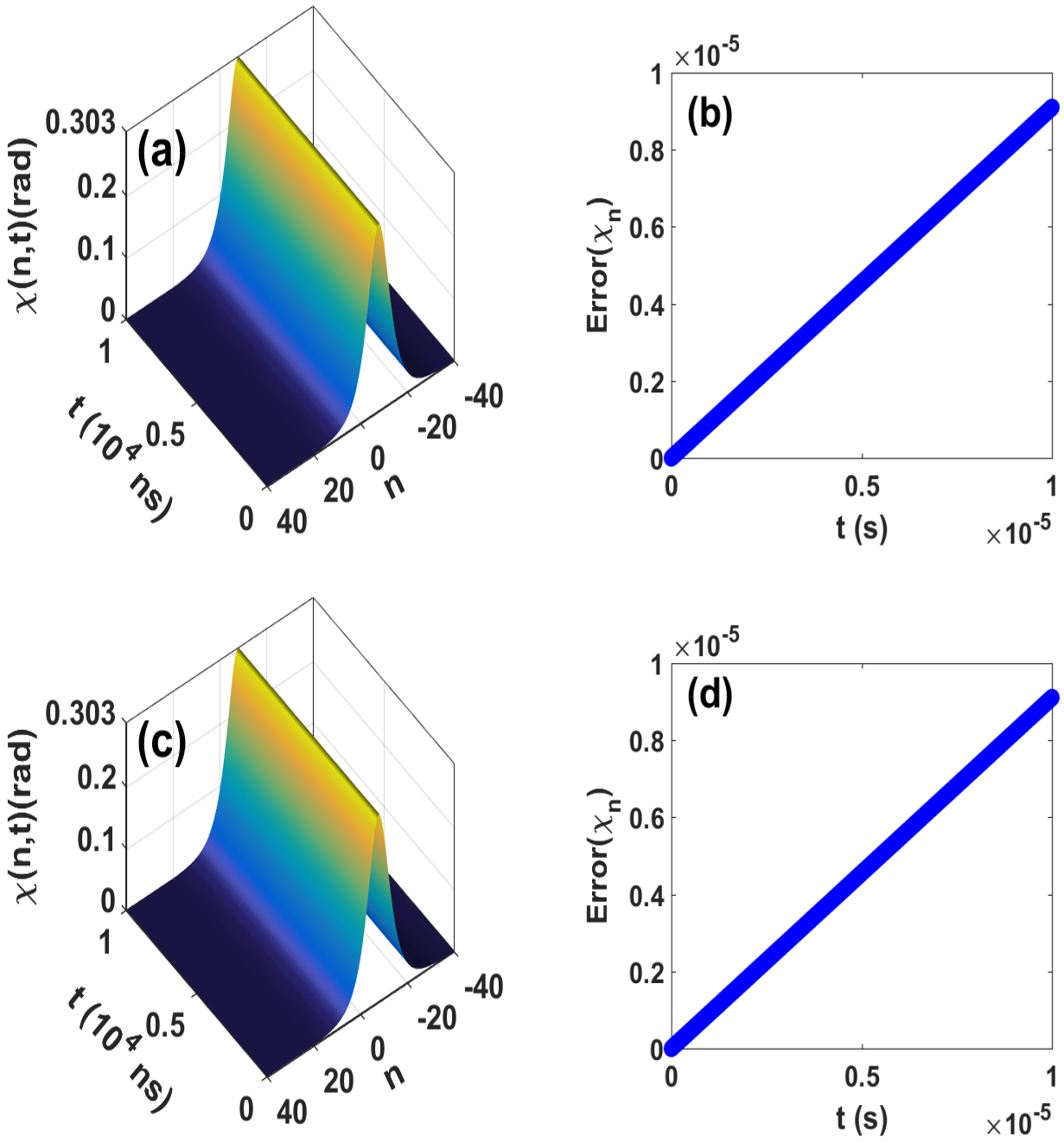

Figure 3.17: *Numerical spatiotemporal evolution of angular displacement* $\epsilon = 1$. *For* $\varepsilon_2 = 0$, *a) bright solitary wave, b) maximum of absolute error. For* $\varepsilon_2 = 1.1\omega_{g_2}$, *c) bright solitary wave, d) maximum of absolute error.*

3.4 Conclusion

This chapter examines the nonlinear dynamics of MTs within the cytosol. We began by investigating the dynamics of radial dislocations of MTs, incorporating a dissipative term that arises due to cytosol viscosity. Through the analysis of MI of plane waves, we demonstrated that cytosol viscosity introduces new unstable modes. However, we observed that the growth rate amplitude of this instability decreases as viscosity increases, and for sufficiently high viscosity values, the instability is completely mitigated. To address these findings, we introduced new stationary solution profiles, specifically the bright and anti-dark profiles, and outlined their conditions for existence. We further explored the relevance of these solutions, discovering that viscosity does not affect them. These stationary profiles were identified as viable candidates for explaining biological mechanisms in which MTs must remain stationary. The results were confirmed through numerical simulations. To further analyze the effects of cytosol viscosity on MT dynamics, we developed new approximate analytical solutions. This enhanced our understanding of MT dynamics, particularly regarding the influence of cytosol viscosity on both longitudinal and angular displacements. We proposed a two degree of freedom model that incorporates cytosol viscosity. Using the modified HBM, we obtained approximate analytical solutions of the solitary wave type to describe MT dynamics. Our findings indicated that for longitudinal displacements, the amplitude of the solution decreases due to viscosity, while for angular displacements, viscosity appeared to have no effect, at least over the total propagation time considered in this study. Thus, viscosity provides a means to control the assembly, disassembly, and stability processes of MTs effectively.

General Conclusion

In this thesis, we studied the influence of viscosity on the distribution of energy within MTs, as well as the potential use of this parameter to regulate their dynamics. This thesis is organized into three parts.

The first chapter addresses MTs, highlighting their composition, structure, and dynamics essential for various cellular processes. Proteins associated with MTs are discussed for their role in regulating MT formation and function, impacting cellular functions such as cell division, intracellular transport, and cell shape. The importance of MTs in maintaining cellular integrity and proper cell function is emphasized, as well as the risks of dysfunction that can lead to pathological consequences, particularly in neurodegenerative diseases and developmental disorders. An in-depth understanding of MTs and their molecular regulation is crucial for deciphering the mechanisms of normal and pathological cellular functions, thus paving the way for new research and therapeutic approaches for diseases associated with MT dysfunction. The chapter concludes with a discussion on solitons and their various manifestations.

The second chapter offers a detailed exploration of mathematical models and analytical methods. We examine several specific mathematical models used to describe MTs, such as the Sataric et al. model, the U model, the radial model, the Priya *et al*. model, and the general model. Regarding analytical methods, we explore approaches such as the rotating wave approximation, modulational instability processes, the direct ansatz method, and Hirota's bilinear method, all of which are crucial for constructing new approaches and solutions in this study. Finally, we introduce the numerical Runge-Kutta 4 method as a complementary tool commonly used to confirm analytical results.

The results and main contributions of this research are presented in the third chapter. Our study focuses on the dynamics of radial dislocations of MTs in the presence of a dissipative term related to cytosol viscosity, denoted as Γ. By analyzing the MI of plane waves, we highlight the significant impact of cytosol viscosity on system stability. Our findings reveal the emergence of new unstable modes in the presence of this viscosity, but the growth of instability decreases with increasing Γ, and for some high values, cy-

tosol viscosity eliminates this instability. Furthermore, it is well-established that MTs adopt stationary states during certain biological processes. To study these phenomena, we transform the original discrete differential equation into a dissipative CGL equation, allowing us to deduce stationary solutions using a direct ansatz method. Two distinct stationary profiles are identified: a bright profile and an anti-dark profile, both of which are relevant candidates for explaining biological mechanisms involving stationary MTs. Our analytical results are confirmed by direct numerical integrations of the original discrete model. The stationary solutions obtained indicate a constant energy, enabling microtubules to maintain their configuration. During this process, MTs act as tracks on which microtubule-associated proteins attach to transport essential elements for proper cellular function. From a biological perspective, these results can be used to halt MT dynamics. In this context, targeted drugs like taxol represent a direct application of our findings.

Furthermore, we have developed new exact solutions to deepen our understanding of MT dynamics, taking into account the influence of cytosol viscosity on both longitudinal and angular movements. To this end, we devised a two-degree-of-freedom model incorporating this viscosity. From our analyses, we employed the rotating wave method to obtain a CGL equation. Subsequently, we converted this discrete equation into a continuous one using a semi-discrete approximation. Hirota's bilinear method enabled us to construct bright two-soliton solutions describing MT dynamics. We observed that during longitudinal displacement, the solution experiences a decrease in amplitude due to viscosity γ, while for angular displacement, no influence of viscosity Γ was noted; the solution retains its shape and amplitude during displacement. Thus, viscosity offers the potential to influence the assembly, disassembly, and stability processes of MTs. The solutions we obtained, defined under certain conditions of existence, were validated by numerical simulations, confirming their reliability. These findings are of paramount importance in regulating cytosol viscosity and could pave the way for the development of targeted therapies for specific pathologies such as cancer. However, several questions remain unanswered and are intended to be explored in the near future.

- ☞ Investigating the use of streamlines within MTs to study the synchronization of dimers during elongation and shortening processes.
- ☞ Exploring the bifurcation phenomena of spiral structures emerging within the streamlines of MTs.
- ☞ Developing a three-dimensional model of MTs by incorporating fractional deriva-

tives to uncover hidden dynamics that are not captured by single-degree-of-freedom models.

Appendix A: Resolution of cubic GLC

To solve the following equation:

$$i\,\varphi_t + P\varphi_{xx} + Q|\varphi|^2\varphi - i\,\gamma\varphi = 0. \qquad (A_1)$$

we consider a solution in the form:

$$\varphi(x,t) = \left[A\,\mathrm{sech}(\beta x) + i\,B\,\tanh(\beta x)\right] e^{(i\,v^2\,t)}. \ (A_2)$$

Inserting Eq. (A_2) into Eq. (A_1) and separating the real and imaginary parts, we obtain:
Real part

$$\begin{aligned}&\left(2\,\alpha\,l^2\varepsilon B\beta^2 + \left(-3B^3 a_0\varepsilon\,{\omega_g}^2 + 2B\varepsilon\,{\omega_g}^2\right)\left(\cosh\left(\beta x\right)\right)^2 - 3\,a_0{\omega_g}^2\varepsilon A^2 B + 3B^3 a_0\varepsilon\,{\omega_g}^2\right)\sinh\left(\beta x\right)\\ &+\left(-6AB^2 a_0{\omega_g}^3 - 2A\alpha\beta^2 l^2\omega_g + A\varepsilon^2 v^2 + 4Av^2{\omega_g}^2 - A\varepsilon^2\omega_g\right)\\ &\times\left(\cosh\left(\beta x\right)\right)^2 - 6\,a_0{\omega_g}^3 A^3 + 6AB^2 a_0{\omega_g}^3 + 4A\alpha\beta^2 l^2\omega_g = 0. \ (A_3)\end{aligned}$$

Imaginary part

$$\begin{aligned}&\left(4\,\alpha\,l^2\omega_g B\beta^2 - 6\,a_0{\omega_g}^3 A^2 B + 6B^3 a_0{\omega_g}^3\right)\sinh\left(\beta x\right)\\ &+\left(-6B^3 a_0{\omega_g}^3 + B\varepsilon^2 v^2 + 4Bv^2{\omega_g}^2 - B\varepsilon^2\omega_g\right)\left(\cosh\left(\beta x\right)\right)^2\sinh\left(\beta x\right)\\ &+\left(3AB^2 a_0\varepsilon\,{\omega_g}^2 + A\alpha\beta^2\varepsilon l^2 - 2A\varepsilon\,{\omega_g}^2\right)\left(\cosh\left(\beta x\right)\right)^2 + 3\,a_0{\omega_g}^2\varepsilon A^3\\ &-3AB^2 a_0\varepsilon\,{\omega_g}^2 - 2A\alpha\beta^2\varepsilon l^2 = 0. \ (A_4)\end{aligned}$$

By setting the coefficients of the terms $\sinh\left(\beta x\right)$, $\cosh\left(\beta x\right)$, $\cosh^2\left(\beta x\right)$ to zero, we obtain the following equations: For the real part (A_3)

$$\begin{aligned}&-3B^3 a_0\varepsilon\,{\omega_g}^2 + 2B\varepsilon\,{\omega_g}^2 = 0,\\ &-3\,a_0{\omega_g}^2\varepsilon A^2 B + 3B^3 a_0\varepsilon\,{\omega_g}^2 + 2\,\alpha\,l^2\varepsilon B\beta^2 = 0,\\ &-6AB^2 a_0{\omega_g}^3 - 2A\alpha\beta^2 l^2\omega_g + A\varepsilon^2 v^2 + 4Av^2{\omega_g}^2 - A\varepsilon^2\omega_g = 0,\\ &-6\,a_0{\omega_g}^3 A^3 + 6AB^2 a_0{\omega_g}^3 + 4A\alpha\beta^2 l^2\omega_g = 0. (A_5)\end{aligned}$$

For the imaginary part (A_4)

$$
\begin{aligned}
&-6B^3a_0{\omega_g}^3+B\varepsilon^2v^2+4Bv^2{\omega_g}^2-B\varepsilon^2\omega_g=0,\\
&-6a_0{\omega_g}^3A^2B+6B^3a_0{\omega_g}^3+4\alpha l^2\omega_gB\beta^2=0,\\
&3AB^2a_0\varepsilon{\omega_g}^2+A\alpha\beta^2\varepsilon l^2-2A\varepsilon{\omega_g}^2=0,\\
&3a_0{\omega_g}^2\varepsilon A^3-3a_0{\omega_g}^2\varepsilon B^2A-2\alpha l^2\varepsilon A\beta^2=0.\ (A_6)
\end{aligned}
$$

Solving equations (A_5) and (A_6) using the Maple 17 Solve command, we obtain:

$$
\left[[A=0,B=0,\beta=\beta,v=v],\left[A=\frac{2}{3}\frac{\sqrt{3}}{\sqrt{a}},B=0,\beta=\frac{\sqrt{2}\omega_g}{\sqrt{\alpha}l},v=\sqrt{\omega_g}\right],\right.
$$
$$
\left[A=2/3\frac{\sqrt{3}}{\sqrt{a}},B=0,\beta=-\frac{\sqrt{2}\omega_g}{\sqrt{\alpha}l},v=\sqrt{\omega_g}\right],\left[A=\frac{2}{3}\frac{\sqrt{3}}{\sqrt{a}},B=0,\beta=-\frac{\sqrt{2}\omega_g}{\sqrt{\alpha}l},v=-\sqrt{\omega_g}\right],
$$
$$
\left[A=-\frac{2}{3}\frac{\sqrt{3}}{\sqrt{a}},B=0,\beta=\frac{\sqrt{2}\omega_g}{\sqrt{\alpha}l},v=\sqrt{\omega_g}\right],\left[A=-\frac{2}{3}\frac{\sqrt{3}}{\sqrt{a}},B=0,\beta=\frac{\sqrt{2}\omega_g}{\sqrt{\alpha}l},v=-\sqrt{\omega_g}\right],
$$
$$
\left[A=-\frac{2}{3}\frac{\sqrt{3}}{\sqrt{a}},B=0,\beta=-\frac{\sqrt{2}\omega_g}{\sqrt{\alpha}l},v=\sqrt{\omega_g}\right],\left[A=-\frac{2}{3}\frac{\sqrt{3}}{\sqrt{a}},B=0,\beta=-\frac{\sqrt{2}\omega_g}{\sqrt{\alpha}l},v=-\sqrt{\omega_g}\right],
$$
$$
\left[A=1/3\frac{\sqrt{6}}{\sqrt{a}},B=1/3\frac{\sqrt{6}}{\sqrt{a}},\beta=0,v=\sqrt{\omega_g}\right],\left[A=-1/3\frac{\sqrt{6}}{\sqrt{a}},B=1/3\frac{\sqrt{6}}{\sqrt{a}},\beta=0,v=\sqrt{\omega_g}\right],
$$
$$
\left[A=1/3\frac{\sqrt{6}}{\sqrt{a}},B=-1/3\frac{\sqrt{6}}{\sqrt{a}},\beta=0,v=\sqrt{\omega_g}\right],\left[A=-1/3\frac{\sqrt{6}}{\sqrt{a}},B=-1/3\frac{\sqrt{6}}{\sqrt{a}},\beta=0,v=\sqrt{\omega_g}\right],
$$
$$
\left[A=1/3\frac{\sqrt{6}}{\sqrt{a}},B=1/3\frac{\sqrt{6}}{\sqrt{a}},\beta=0,v=-\sqrt{\omega_g}\right],\left[A=-1/3\frac{\sqrt{6}}{\sqrt{a}},B=1/3\frac{\sqrt{6}}{\sqrt{a}},\beta=0,v=-\sqrt{\omega_g}\right],
$$
$$
\left[A=1/3\frac{\sqrt{6}}{\sqrt{a}},B=-1/3\frac{\sqrt{6}}{\sqrt{a}},\beta=0,v=-\sqrt{\omega_g}\right],\left[A=-1/3\frac{\sqrt{6}}{\sqrt{a}},B=-1/3\frac{\sqrt{6}}{\sqrt{a}},\beta=0,v=-\sqrt{\omega_g}\right],
$$
$$
\left[A=0,B=1/3\frac{\sqrt{6}}{\sqrt{a}},\beta=-\frac{\omega_g}{\sqrt{-\alpha}l},v=\sqrt{\omega_g}\right],\left[A=0,B=1/3\frac{\sqrt{6}}{\sqrt{a}},\beta=-\frac{\omega_g}{\sqrt{-\alpha}l},v=-\sqrt{\omega_g}\right],
$$
$$
\left[A=0,B=1/3\frac{\sqrt{6}}{\sqrt{a}},\beta=\frac{\omega_g}{\sqrt{-\alpha}l},v=\sqrt{\omega_g}\right],\left[A=0,B=1/3\frac{\sqrt{6}}{\sqrt{a}},\beta=\frac{\omega_g}{\sqrt{-\alpha}l},v=-\sqrt{\omega_g}\right],
$$
$$
\left[A=0,B=-1/3\frac{\sqrt{6}}{\sqrt{a}},\beta=-\frac{\omega_g}{\sqrt{-\alpha}l},v=\sqrt{\omega_g}\right],\left[A=0,B=-1/3\frac{\sqrt{6}}{\sqrt{a}},\beta=-\frac{\omega_g}{\sqrt{-\alpha}l},v=-\sqrt{\omega_g}\right]
$$
$$
,\left[A=0,B=-1/3\frac{\sqrt{6}}{\sqrt{a}},\beta=\frac{\omega_g}{\sqrt{-\alpha}l},v=\sqrt{\omega_g}\right],\left[A=0,B=-1/3\frac{\sqrt{6}}{\sqrt{a}},\beta=\frac{\omega_g}{\sqrt{-\alpha}l},v=-\sqrt{\omega_g}\right],
$$
$$
\left.\left[A=\frac{2}{3}\frac{\sqrt{3}}{\sqrt{a}},B=0,\beta=\frac{\sqrt{2}\omega_g}{\sqrt{\alpha}l},v=-\sqrt{\omega_g}\right]\right].\ (A_7)
$$

For $a_0 = a/h^2$, we consider the following solutions:

$$A = \pm 2h\sqrt{2}, B = 0, v = \pm\sqrt{\omega_g}, \beta = \frac{\sqrt{2}\,\omega_g}{\sqrt{\alpha}\,l}. \quad (A_8)$$

References

[1] A. Claude, Fractionation of mammalian liver cells by differential centrifugation: II. Experimental procedures and results, J. Exp. Med. **84**, 1 (1946).

[2] S. Forth and T. M. Kapoor, The mechanics of microtubule networks in cell division, J. Cell Biol. **216**, 6 (2017).

[3] I. M. Tolić-Nørrelykke, Push-me-pull-you: how microtubules organize the cell interior, Eur. Biophys. J. **37**, 1271 (2008).

[4] C. Garzon-Coral, H. A. Fantana, and J. Howard, A force-generating machinery maintains the spindle at the cell center during mitosis, Science **352**, 6289 (2016).

[5] I. M. Tolić-Nørrelykke, L. Sacconi, G. Thon, and F. S. Pavone, Positioning and elongation of the fission yeast spindle by microtubule-based pushing, Curr. Biol. **14**, 13 (2004).

[6] G. Fink, I. Schuchardt, J. Colombelli, E. Stelzer, and G. Steinberg, Dynein-mediated pulling forces drive rapid mitotic spindle elongation in Ustilago maydis, EMBO J. **25**, 30 (2006).

[7] S. W. Grill, P. GoÈnczy, E. H. Stelzer, and A. A. Hyman, Polarity controls forces governing asymmetric spindle positioning in the Caenorhabditis elegans embryo, Nature **409**, 6820 (2001).

[8] S. W. Grill, J. Howard, E. Schaffer, E. H. Stelzer, and A. A. Hyman, The distribution of active force generators controls mitotic spindle position, Science **301**, 5632 (2003).

[9] S. W. Grill and A. A. Hyman, Spindle positioning by cortical pulling forces, Dev. Cell **8**, 4 (2005).

[10] T. Kiyomitsu and I. M. Cheeseman, Cortical dynein and asymmetric membrane elongation coordinately position the spindle in anaphase, Cell **154**, 2 (2013).

[11] K. Kimura and A. Kimura, Intracellular organelles mediate cytoplasmic pulling force for centrosome centration in the Caenorhabditis elegans early embryo, Proc. Natl. Acad. Sci. U.S.A. **108**, 1 (2011).

[12] T. Shinar, M. Mana, F. Piano, and M. J. Shelley, A model of cytoplasmically driven microtubule-based motion in the single-celled Caenorhabditis elegans embryo, Proc. Natl. Acad. Sci. U.S.A. **108**, 26 (2011).

[13] H.-Y. Wu, E. Nazockdast, M. J. Shelley, and D. J. Needleman, Forces positioning the mitotic spindle: Theories, and now experiments, BioEssays **39**, 2 (2017).

[14] E. Mandelkow, E.-M. Mandelkow, H. Hotani, B. Hess, and S. C. Müller, Spatial patterns from oscillating microtubules, Science **246**, 4935 (1989).

[15] S. Zdravković, M. V. Satarić, A. Maluckov, and A. Balaž, Localized modulated waves in microtubules, Appl. Math. Comput. **24**, 2 (2014).

[16] E. M. Witkin, The role of DNA repair in aging of the adult Drosophila melanogaster, Mutat. Res. Fundam. Mol. Mech. Mutagen. **214**, 67 (1989).

[17] T. Mitchison and M. W. Kirschner, Dynamic instability of microtubule growth, Nature **312**, 237 (1984).

[18] H. Hess, J. Howard, and V. Vogel, A piconewton forcemeter assembled from microtubules and kinesins, Nano Lett. **2**, 10 (2002).

[19] M. G. Van den Heuvel and C. Dekker, Motor proteins at work for nanotechnology, Science **317**, 5836 (2007).

[20] K. R. Foster and J. W. Baish, Viscous damping of vibrations in microtubules, J. Biol. Phys. **26**, 255 (2000).

[21] D. B. Belobo, G. H. Ben-Bolie, T. B. Ekogo, C. Latchio Tiofack, and T. C. Kofane, Modulational instability of a Bose–Einstein condensate beyond the Fermi pseudopotential with a time-dependent complex potential, Int. J. Mod. Phys. B **26**, 30 (2012).

[22] M. L. Williams, R. F. Landel, and J. D. Ferry, The temperature dependence of relaxation mechanisms in amorphous polymers and other glass-forming liquids, J. Am. Chem. Soc **77**, 14 (1955).

[23] T. Yeung, B. Heit, J. F. Dubuisson, G. D. Fairn, B. Chiu, R. Inman, A. Kapus, M. Swanson, S. Grinstein, Contribution of phosphatidylserine to membrane surface charge and protein targeting during phagosome maturation, Cell. Motil. **5**, 17 (2009).

[24] C. B. Tabi, E. Tankou, and A. Mohamadou, Nonlinear coupled mode excitations in microtubules, Chaos, Solitons Fractals **95**, 187 (2017).

[25] M. C. Ekosso, A. J. Fotue, S. C. Kenfack, H. Fotsin, and L. C. Fai, Effects of temperature variations on the dynamics of microtubules, Mod. Phys. Lett. B **33**, 34 (2019).

[26] S. Shirmovsky and D. V. Shulga, Microtubules lattice equal-frequency maps: The dynamics of relief changes in dependence on elastic properties, tubulins dipole-dipole interaction and viscosity, Phys. A Stat. Mech. its Appl. **534**, 122165 (2019).

[27] A. T. Molines, J. Lemière, M. Gazzola, E. I. Steinmark, C. H. Edrington, C.-T. J. Hsu, K. Suhling, G. Goshima, L. J. Holt, M. Thery, G. J. Brouhard, and F. Chang, Physical properties of the cytoplasm modulate the rates of microtubule polymerization and depolymerization, Preprint Cell. Biol. (2020).

[28] M. D. Betterton, A new view of how cytoplasmic viscosity affects microtubule dynamics, Dev. Cell. **57**, 4 (2022).

[29] A. T. Molines, J. Lemière, M. Gazzola, I. E. Steinmark, C. H. Edrington, C. T. Hsu, P. Real-Calderon, K. Suhling, G. Goshima, L. J. Holt, M. Thery, G. J. Brouhard, and F. Chang, Physical properties of the cytoplasm modulate the rates of microtubule polymerization and depolymerization, Dev. Cell. **57**, 4 (2022).

[30] E. Nogales, S. G. Wolf, and K. H. Downing, Erratum: Structure of the $\alpha\beta$ tubulin dimer by electron crystallography, Nature **393**, 6681 (1998).

[31] E. Nogales, M. Whittaker, R. A. Milligan, and K. H. Downing, High-resolution model of the microtubule, Cell. **96**, 1 (1999).

[32] T. Mitchison, Localization of an exchangeable gtp bzinding site at the plus end of microtubules, Science **261**, 5124 (1993).

[33] M. F. Carlier, D. Didry, C. Simon and D. Pantaloni, Mechanism of GTP hydrolysis in tubulin polymerization: characterization of the kinetic intermediate microtubule-GDP-Pi using phosphate analogues, Biochemistry (Mosc.) **28**, 178 (1989).

[34] D. Pantaloni and M. F. Carlier, Involvement of guanosine triphosphate (GTP) hydrolysis in the mechanism of tubulin polymerization: regulation of microtubule dynamics at steady state by a GTP cap, Ann. N. Y. Acad. Sci. **466**, 496 (1986).

[35] T. Horio and T. Murata, The role of dynamic instability in microtubule organization, Front. Plant Sci. **5**, 511 (2014).

[36] H. Y. Kueh and T. J. Mitchison, Structural plasticity in actin and tubulin polymer dynamics, Science **325**, 960 (2009).

[37] E. Nogales and H.-W. Wang, Structural mechanisms underlying nucleotidedependent self-assembly of tubulin and its relatives. Curr. Opin. Struct. Biol. **16**, 221 (2006).

[38] D. Panda, H. P. Miller and L. Wilson, Determination of the size and chemical nature of the stabilizing ”cap” at microtubule ends using modulators of polymerization dynamics, Biochemistry (Mosc.) **41**, 1609 (2002).

[39] O. Valiron, I. Arnal, N. Caudron and D. Job, GDP-tubulin incorporation into growing microtubules modulates polymer stability. J. Biol. Chem. **285**, 17507 (2010).

[40] A. Dimitrov, M. Quesnoit, S. Moutel, I. Cantaloube, C. Poüs and F. Perez, Detection of GTP-tubulin conformation in vivo reveals a role for GTP remnants in microtubule rescues. Science **322**, 1353 (2008).

[41] L. G. Tilney, J. Bryan, D. J. Bush, K. Fujiwara, M. S. Mooseker, D. B. Murphy, and D. H. Snyder, Microtubules: evidence for 13 protofilaments, J. Cell. Biol. **59**, 2 (1973).

[42] M. F. Carlier, Guanosine-5-triphosphate hydrolysis and tubulin polymerization - Review article, Mol. Cell. Biochem. **47**, 2 (1982).

[43] J. Fan, A. D. Griffiths, A. Lockhart, R. A. Cross, and L. A. Amos, Microtubule minus ends can be labelled with a phage display antibody specific to alpha-tubulin, J. Mol. Biol. **259**, 3 (1996).

[44] K. Hirose, J. Fan, and L. A. Amos, Re-examination of the polarity of microtubules and sheets decorated with kinesin motor domain, J. Mol. Biol. **251**, 3 (1995).

[45] H. F. Lodish, Molecular cell biology, publisher by Macmillan 2008.

[46] A. Fokin, I. Brodsky, A. Burakov, and E. Nadezhdina, Interaction of early secretory pathway and Golgi membranes with microtubules and microtubule motors, Biochemistry (Moscow) **79**, 879 (2014).

[47] D. Job, O. Valiron, and B. Oakley, Microtubule nucleation, Curr. Opin. Cell. Biol. **15**, 1 (2003).

[48] F. Gittes, B. Mickey, J. Nettleton and J. Howard, Flexural rigidity of microtubules and actin filaments measured from thermal fluctuations in shape. J. Cell Biol. **120**, 923 (1993).

[49] R. Dixit, J. L. Ross, Y. E Goldman and E. L. F. Holzbaur, Differential regulation of dynein and kinesin motor proteins by tau. Science **319**, 1086 (2008).

[50] C. P. Brangwynne, F. C. MacKintosh, S. Kumar, N. A. Geisse, J. Talbot, L. Mahadevan, K. K. Parker, D. E. Ingber and D. A. Weitz, Microtubules can bear enhanced compressive loads in living cells because of lateral reinforcement, J. Cell Biol. **173**, 733 (2006).

[51] G. O. Wasteneys and J. C. Ambrose, Spatial organization of plant cortical microtubules: close encounters of the 2D kind, Trends Cell Biol. **19**, 62 (2009).

[52] R. B. Dye, S. P. Fink and R. C. Williams, Taxol-induced flexibility of microtubules and its reversal by MAP-2 and Tau, J. Biol. Chem. **268**, 6847 (1993).

[53] B. Mickey and J. Howard, Rigidity of microtubules is increased by stabilizing agents, J. Cell Biol. **130**, 909 (1995).

[54] H. Felgner, R. Fran and M. Schliwa, Flexural rigidity of microtubules measured with the use of optical tweezers, J. Cell. Sci. **109**, 509 (1996).

[55] D. Portran, M. Zoccoler, J. Gaillard, V. Stoppin-Mellet, E. Neumann, I. Arnal, J. L. Martiel and M. Vantard, MAP65/Ase1 promote microtubule flexibility. Mol. Biol. Cell **24**, 1964 (2013).

[56] C. Elie-Caille, F. Severin, J. Helenius, J. Howard, D. J. Muller and A. A. Hyman, . Straight GDP-tubulin protofilaments form in the presence of taxol, Curr. Biol. **17**, 1765 (2007).

[57] K. Kawaguchi, S. Ishiwata, S. ichi and T. Yamashita, Temperature dependence of the flexural rigidity of single microtubules. Biochem. Biophys. Res. Commun. **366**, 637 (2008).

[58] K. Kawaguchi and A. Yamaguchi, Temperature dependence rigidity of non-taxol stabilized single microtubules, Biochem. Biophys. Res. Commun. **402**, 66 (2010).

[59] A. Mitra and D. Sept, Taxol allosterically alters the dynamics of the tubulin dimer and increases the flexibility of microtubules, Biophys. J. **95**, 3252 (2008).

[60] M. E. Janson and M. Dogterom, A bending mode analysis for growing microtubules: evidence for a velocity-dependent rigidity, Biophys. J. **87**, 2723 (2004).

[61] F. Pampaloni, G. Lattanzi, A. Jonàs, T. Surrey, E. Frey and E.-L. Florin, Thermal fluctuations of grafted microtubules provide evidence of a length-dependent persistence length. Proc. Natl. Acad. Sci. U.S.A. **103**, 10248 (2006).

[62] S. Inoué and H. Sato, Cell motility by labile association of molecules. The nature of mitotic spindle fibers and their role in chromosome movement, J. Gen. Physiol. **50**, Suppl:259?292 (1967).

[63] N. Caudron, O. Valiron, Y. Usson, P. Valiron, and D. Job, A reassessment of the factors affecting microtubule assembly and disassembly in vitro, J. Mol. Biol. **297**, 211?220 (2000).

[64] H. Flyvbjerg, E. Jobs, and S. Leibler, Kinetics of self-assembling microtubules: an inverse problem in biochemistry, Proc. Natl. Acad. Sci. U.S.A. **93**, 5975?5979 (1996).

[65] M. Seggio, Étude in vitro des effets de la protéine MAP6 sur le cytosquelette, thèse de doctorat, Communauté Université Grenoble (2016).

[66] M. Moritz, M.B. Braunfeld, J.W. Sedat, B. Alberts, and D.A. Agard, Microtubule nucleation by gamma-tubulin-containing rings in the centrosome, Nature **378**, 638 (1995).

[67] J.M. Kollman, A. Merdes, L. Mourey, and D.A. Agard, Microtubule nucleation by γ-tubulin complexes, Nat. Rev. Mol. Cell Biol. **12**, 709 (2011).

[68] K. Chabin-Brion, J. Marceiller, F. Perez, C. Settegrana, A. Drechou, G. Durand, and C. Poüs, The Golgi complex is a microtubule-organizing organelle, Mol. Biol. Cell. **12**, 2047 (2001).

[69] S. Rivero, J. Cardenas, M. Bornens, and R.M. Rios, Microtubule nucleation at the cis-side of the Golgi apparatus requires AKAP450 and GM130, EMBO J. **28**, 1016 (2009).

[70] M.K.E. Schaefer, H. Schmalbruch, E. Buhler, C. Lopez, N. Martin, J.-L. Guénet, and G. Haase, Progressive motor neuronopathy: a critical role of the tubulin chaperone

TBCE in axonal tubulin routing from the Golgi apparatus, J. Neurosci. **27**, 8779 (2007).

[71] R. Roubin, C. Acquaviva, V. Chevrier, F. Sedjaï, D. Zyss, D. Birnbaum, and O. Rosnet, Myomegalin is necessary for the formation of centrosomal and Golgi-derived microtubules, Biol. Open **2**, 238 (2013).

[72] E.M. Mandelkow, E. Mandelkow, and R.A. Milligan, Microtubule dynamics and microtubule caps: a time-resolved cryo-electron microscopy study, J. Cell Biol. **114**, 977 (1991).

[73] R.I. Koning, S. Zovko, M. Bárcena, G.T. Oostergetel, H.K. Koerten, N. Galjart, A.J. Koster, and A. Mieke Mommaas, Cryo electron tomography of vitrified fibroblasts: microtubule plus ends in situ, J. Struct. Biol. **161**, 459 (2008).

[74] I.M. Jánosi, D. Chrétien, and H. Flyvbjerg, Modeling elastic properties of microtubule tips and walls, Eur. Biophys. J. **27**, 501 (1998).

[75] A. A. Hyman, S. Salser, D. Drechsel, N. Unwin, and T. J. Mitchison, Role of GTP hydrolysis in microtubule dynamics: information from a slowly hydrolyzable analogue, GMPCPP, Mol. Biol. Cell **3**, 10 (1992).

[76] M. Le Grand, La protéine Akt, lien entre mitochondries et microtubules dans le mécanisme d'action des agents anti-microtubules ou quand les MTA s'invitent dans de nouvelles stratégies thérapeutiques, Ph.D. thesis, Aix-Marseille (2015).

[77] H. C. Joshi, Microtubule organizing centers and γ-tubulin, Curr. Opin. Cell. Biol. **6**, 1 (1994).

[78] G. Pereira and E. Schiebel, Centrosome-microtubule nucleation, J. Cell. Sci. **110**, 3 (1997).

[79] R. L. Margolis and L. Wilson, Opposite end assembly and disassembly of microtubules at steady state in vitro, Cell. **13**, 1 (1978).

[80] R. L. Margolis and L. Wilson, Microtubule treadmills?possible molecular machinery, Nature **293**, 5835 (1981).

[81] G. Arpag, E. J. Lawrence, V. J. Farmer, S. L. Hall, and M. Zanic, Collective effects of XMAP215, EB1, CLASP2, and MCAK lead to robust microtubule treadmilling, Proc. Natl. Acad. Sci. U. S. A. **117**, 23 (2020).

[82] C. M. Waterman-Storer and E. D. Salmon, Microtubule dynamics: Treadmilling comes around again, Curr. Biol. **7**, 6 (1997).

[83] R. L. Margolis and L. Wilson, Margolis, Microtubule treadmilling: What goes around comes around, BioEssays **20**, 10 (1998).

[84] K. W. Farrell, M. A. Jordan, H. P. Miller, and L. Wilson, Phase dynamics at microtubule ends: The coexistence of microtubule length changes and treadmilling, J. Cell. Biol. **104**, 4 (1987).

[85] B. Franco, Régulation de la stabilité du cytosquelette microtubulaire: conséquences sur la croissance de la jonction neuromusculaire chez la Drosophile, Ph.D. thesis, Université Montpellier (2007).

[86] D. Chrétien, S. D. Fuller, and E. Karsenti, Structure of growing microtubule ends: two-dimensional sheets close into tubes at variable rates, J. Cell Biol. **129**, 5 (1995).

[87] D. Chretien, I. Jànosi, J.-C. Taveau, and H. Flyvbjerg, Microtubule's conformational cap, Cell Struct. Funct. **24**, 5 (1999).

[88] A. Molines, Organisation du Réseau Cortical de Microtubules chez Arabidopsis thaliana: Contribution des protéines EB1 et MAP65-1, Ph.D. thesis, Université Paris-Saclay, Préparée à l'Université Paris-Sud (2016).

[89] A. Guesdon, F. Bazile, R. M. Buey, R. Mohan, S. Monier, R. R. Garca, M. Angevin, C. Heichette, R. Wieneke, R. Tampe, L. Duchesne, A. Akhmanova, M. O. Steinmetz, and D. Chretin, Nat. Cell. Biol. **18**, 1102 (2016).

[90] F. M. Coquelle, B. Vitre, and I. Arnal, Structural basis of EB1 effects on microtubule dynamics, Biochem. Soc. Trans. **37**, 5 (2009).

[91] B. Vitre, F. M. Coquelle, C. Heichette, C. Garnier, D. Chrétien and I. Arnal, EB1 regulates microtubule dynamics and tubulin sheet closure in vitro, Nat. Cell Biol. **10**, 4 (2008).

[92] T. Mitchison and M. Kirschner, Microtubule assembly nucleated by isolated centrosomes, Nature **312**, 5991 (1984).

[93] A. A. Hyman, D. Chrétien, I. Arnal, and R. H. Wade, Structural changes accompanying GTP hydrolysis in microtubules: information from a slowly hydrolyzable analogue guanylyl-(alpha, beta)-methylene-diphosphonate, J. Cell. Biol. **128**, 1 117 (1995).

[94] R. Melki, M. Carlier, D. Pantaloni, and S. Timashe, Cold depolymerization of microtubules to double rings: geometric stabilization of assemblies, Biochemistry **28**, 9143 (1989).

[95] D. Chrétien and S. D. Fuller, Microtubules switch occasionally into unfavorable configurations during elongation, J. Mol. Biol. **298**, 663 (2000).

[96] V. Hunyadi, D. Chrétien, and I. M. Jánosi, Mechanical stress induced mechanism of microtubule catastrophes, J. Mol. Biol. **348**, 927 (2005).

[97] R. D. Sloboda, W. L. Dentler, and J. L. Rosenbaum, Microtubule-associated proteins and the stimulation of tubulin assembly in vitro, Biochemistry **15**, 4497 (1976).

[98] J. Olmsted, Microtubule-associated proteins, Annu. Rev. Cell Biol. **2**, 421 (1986).

[99] M. D. Weingarten, A. H. Lockwood, S.-Y. Hwo, and M. W. Kirschner, A protein factor essential for microtubule assembly, Proc. Natl. Acad. Sci. U.S.A. **72**, 1858 (1975).

[100] D. W. Cleveland, S.-Y. Hwo, and M. W. Kirschner, Purification of tau, a microtubule-associated protein that induces assembly of microtubules from purified tubulin, J. Mol. Biol. **116**, 207 (1977).

[101] S. A. Lewis, I. E. Ivanov, G.-H. Lee, and N. J. Cowan, Organization of microtubules in dendrites and axons is determined by a short hydrophobic zipper in microtubule-associated proteins MAP2 and tau, Nature **342**, 498 (1989).

[102] C. Scott, A. Klika, M. Lo, T. Norris, and C. Caputo, Tau protein induces bundling of microtubules in vitro: comparison of different tau isoforms and a tau protein fragment, J. Neurosci. Res. **33**, 19 (1992).

[103] Y. Kanai, J. Chen, and N. Hirokawa, Microtubule bundling by tau proteins in vivo: analysis of functional domains, EMBO J. **11**, 3953 (1992).

[104] S. Kar, J. Fan, M. J. Smith, M. Goedert, and L. A. Amos, Repeat motifs of tau bind to the insides of microtubules in the absence of taxol, EMBO J. (2003).

[105] R. A. Santarella, G. Skiniotis, K. N. Goldie, P. Tittmann, H. Gross, E.-M. Mandelkow, E. Mandelkow, and A. Hoenger, Surface-decoration of microtubules by human tau, J. Mol. Biol. **339**, 539 (2004).

[106] D. N. Drechsel, A. Hyman, M. H. Cobb, and M. Kirschner, Modulation of the dynamic instability of tubulin assembly by the microtubule-associated protein tau, Mol. Biol. Cell. **3**, 1141 (1992).

[107] S. Barlow, M. L. Gonzalez-Garay, R. R. West, J. B. Olmsted, and F. Cabral, Stable expression of heterologous microtubule-associated proteins (MAPs) in Chinese hamster ovary cells: evidence for differing roles of MAPs in microtubule organization, J. Cell. Biol. **126**, 1017 (1994).

[108] B. Trinczek, J. Biernat, K. Baumann, E.-M. Mandelkow, and E. Mandelkow, Domains of tau protein, differential phosphorylation, and dynamic instability of microtubules, Mol. Biol. Cell. **6**, 1887 (1995).

[109] J.-H. Cho and G. V. Johnson, Glycogen synthase kinase 3β phosphorylates tau at both primed and unprimed sites: differential impact on microtubule binding, J. Biol. Chem **278**, 187 (2003).

[110] G. Lindwall and R. D. Cole, Phosphorylation affects the ability of tau protein to promote microtubule assembly, J. Biol. Chem **259**, 5301 (1984).

[111] R. D. Vale, T. S. Reese, and M. P. Sheetz, Identification of a novel force-generating protein, kinesin, involved in microtubule-based motility, Cell **42**, 39 (1985).

[112] N. Hirokawa, Y. Shiomura, and S. Okabe, Tau proteins: the molecular structure and mode of binding on microtubules, J. Cell Biol. **107**, 1449 (1988).

[113] T. A. Schroer and M. P. Sheetz, Functions of microtubule-based motors, Annual review of physiology **53**, 1 (1991).

[114] R. B. Vallee, J. C. Williams, D. Varma, and L. E. Barnhart, Dynein: An ancient motor protein involved in multiple modes of transport, J. Neurobiol. **58**, 189 (2004).

[115] W. Steffen, S. Karki, K. T. Vaughan, R. B. Vallee, E. L. Holzbaur, D. G. Weiss, and S. A. Kuznetsov, The involvement of the intermediate chain of cytoplasmic dynein in binding the motor complex to membranous organelles of Xenopus oocytes, Mol. Biol. Cell. **8**, 2077 (1997).

[116] F. Nagano, S. Orita, T. Sasaki, A. Naito, G. Sakaguchi, M. Maeda, T.Watanabe, E. Kominami, Y. Uchiyama, and Y. Takai, Interaction of Doc2 with tctex-1, a light chain of cytoplasmic dynein: implication in dynein-dependent vesicle transport, J. Biol. Chem. **273**, 30065 (1998).

[117] Y.-K. Mok, K. W.-H. Lo, and M. Zhang, Structure of Tctex-1 and its interaction with cytoplasmic dynein intermediate chain, J. Biol. Chem. **276**, 14067 (2001).

[118] S. C. Schuyler and D. Pellman, Microtubule "plus-end-tracking proteins": the end is just the beginning, Cell. **105**, 421 (2001).

[119] J. R. McIntosh, E. L. Grishchuk, and R. R. West, Chromosome-microtubule interactions during mitosis, Annu. Rev. Cell. Dev. Biol. **18**, 193 (2002).

[120] J. W. VOS, Microtubule become more dynamic but not shorter during preprophase band formation: a possible "search-and-capture" mechanism for microtubule translocation, Cell. Motil. Cytoskeleton **38**, 278 (2003).

[121] R. Wollman, E. Cytrynbaum, J. Jones, T. Meyer, J. Scholey, and A. Mogilner, Efficient chromosome capture requires a bias in the 'search-and-capture'process during mitotic-spindle assembly, Curr. Biol. **15**, 828 (2005).

[122] A. A. Hyman and T. J. Mitchison, Two different microtubule-based motor activities with opposite polarities in kinetochores, Nature **351**, 206 (1991).

[123] D. J. Sharp and G. C. Rogers, A Kin I-Independent Pacman: Flux Mechanism for Anaphase A, Cell. Cycle **3**, 705 (2004).

[124] J. M. Vasiliev, I. Gelfand, L. Domnina, O. Y. Ivanova, S. Komm, and L. Olshevskaja, Effect of colcemid on the locomotory behaviour of fibroblasts, Development **24**, 625 (1970).

[125] A. Zlotnik, A. M. Burkhardt, and B. Homey, Homeostatic chemokine receptors and organ-specific metastasis, Nat. Rev. Immunol. **11**, 597 (2011).

[126] M. L. de Heredia and R.-P. Jansen, mRNA localization and the cytoskeleton, Curr. Opin. Cell. Biol. **16**, 80 (2004).

[127] H. Stebbings, Cytoskeleton-dependent transport and localization of mRNA, Int. Rev. Cytol. **211**, 1 (2001).

[128] I. R. Boldogh and L. A. Pon, Mitochondria on the move, Trends Cell. Biol. **17**, 502 (2007).

[129] L. Buée, T. Bussièr, V. Buée-Scherrer, A. Delacourte, and P. R. Hof, Tau protein isoforms, phosphorylation and role in neurodegenerative disorders, Brain Res. Rev. **33**, 95 (2000).

[130] A. Delacourte and L. Buée, Tau pathology: a marker of neurodegenerative disorders, Curr. Opin. Neurol. **13**, 371 (2000).

[131] V. M. Lee, M. Goedert, and J. Q. Trojanowski, Neurodegenerative tauopathies, Annu. Rev. Neurosci. **24**, 1121 (2001).

[132] A. Alzheimer, Uber eigenartige Erkrankung der Hirnrinde, Allg. Z. Psychiatr. **64**, 146 (1907).

[133] M. Hafezparast, R. Klocke, C. Ruhrberg, A. Marquardt, A. Ahmad-Annuar, S. Bowen, G. Lalli, A. S. Witherden, H. Hummerich, S. Nicholson, et al., Mutations in dynein link motor neuron degeneration to defects in retrograde transport, Mutations in dynein link motor neuron degeneration to defects in retrograde transport, Science **300**, 808 (2003).

[134] K. Ikenaka, M. Katsuno, K. Kawai, S. Ishigaki, F. Tanaka, and G. Sobue, Disruption of axonal transport in motor neuron diseases, Int. J. Mol. Sci. **13**, 1225 (2012).

[135] S. K. Dutcher, The tubulin fraternity: alpha to eta, Curr. Opin. Cell. Biol. **13**, 49 (2001).

[136] N. Hirokawa, S. Niwa, and Y. Tanaka, Molecular motors in neurons: transport mechanisms and roles in brain function, development, and disease, Neuron **68**, 610 (2010).

[137] B. H. LaMonte, K. E. Wallace, B. A. Holloway, S. S. Shelly, J. Asca no, M. Tokito, T. Van Winkle, D. S. Howland, and E. L. Holzbaur, Disruption of dynein/dynactin inhibits axonal transport in motor neurons causing late-onset progressive degeneration, Neuron **34**, 715 (2002).

[138] M. Fliegauf, T. Benzing, and H. Omran, When cilia go bad: cilia defects and ciliopathies, Nat. Rev. Mol. Cell. Biol. **8**, 880 (2007).

[139] J. S. Russell, Report on Waves, Report of the fourteenth Meeting of the British Association for the Advancement of Science, John Murray, Londres, 311 (1844).

[140] D. J. Korteweg, G. De Vries, On the change of form of long waves advancing in a rectangular canal and on a new type of long stationary waves, Philosophical Magazine 5th Series **36**, 422 (1895).

[141] E. Fermi, J. Pasta, S. Ulam, Studies of nonlinear problems. Los Alamos report, LA - 1940 (1955).

[142] N. J. Zabusky, M. D. Kruskal, Interaction of solitons in a collisionless plasma and the recurrence of initial states, Phys. Rev. Lett. **15**, 240 (1965).

[143] A. C. Newell, Nonlinear tunelling, J. Math. Phys. **19**, 1126 (1978).

[144] D.J. Korteweg and G. de Vries, On the change of form of long waves advancing in a rectangular canal, and on a new type of long stationary waves, Phil. Mag., **39**, 422-443 (1895).

[145] T. Dauxois and M. Peyrard, Physics of Solitons, Cambridge University Press, Cambridge, (2006).

[146] M. Peyrard and T. Dauxois. Wave called soliton, (1994).

[147] R. H. Enns, It a Nonlinear World, Springer, New York, (2011).

[148] N. Akhmediev and A. Ankiewicz, Dissipative solitons, Springer, (2005).

[149] M. Brambilla, L.A. Lugiato, F. Prati, L. Spinelli, and W.J. Firth, Transverse laser patterns. I. Phase singularity crystals, Phys. Rev. Lett.**79**, 2042 (1997)

[150] J.C. Misra and M.K. Patra, Nonlinear analysis of blood flow in a stenosed artery under an external magnetic field, Comput. Math. Appl. **54**, 242 (2007).

[151] T. Heimburg and A.D. Jackson, A thermodynamic approach to understanding the influence of lipid composition on membrane properties, Proc. Natl. Acad. Sci. U.S.A. **102**, 9790 (2005).

[152] T. Heimburg and A.D. Jackson, The thermal properties of lipid membranes and phase transitions: A thermodynamic approach, Biophys. Rev. Lett. **2**, 57 (2007).

[153] A. L. Hodgkin and A. F. Huxley, A quantitative description of membrane current and its application to conduction and excitation in nerve, J. Physiol. **117**, 500 (1952).

[154] D. H. Peregrine, Water waves, nonlinear Schrödinger equations and their solutions, J. Aust. Math. Soc. Ser. B **25**, 16-43 (1983).

[155] E. Tankou, C. B. Tabi, and T. C. Kofané, Soliton-mediated ionic pulses and coupled ionic excitations in a dissipative electrical network model of microtubules, Chaos Solitons Fractals. **162**, 112446 (2022).

[156] C. B. Tabi, A. Mohamadou, and T. C. Kofané, Modulational instability and pattern formation on DNA dynamics with viscosity, J. Comput. Theor. Nanosci. **5**, 647 (2008).

[157] C. B. Tabi, A. Mohamadou, and T. C. Kofané, Modulational instability in DNA model with competing short- and long-range dispersive interactions, J. Bionanoscience **2**, 89 (2008).

[158] H. Ngoubi, G. H. Ben-Bolie, and T. C. Kofané, Charge transport in a DNA model with solvent interaction, J. Biol. Phys. **44**, 483 (2018).

[159] A. Mvogo, G. H. Ben-Bolie, and T. C. Kofané, Long-range interactions in a-helical proteins with interspine coupling: Modulational instability and exact soliton solutions, Eur. Phys. J. B **86**, 10.1140/epjb/e2013-40517-1 (2013).

[160] C. B. Tabi, A. Mohamadou, and T. C. Kofané, Wave propagation of nonlinear modes and formation of bubble in a two-component helicoidal lattice, J. Bionanoscience **2**, 1 (2008).

[161] C. B. Tabi, A. Mohamadou, and T. C. Kofané, Phys. Lett. Sect. A Gen. At. Solid State Phys. **373**, 2476 (2009).

[162] B. P. Edouma Biloa, C. B. Tabi, H. P. Ekobena Fouda, and T. C Kofané, Nonlinear dissipative wave trains in a system of self-propelled particles, Phys. Scr. **98**, 10.1088/1402-4896/acfb46 (2023).

[163] E. Armand Sylvin, Consistency between modulational instability and energy localization in time-delay-memristive neural network, Pap. Knowl. Towar. a Media Hist. Doc. **143**, 42002 (2023).

[164] Y. S. Kivshar and M. Peyrard, Modulational instabilities in discrete lattices, Phys. Rev. A **46** (1992).

[165] M. V. Satarić, J. A. Tuszyński, and R. B. Akula, Kinklike excitations as an energy-transfer mechanism in microtubules, Phys. Rev. E **48**, 589 (1993).

[166] M. Satarić, D. Koruga, Z. Ivić, and R. B. Žakula, The detachment of dimers in the tube of microtubulin as a result of a solitonic mechanism, J. Mol. Electron. **6**, 63 (1990).

[167] M. A. Collins, A. Blumen, J. F. Currie, and J. Ross, Dynamics of domain walls in ferrodistortive materials. I. Theory, Phys. Rev. B **19**, 3630 (1979).

[168] S. Zeković, A. Muniyappan, S. Zdravković, and L. Kavitha, Employment of Jacobian elliptic functions for solving problems in nonlinear dynamics of microtubules, Chinese Phys. B **23**, 10.1088/1674-1056/23/2/020504 (2014).

[169] S. Zdravković, L. Kavitha, M. V. Satarić, S. Zeković, and J. Petrović, Modified extended tanh-function method and nonlinear dynamics of microtubules, Chaos, Solitons and Fractals **45**, 1378 (2012).

[170] S. Zdravković, M. V. Satarić, and S. Zeković, Employment of Jacobian elliptic functions for solving problems in nonlinear dynamics of microtubules, EPL **102**, 38002 (2013).

[171] S. Zdravković, M. V. Satarić and S. Zeković, Nonlinear dynamics of microtubules - A longitudinal model, EPL **102**, 3 (2013).

[172] M. V. Satarić and J. A. Tuszyński, Relationship between the nonlinear ferroelectric and liquid crystal models for microtubules, Phys. Rev. E - Stat. Physics, Plasmas, Fluids, Relat. Interdiscip. Top. **67**, 11 (2003).

[173] S. Zdravković, S. Zeković, A. N. Bugay, and M. V. Satarić, Localized modulated soliton, Microtubule, Nonlinear Schrödinger equation, Semi-discrete approximation, Appl. Math. Comput. **285**, 248 (2016).

[174] L. A. Amos and D. Schlieper, Microtubules and maps, Advances in protein chemistry **71**, 257 (2005).

[175] N. R. Watts, N. Cheng, W. West, A. C. Steven, and D. L. Sackett, The cryptophycin-tubulin ring structure indicates two points of curvature in the tubulin dimer, Biochemistry **41**, 12662 (2002).

[176] P. Drabik, S. Gusarov, and A. Kovalenko, Microtubule stability studied by three-dimensional molecular theory of solvation, Biophys. J **92** (2007).

[177] M. V. Satarić, L. Matsson, and J. A. Tuszyński, Complex movements of motor protein relay helices during the power stroke, Physical Review E **74**, 051902 (2006).

[178] R. Priya, L. Kavitha, and D. Gopi, Dynamic instability in neuronal microtubules, Mater. Today Proc. **26**, 3552 (2019).

[179] M. Remoissenet, Low-amplitude breather and envelope solitons in quasi-one-dimensional physical models, Phys. Rev. B **33**, 2386 (1986).

[180] I. Daumont, T. Dauxois, and M. Peyrard, Modulational instability: first step towards energy localization in nonlinear lattices, Nonlinearity **10**, 617 (1997).

[181] I. Kourakis, V. Basios, and P. K. Shukla, Intrinsic localized modes in dust lattices, ArXiv (2004).

[182] G. P. Agrawal, Nonlinear Fiber Optics, in Nonlinear Sci. Daw. 21st Century (Springer Berlin Heidelberg, 2007) pp. 195-211.

[183] F. I. Ndzana, A. Mohamadou, and T. C. Kofané, Discrete Lange-Newell criterion for dissipative systems, Physical Review E **79**, 056611 (2009).

[184] C. B. Tabi, A. Mohamadou, and T. C. Kofané, Discrete instability in the DNA double helix, Chaos **19**, 4 (2009).

[185] H. E. Fouda, C. Tabi, A. Mohamadou, and T. Kofané, Intramolecular vibrations and noise effects on pattern formation in a molecular helix, Journal of Physics: Condensed Matter **23**, 375104 (2011).

[186] R. Ondoua, C. Tabi, H. Ekobena Fouda, A. Mohamadou, and T. Kofané, Discrete energy transport in the perturbed Ablowitz-Ladik equation for Davydov model of α-helix proteins, Eur. Phys. J. B **85**, 1 (2012).

[187] J. M. Fewu, C. Tabi, H. Edongue, H. E. Fouda, and T. Kofané,vWave patterns in α-helix proteins with interspine coupling, Phys. Scr. **87**, 025801 (2013).

[188] A. Mvogo, G. H. Ben-Bolie, and T. C. Kofané, Discrete energy transport in collagen molecules, Chin. Phys. B **23**, 098701 (2014).

[189] K. Tai, A. Hasegawa, and A. Tomita, Observation of modulational instability in optical fibers, Phys. Rev. Lett. **56**, 135 (1986).

[190] G. B. Whitham, Non-linear dispersive waves, Proc. R. Soc. London. Ser. A. Math. Phys. Sci. **283**, 238 (1965).

[191] T. B. Benjamin and J. E. Feir, The disintegration of wave trains on deep water Part 1. Theory, J. Fluid Mech. **27**, 417 (1967).

[192] M. Peyrard and A. R. Bishop, Statistical mechanics of a nonlinear model for DNA denaturation, Phys. Rev. Lett. **62**, 2755 (1989).

[193] Y. S. Kivshar, Nonlinear localized modes in inhomogeneous chains, Physics Letters A **161**, 80 (1991).

[194] A. Sievers and S. Takeno, Intrinsic localized modes in anharmonic crystals, Phys. Rev. Lett. **61**, 970 (1988).

[195] S. Takeno, K. Kisoda, and A. Sievers, Intrinsic localized vibrational modes in anharmonic crystals: stationary modes, Progress of Theoretical Physics Supplement **94**, 242 (1988)

[196] B. Heidelberg, Integrability, Lect. Notes Phys. 767, Springer Berlin Heidelberg **737** (2009).

[197] R. Hirota, The Direct Method in Soliton Theory, Cambridge University Press, New York (2004).

[198] E. Kengne and R. Vaillancourt, Transmission of solitary pulse in dissipative nonlinear transmission lines, Commun. Nonlinear Sci. Numer. Simul. **14**, 3804 (2009).

[199] Kazuhiro Nozaki and Naoaki Bekki, Exact Solutions of the Generalized Ginzburg-Landau Equation, J. Phys. Soc. Japan **53**, 1581 (1984).

[200] G. A. Zakeri and E. Yomba, J. Phys. Soc. Japan **82**, 1 (2013).

[201] W. Liu, W. Yu, C. Yang, M. Liu, Y. Zhang, and M. Lei, Nonlinear Dyn. **89**, 2933 (2017).

[202] E. Yomba, T. C. Kofané, and F. B. Pelap, J. Phys. Soc. Japan **65**, 2337 (1996).

[203] F. B. Pelap, T. C. Kofané, N. Flytzanis, and M. Remoissenet, J. Phys. Soc. Japan **70**, 2568 (2001).

[204] J. Pokornỳ, F. Jelinek, V. Trkal, I. Lamprecht, and R. Hölzel, Vibrations in Microtubules, Journal of Biological Physics **23**, 171 (1997).

[205] J. E. Schoutens, Dipole-dipole interaction in microtubules, J. Biol. Phys. **31**, 35 (2005).

[206] S. Zdravković, A. N. Bugay, G. F. Aru, and A. Maluckov, Localized modulated waves in microtubules, Chaos **24**, 2 (2014).

[207] J. Pokornỳ and J. Vrba, Generation of electromagnetic field by microtubules, Int. J. Mol. Sci. **22**, 15 (2021).

[208] S. Zdravković, S. Zeković, A. N. Bugay, and J. Petrović, Chaos, Two component model of microtubules and continuum approximation, Chaos Solitons Fractals **152**,111352 (2021).

[209] H. D. Wahlquist and F. B. Estabrook, Prolongation structures of nonlinear evolution equations, J Math. Phys. **16**, 1 (1975).

[210] A. Pickering, The Mangle of Practice: Time, Agency, and Science, J. Phys. A Math. Gen **26**, 17 (1993).

[211] A. H. He and L. N. Zhang, Large lateral optical beam displacements due to surface plasmon resonance, Phys. Lett. A **372**, 1044 (2008).

[212] Ondoua, R. Y. and Mimshe Fewu, J. C. and Belobo Belobo, D. and Tabi, C. B. and Ekobena Fouda, H. P., Excitons dynamic in a three-stranded α-helix protein chains with diagonal and off-diagonal couplings: effects of strong long-range interactions, Eur. Phys. J. Plus **136**, 3 (2021).

[213] S. Issa, C. B. Tabi, H. P. Ekobena and T. C. Kofane, Three excitons states in non-linear saturation α-helix protein, Eur. Phys. J. Plus **233**, 233 (2018).

[214] Naher, Hasibun and Abdullah, Farah Aini, The Basic (G'/G)-expansion method for the fourth order Boussinesq equation, Appl. Math. **3**, 10 (2012).

[215] J. R. Bogning, D. T. C. Djeumen, T. C. Kofané, Construction of the Soliton Solutions of the Ginzburg-Landau Equations by the New Bogning-Djeumen Tchaho-Kofané Method, Phys. Scr. **20**, 025013 (2012).

[216] J. R. Bogning, D. T. C. Djeumen, T. C. Kofane, Generalization of the Bogning-Djeumen Tchaho-Kofané method for the construction of the solitary waves and the survey of the instabilities, Far East J. Dyn. Syst. **20**, 101 (2012).

[217] L. Pimonow, Modulation d'ondes stationnaires ultra-sonores dans l'air, Annales Des Télécommunications **9**, (1954).

[218] P. Minotti and V. Nocton, Etude théorique d'un microtranslateur piezoelectrique à ondes stationnaires: une introduction aux futurs micromoteurs multi degrés de liberté, Mechanism and machine theory **31**, 1 (1996).

[219] P. Minotti and V. Nocton Etude théorique d'un microtranslateur piezoelectrique à ondes stationnaires: une introduction aux futurs micromoteurs multi degrés de liberté, Mechanism and machine theory **31**, 1 (1996).

[220] J. Pouget, M. Remoissenet, J. M. Tamga, Energy self-localization and gap local pulses in a two-dimensional nonlinear lattice, Phys. Rev. B **47**, 14866 (1993).

[221] A. Kolman, Epothilone D (Kosan/Roche), Current opinion in investigational drugs (London, England: 2000) **5**, 6 (2004).

[222] H. Wang, Z. Wang, S. Wang, M. Li, L. Nan, J. K. Rhie, J. M. Covey, R. Zhang, D. L. Hill, Preclinical pharmacology of epothilone D, a novel tubulin-stabilizing antitumor agent, Cancer Chemoth. Pharm. 56, 255 (2005).

[223] S. Zdravković, M. V. Satarić, and V. Sivčević, General model of microtubules, Nonlinear Dyn. **92**, 479 (2018).

[224] S. Zdravković, A. N. Bugay, G. F. Aru and A. Maluckov, Localized modulated waves in microtubules, Chaos **24**, 2 (2014).

[225] S. Latifah, S. F. Rohmah, I. A. Ramadhan, D. Dwiputra, W. Hidayat and F. P. Zen, The solvent effect on the nonlinear dynamics of U-model microtubules, J. Phys. Conf. Ser. **1204**, 1 (2019).

[226] A. Desai and T. J. Mitchison, Microtubules polymerization dynamics, Annu. Rev. Cell. Dev. Biol. **13**, 83 (1997).

[227] Z. Wang, H. Wang, J. K. Rhie, J. M. Covey, P. Liang, S. Wang, C. Wang, Y. Hu, G. Prasad, L. Nan, D. L. Hill, and R. Zhang, Development and validation of a liquid chromatography-tandem mass spectrometry method for the determination of paclitaxel in human plasma, J. Pharm. Biomed. Anal. **42**, 272 (2006).

List of publications

1. **R. Tabapsi Kamdem**, D. Belobo Belobo, A. Dang Koko, C. B. Tabi, and T. C. Kofané, "*Energy Localization in Microtubules with Radial Dislocation*" Eur. Phys. J. Plus **138**, 1 (2023).

2. **R. Tabapsi Kamdem**, D. Belobo Belobo, C. D. Bansi Kamdem, A. Dang Koko, C. B. Tabi, and T. C. Kofané, "*Nonlinear dynamics effect of viscosity of cytosol into the microtubules and exact solutions*" Commun. Nonlinear. Sci. Numer. Simulat. **143**, 108615 (2025).

Eur. Phys. J. Plus (2023) 138:433
https://doi.org/10.1140/epjp/s13360-023-04051-9

THE EUROPEAN PHYSICAL JOURNAL PLUS

Regular Article

Energy localization in microtubules with radial dislocation

R. Tabapsi Kamdem[1,2,a], **D. Belobo Belobo**[1,2,3], **A. Dang Koko**[1,2,4], **C. B. Tabi**[5], **T. C. Kofané**[1,5]

[1] Laboratory of Biophysics, Department of Physics, Faculty of Science, University of Yaounde I, P.O. Box 812, Yaounde, Cameroon
[2] African Centre for Advanced Studies, P.O. Box 4477, Yaounde, Cameroon
[3] Department of Mathematics and Physical Sciences, National Advanced School of Engineering of Yaounde, University of Yaounde I, P.O. Box 8390, Yaounde, Cameroon
[4] Departement of maintenance, Higher Technical Teachers' Training College, University of Ebolowa, P.O. Box 886, Ebolowa, Cameroon
[5] Department of Physics and Astronomy, Botswana University of Science and Technology, Private Bag 16, Palapye, Botswana

Received: 13 April 2022 / Accepted: 28 April 2023

Abstract In this study, we investigate the dynamics of microtubules in the presence of the cytosol viscosity using a discrete radial dislocations model. Applying the semi-discrete approximation, the discrete model is first converted into its continuous counterpart which is nothing else but the cubic Complex Ginzburg–Landau equation. Performing a linear stability analysis of plane waves, it is shown that the cytosol viscosity modifies the modulation instability of the system by enlarging the width of unstable zones but softens the instability as it shrinks the growth rate of instability. Furthermore, motivated by the existence of a range of biological processes during which microtubules exhibit a stationary behavior, we look for stationary state solutions and first apply a direct method to the cubic Complex Ginzburg–Landau equation. Coming back to the original discrete model, we show that both bright and anti-dark profiles solitary waves are good candidates likely to explain biological mechanisms that necessitate stationary microtubules. Our analytical predictions are corroborated by intensive numerical simulations with a pretty high accuracy. By providing system parameters related to obtaining stationary states, our work may find applications in targeted microtubules drugs that aim to stabilize cells growth like cancers.

1 Introduction

Eukaryotic cells are structurally and dynamically organized by a network of protein polymers called the cytoskeleton [1]. The cytoskeleton is organized as a framework consisting of three types of well-organized structures that extend throughout the cytoplasm, namely microfilaments, actin filaments and largely microtubules (MTs). MTs are defined as a network of proteins that are superimposed on each other in the form of dimers. They are present in all eukaryotic cells, where they have a wide range of tasks such as maintaining and protecting cell structures and are involved in a large number of biological processes such as cell division and motility. They also serve as transport networks for motor proteins and intracellular organelles [2]. MTs result from the assembly of α and β tubulins, which are composed of positive and negative electric charges. The association of these sub-units leads to the formation of dimers each of length 8 nm [3, 4]. The addition of dimers along the length leads to the formation of a protofilament (PF), whose reconstitution in a helical manner yields to the formation of a MT, with internal and external diameters are 15 and 25 nm, respectively. Given their different functions, the propagation of waves along MTs is a fundamental concern and relies on the hydrolysis of guanosine triphosphate (GTP) which releases energy. According to recent theoretical results, it is believed that energy propagates through MTs as solitary waves [5]. We recall that solitary waves are approximate analytical solutions of nonintegrable partial differential equations that are localized with respect to the transverse variable(s) while solitons are exact solutions of integrable nonlinear partial differential equations localized with respect to the transverse variable(s) which collide elastically except a phase shift that might appear after the collision [6].

In general, all physical systems can be considered open due to interaction with the environment [7]. The cytosol in which the cellular organelles are immersed in represents the environment that directly affects the dynamics of the MT via its viscosity and shear strength which are firmly linked to the concept of rheology where temperature plays an important role [8]. In 2000, Foster **et al.** [9] studied the effect of viscosity on vibrations in MTs and reported that electrical signals from yeast cells at 8.18 MHz with an extremely narrow bandwidth (< 0.01 MHz) correspond to MT oscillations. Using the so-called φ-model (though we choose for convenience to denote φ by χ below), Zdravkovic et al. [10] showed that the nonlinear dynamic of MTs can be explained by a kink soliton moving through the MTs. Elaborating on the coupled modes theory and in the absence of the cytosol viscosity, it has been shown that the polymerization and depolymerization mechanisms are better described by coupled nonlinear waves [11]. The temperature

[a] e-mail: rostandtabapsi@gmail.com (corresponding author)

Published online: 22 May 2023

substantially modifies the cytosol viscosity hence giving rise to hybrid solitons [12]. Assuming that the cytosol viscosity and the dipole moment direction depend on both internal and external factors, it was revealed that the viscosity dampens the vibrational processes while the oscillations of the tubules become harmonically damped only in certain areas on the equal frequency maps [13]. It was suggested that the variation of the cytosol viscosity deeply alters the MTs polymerization in depolymerization processes [14]. It is clear from the above results that the cytosol viscosity plays an important role on the dynamics of MTs. In particular, it is expected that nonlinear waves that explain the dynamics of MTs are affected by the cytosol viscosity. Indeed, taking into account the cytosol viscosity, the original MT partial differential equation was converted into the conservative nonlinear Schrödinger equation whose breather solitons have been used to explain the MTs dynamics [15]. Instead of casting the original equation into a nonlinear Schrödinger type equation in order to exploit its known solution, direct approaches may be used to find other profile solutions like bright and antikink solitary waves [10, 16]. The dynamics of the MTs is governed by a nonlinear partial differential equation, which in principle, admits a large number of solutions that remain to be constructed. Apart from the above few analytical solutions [10, 15, 16], the dynamics of the MTs is not spill out in details. Other nonlinear wave structures are still awaiting to be unveiled. On the other hand, it is well known that the modulation instability (MI) mechanism is a very good tool to easily activate solitary waves in different media like DNA, proteins, active matter [19] and Bose-Einstein condensates [20], to name just a few. The effect of the cytosol viscosity on the MI of MTs needs to be clarified. The aim of the current work is to fill in our gap on the knowledge of the influence of the cytosol viscosity on the MI of MTs. In addition, we construct new solitary wave solutions that explain the dynamics of MTs in the presence of the cytosol viscosity which, in fact, does not affect the dynamics of the MT.

The rest of the manuscript is organized as follows. In Sect. 2, starting from a MT Hamiltonian, we first derive the discrete nonlinear differential equation that governs the dynamics of MTs in the presence of the cytosol viscosity. Then, after performing a linear perturbation, we analyze the impact of cytosol viscosity on MI of MTs. Applying the direct ansatz method, analytical solutions with bright and anti-dark profiles are constructed and their main characteristics analyzed in Sect. 3. It is shown that the cytosol viscosity does not affect any characteristic of the stationary solitary waves constructed. Numerical simulations performed corroborate there analytical counterparts with a pretty high accuracy. The manuscript is concluded in Sect. 4.

2 Model and analytical prediction of MI

2.1 The model

In order to derive the equation of motion that governs the dynamic of a dimer in a PF of the MT, we start by writing the Hamiltonian given by [10]

$$H = \sum_n \left[\frac{I}{2} \dot{\chi_n}^2 + \frac{K}{2} (\chi_{n+1} - \chi_n)^2 + pE \left(\frac{\chi_n^2}{2} - \frac{\chi_n^4}{24} - 1 \right) \right]. \tag{1}$$

In Eq. (1), χ_n represents the angular displacement of a dimer at site n from its equilibrium position. The dot over χ_n accounts for a derivation with respect to time t. $I = mL^2/12$ is the moment of inertia of each dimer where $m = 1.8 \times 10^{-22}$ kg is the mass of the dimer [21] and $L = 8$ nm its length [10]. $K = 0.1$ eV [11] is an intra-dimer stiffness parameter, $p = 337$ Debye $= 1.13 \times 10^{-27}$ Cm [22] is the electric dipole moment, and $pE = 0.25$ eV where E ($E = 4 \times 10^7$ V/m) is the intrinsic electric field strength. The order of magnitude is given in [15, 23] such that $p, E > 0$. The physical meaning of the terms in the right-hand side of Eq. (1) is as follows. The first term accounts for the kinetic energy, the second one describes the chemical potential energy of two neighboring dimers that belong to the same PF, and the last term is the dipole-dipole potential energy of the dimer χ_n. The Hamiltonian (1) corresponds to a conservative system. The cytosol viscosity which is a damping term may be included in the dynamics by considering the viscosity momentum $M_v = -\Gamma \dot{\chi_n}$, where Γ represents the viscosity coefficient [10]. Applying the Hamilton–Jacobi formalism, one derives the equation of motion satisfied by the dimer as [10]

$$\ddot{\chi_n} + \varepsilon \dot{\chi_n} = \alpha (\chi_{n+1} - 2\chi_n + \chi_{n-1}) + \omega_g^2 (a \chi_n^3 - \chi_n), \tag{2}$$

with $\alpha = \frac{K}{I}$, $\omega_g^2 = pE/I$, $\varepsilon = \frac{\Gamma}{I}$ and $a = \frac{1}{6}$. α measures the potential energy of the chemical bonds during their rotation; ω_g is the lowest cut-off frequency where pE plays a decisive role in stabilizing PFs and the MT itself, hence has a stabilizing effect on the polymerization [10]. We neglect the nonlinear terms and the viscosity in Eq. (2) by introducing the expression $\chi_n(t) = \propto e^{i(qn-\omega t)}$, and the resulting dispersion relation is given by

$$\omega^2 = \omega_g^2 + 4\alpha \sin^2\left(\frac{q}{2}\right), \tag{3}$$

where ω is the linear angular frequency and q is an angle.

Insights on the dynamics of MTs rely on analytical solutions of Eq. (2), but only a few of them are available in the existing literature [10, 15, 16]. To obtain deeper insights in Eq. (2), we start by assuming that χ_n is a slowly modulated wave of the original nonlinear problem Eq. (1) whose frequency is in the linear band such that one may write

$$\chi_n(t) = F_n(t) e^{-i\omega_g t} + F_n^*(t) e^{i\omega_g t}. \tag{4}$$

$F_n(t)$ and $F_n(t)^*$ are complex conjugate functions assumed to vary slowly in time with respect to the main oscillation at frequency ω_g, i.e., $\dot{\chi_n} \ll \omega_g\, \chi_n$ [17]. Inserting Eq. (4) into Eq. (2) and applying the so-called rotating-wave approximation, after a few algebra, leads to the discrete cubic complex Ginzburg–Landau (CGL) equation satisfied by $F_n(t)$

$$(\varepsilon - 2\,i\,\omega_g)\,\dot{F_n} - \alpha\left[F_{n+1} - 2\,F_n + F_{n-1}\right] - 3\,a\,\omega_g^2\,|F_n|^2\,F_n - i\,\varepsilon\,\omega_g\,F_n = 0. \tag{5}$$

2.2 Analytical prediction of MI

In this part of the work, we analyze the MI of the CGL Eq. (5) since we expect it may manifest itself in Eq. (2). To this end, we first look for plane wave solutions of Eq. (5) in the form

$$F_n(t) = \phi_0\, \exp[i\,(q\,n - \omega_0\,t)], \tag{6}$$

q, ω_0 and ϕ_0 represent an angle, the angular frequency and amplitude of the wave, respectively, $\omega_0 = -\omega_g$ and all are related by the nonlinear dispersion relation

$$-\omega_0\,(2\,\omega_g + i\,\varepsilon) + 4\,\alpha\,\sin^2\left(\frac{q}{2}\right) - 3\,a\omega_g^2\,|\phi_0|^2 - i\,\omega_g\,\varepsilon = 0. \tag{7}$$

Eq. (7) is verified if and only if $\phi_0^2 > 4$. To examine the linear stability of the initial plane wave, we slightly disturb both its amplitude and phase and look for a solution in the form

$$F_n(t) = [(\phi_0 + b_n(t))]e^{i\,\psi_n(t) + i\,\theta_n(t)} \tag{8}$$

where $\theta_n(t) = qn - \omega_0 t$. Assuming that $|b_n(t)| \ll |\phi_0|$ and $|\psi_n(t)| \ll |\theta_n(t)|$ [17, 18], we introduce Eq. (8) into Eq. (5), then separating the real and imaginary parts, we obtain

$$\begin{aligned}
\dot{b_n} &= N_1\,b_n + N_2\,(b_{n+1} - 2b_n + b_{n-1}) \\
&\quad + N_3(\psi_{n+1} - 2\psi_n + \psi_{n-1}) + N_4\,(b_{n+1} - b_{n-1}) \\
&\quad + N_5\,(\psi_{n+1} - \psi_{n-1}) \\
\dot{\psi_n} &= P_1\,b_n + P_2\,(b_{n+1} - 2b_n + b_{n-1}) \\
&\quad + P_3(\psi_{n+1} - 2\psi_n + \psi_{n-1}) + P_4\,(b_{n+1} - b_{n-1}) \\
&\quad + P_5\,(\psi_{n+1} - \psi_{n-1}).
\end{aligned} \tag{9}$$

In Eq. (9), coefficients N_i, P_i $(i = 1, \cdots, 8)$ are provided in Appendix (A) as well as a full derivation of the perturbed equation Eq. (9). Solutions of Eq. (9) are supposed to have the forms

$$\begin{bmatrix} b_n(t) \\ \psi_n(t) \end{bmatrix} = \begin{bmatrix} b_1 & b_1 \\ \psi_1 & \psi_1 \end{bmatrix} \begin{bmatrix} \exp(i(Q\,n + \Omega\,t)) \\ \exp(-i(Q\,n + \Omega^*\,t)) \end{bmatrix}, \tag{10}$$

where b_1, ψ_1, being real constants, Q and Ω the wave number and frequency of the disturbance, respectively. The asterisk (*) represents conjugate of a variable. By inserting Eq. (10) into Eq. (9) and after linearization around the perturbed plane waves, we obtain the linear system

$$\begin{bmatrix} i\Omega + a_{11} & a_{12} \\ a_{21} & i\Omega + a_{22} \end{bmatrix} \begin{bmatrix} b_1 \\ \psi_1 \end{bmatrix} = \begin{bmatrix} 0 \\ 0 \end{bmatrix}. \tag{11}$$

with all the coefficients given in Appendix (B). The system of Eq. (11) admits a nontrivial solution if its determinant vanishes. This leads to the second-order polynomial dispersion relation

$$\Omega^2 + A_1\,\Omega + A_0 = 0, \tag{12}$$

A_1, A_0 are given in Appendix (C) as well as a full derivation of Eq. (11). The existence of MI is possible if Ω is a complex number $(\Omega = \Omega_r + i\,\Omega_i)$ with a nonzero imaginary part. The system is unstable provided that $\Omega_i < 0$ with an instability growth rate $G = \text{Max}(-\Omega_i)\,(i = 1, 2)$. The MI growth rate is plotted as a function of the unstable wavenumbers Q and the parameter ε (Fig. 1). In this figure, the width of the unstable mode regions increases along the unstable wavenumber axis for small values of ε (ε is order of ω_g [15]), while for increasing values of ε, the magnitude of the instability growth rate decreases down to zero. This means that the cytosol viscosity extends the unstable mode parameter region for Q, but its large values alleviate the instability. The latter result agrees with observations in [14].

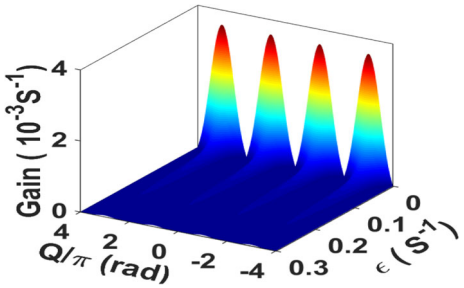

Fig. 1 MI growth rate versus unstable wavenumber Q and the ε parameter when $q = 1.18$. The presence of the cytosol viscosity stabilizes the system as it induces a decrease in the magnitude of the MI growth rate. However, by widening the unstable wavenumber region, the cytosol viscosity drives the system to instability. Parameters are: $K = 0.1$ eV, $pE = 0.25$ eV and $\phi_0 = \sqrt{5}$

3 Analytical solutions and numerical analysis

The MI analysis helps to determine parameter zones in which solitary waves are likely to be found. However, important characteristics of solitary waves that can propagate through the MTs such as their shape, amplitude and phase are not predicted by the MI analysis. To fill in such a gap and provide useful information about other types of waves that may propagate through MTs, analytical solutions are needed. Other advantages of analytical solutions are that they help to test the validity of the numerical solutions of the model under consideration. Several powerful methods are designed to solve nonlinear partial differential equations similar to Eq. (2). Among these are the inverse scattering transform method [24], the tanh method [25], the Exponential-expansion method [26], the modified Hirota method [27, 28], the F-expansion method [29, 30], the (G'/G)-expansion method [31] and the BDK method [32, 33]. In this work, we apply a direct method to construct solitary wave solutions of Eq. (5). To this end, we redefine the solution (4) in the form:

$$h\,\chi_n(t) = h\,F_n(t)\,e^{-i\,\omega_g\,t} + h\,F_n^*(t)\,e^{i\,\omega_g\,t}$$
$$\text{with } 0 \le \chi_n(t) \le \frac{\pi}{6} \tag{13}$$

where h is a constant whose value will be specified later to respect the experimental conditions [34]. We first assume that the function $F_n(t)$ and $F_n(t)^*$ vary weakly in time near the cut-off frequency. This means that $F_n(t)$ and $F_n(t)^*$ may be considered as continuous functions of space $x = n\,l$ (where $l = 80$ Å is the tubulin dimers spacing [11]) and time t. The latter arguments imply that the discrete functions in Eq. (5) should be replaced by the continuous versions after adequate Taylor series expansions. In the following, the continuous version of the function $F_n(t)$ is denoted $\varphi(x,t)$. After a little algebra, one recovers the continuous version of the discrete cubic CGL Eq. (5) given by

$$i\varphi_t + P\varphi_{xx} + Q|\varphi|^2\varphi - i\gamma\varphi = 0. \tag{14}$$

The expressions of P, Q and γ are

$$P = \begin{cases} P_r = \frac{2\alpha l^2\omega_g}{4\omega_g^2+\varepsilon^2}, \\ P_i = -\frac{\alpha l^2\varepsilon}{4\omega_g^2+\varepsilon^2}, \end{cases} \quad Q = \begin{cases} Q_r = \frac{6a_0\omega_g^3}{4\omega_g^2+\varepsilon^2}, \\ Q_i = -\frac{3a_0\omega_g^2\varepsilon}{4\omega_g^2+\varepsilon^2}, \end{cases}$$
$$\gamma = \begin{cases} \gamma_r = -\frac{2\omega_g^2\varepsilon}{4\omega_g^2+\varepsilon^2}, \\ \gamma_i = \frac{\omega_g\varepsilon^2}{4\omega_g^2+\varepsilon^2}, \text{ with } a_0 = h^2 a. \end{cases} \tag{15}$$

Applying the direct method, we assume the solution of Eq. (14) as

$$\varphi(x,t) = [A\,sech(\beta x) + i\,B\tanh(\beta x)]e^{(i v^2 t)}. \tag{16}$$

Then, inserting Eq. (16) into Eq. (5) and separating the real and imaginary parts leads to a system of over-determined equations, whose solutions found with the computer algebra software MAPLE 13 are

$$A = \pm 2\,h\,\sqrt{2},\ B = 0,\ v = \pm\sqrt{\omega_g},\ \beta = \frac{\sqrt{2}\omega_g}{\sqrt{\alpha}l}. \tag{17}$$

From Eq. (17), we rewrite the solution (16) as

$$\varphi(x,t) = \left[\pm 2\,h\,\sqrt{2}\frac{1}{\cosh(\beta x)}\right]\exp i(v^2 t). \tag{18}$$

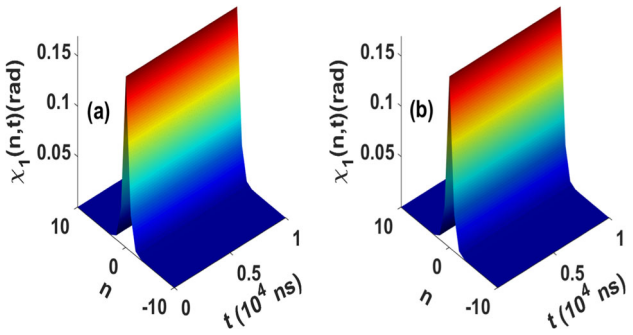

Fig. 2 Spatiotemporal evolutions of the bright solitary wave: ***a*** analytical, ***b*** numerical solutions. The numerical solution matches the analytical one with good accuracy. $pE = 0.25$ eV, $K = 0.1$ eV, $l = 80$ Å, $\varepsilon = 1.1\,\omega_g$

In order to retrieve the solution of the original discrete problem Eq. (2), we insert Eq. (18) into Eq. (4) with $x = nl$ to come back to the discrete situation. This corresponds to the solutions of Eq. (2) written as

$$\chi_n(t) = \pm 2\,A\;sech(\beta n\,l). \tag{19}$$

The solution Eq. (19) satisfies the experimental condition Eq. (13) provided that $h \leq \dfrac{\pi}{24\sqrt{2}}$. It is worth noting that the solutions Eq. (19) are stationary ones rather different from breather solutions previously derived [10, 15, 16]. Stationary states are well-known solutions that appear in many fields in physics [35–37]. The stationary solutions found above may explain biological processes during which the MTs do not change in time. Such processes occur for example during cytoplasmic transport by Microtubules Associated Proteins (MAPs). Moreover, the width of the solution Eq. (19) $(\beta l)^{-1} = \frac{1}{\sqrt{2}}\sqrt{\dfrac{K}{pE}}$ is proportional to ration of the stiffness and the dimer electric energy; its value decreases with increasing values of the dimer electric energy. This implies that for different MTs, it is the electric and chemical potential energies of two neighboring dimers belonging to the same PF and the inertia that alter the width of the solitary waves. Our solutions may be applied to distinguish MTs with different masses, hence different kinds. In addition, since there are two values of A, they lead to two different profiles of solutions, namely a bright solitary wave for $A > 0$ (see Fig. 2) and an anti-dark solitary wave for $A < 0$ (see Fig. 3). It is well known that exact or approximate analytical solutions as Eq. (19) of nonlinear partial differential equations may be unstable in real physical experiments. Unstable solutions not observed in experiments are not considered as real physical objects. One way to study the stability of analytical solutions of a time evolution partial differential equation is to insert them at initial time into the underlying equation and solve the latter one numerically. The stability of the numerical solution is confirmed by its evolution without disintegration after a sufficient long time for which the phenomenon under investigation is observed in experiment. In what follows, we use the fourth-order Runge–Kutta computational scheme with periodic boundary conditions [38]. The time step has been chosen as $\Delta t = 10^{-10}$ s while the spatial grid is [-10, 10]. Let us analyze the numerical stability of the two cases of solutions presented above.

3.1 Bright solitary wave

We obtain a stationary bright solitary wave for a positive amplitude of the solution (19) written as $\chi_n(t) = 4\sqrt{2}/\cosh(\beta nl)$, that is inserted at initial time $t = 0$ for numerical integration. We display in Fig. 2 spatiotemporal evolutions of the analytical (Fig. 2a) and numerical (Fig. 2b) solutions. A scrutiny analysis of both panels of Fig. 2 shows that the numerical solution corroborate the analytical prediction with a very high accuracy. As stated above, the numerical solution remains stable up to a final time equals to 10^4 ns, a lifetime 100 times longer than the ones presented in previous works [11, 15]. Stationary state solutions like the ones presented in Fig. 2 imply a constant energy that could be used by the MT to stay in a spatial configuration during a sufficiently longer time that would allow MAPs to use the MT as an intracellular transport channel [39]. During this transport, the MT behaves like a railway on which the MAPs attach themselves in order to transport the elements necessary for the proper functioning of the cell. Knowledge of stationary states of MTs are also important since it was suggested that they could explain the presence of a GTP or the conformation cap at its end. The GTP cap keeps the MT in a stable position and prevents it from tipping over in a catastrophic event. In the conformational capping approach, MTs are prone to keep a stable position in case the PFs have straight positions or bending angles $\leq \dfrac{\pi}{6}$. In our case, the amplitude of the dimer angle which is in the range $[0.15, 0.16]\,rad$ is in good agreement with the results of the work of [34] where the limiting angle of PF dislocations is $\pi/6$ rad [10]. Moreover, a stationary MT implies the death of the cell. This might be used to stop cell dynamic leading to its death. In this perspective, drugs that target MTs may be applied to arrest their dynamics instability to kill cancer cells for example. A striking example is the taxol, a drug that stabilizes MTs and is used in cancerology for its ability to freeze the mitotic network [40, 41].

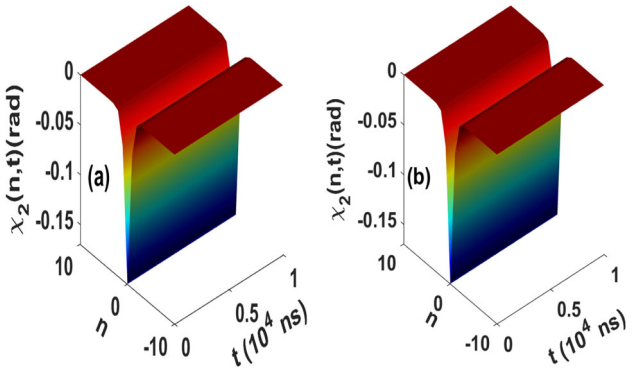

Fig. 3 Spatiotemporal evolutions of the anti-dark solitary wave: ***a*** analytical, ***b*** numerical solutions. The numerical solution recovers the analytical solution with high accuracy. $pE = 0.25$ eV, $K = 0.1$ eV, $l = 80$ Å, $\varepsilon = 1.1\,\omega_g$

3.2 Anti-dark solitary wave

The initial condition for numerical integration of Eq. (2) is now the anti-dark solitary wave of Eq. (19) given by $\chi_n(t) = -4\sqrt{2}\ sech(\beta nl)$. Spatiotemporal evolutions of the angular variation of the dimers are presented in panels (a) (analytics) and (b) (numerics) of Fig. 3, respectively. Once again, the numerical solution maintains the initial spatial distribution up to $t = 10^4$ ns, hence confirming the stability of our anti-dark solitary wave solution. As mentioned above, the anti-dark solitary wave solutions are also a good candidate to explain MAPs displacements on the top of MTs or the stable position MTs induced by the GTP cap.

4 Conclusion

In this work, we have studied the dynamics of MTs radial dislocations in the presence of a dissipative term originating from the cytosol viscosity Γ. Through the MI analysis of plane waves, we have shown that the viscosity of the cytosol has a major impact on the stability of the system. To be more precise, our results show that in the presence of the cytosol viscosity, new unstable modes appear, nevertheless, the magnitude of the instability growth rate decreases with increasing values of Γ and for some large values the cytosol viscosity wipes out the instability of the system. Moreover, it is well known that MTs during some biological processes behave like stationary states. Converting the original discrete ordinary differential equation into a dissipative complex Ginzburg–Landau equation in which the dissipation viscosity coefficient no longer acts, we constructed using a direct ansatz method, stationary solutions of the original discrete problem. We provided two distinct profile stationary states, a bright and an anti-dark profiles that as explained above, are good candidates to explain biological mechanisms where MTs should keep stationary. Our analytical results are supported by direct numerical integrations of the original discrete model. The model [10] considered here works well for different collective conformations of dimers in PFs [42]. It is well known that the hydrolysis of GTP that triggers the dynamics of the MTs is a stochastic process which in principle should alter the MTs dynamics. In future works, we aim to include in the governing equation the random mechanisms due to the hydrolysis of GTP.

Data Availability Statement This manuscript has no data associated.

Declarations

Conflict of interest The authors declare that they have no conflict of interest.

Appendix A

We consider the perturbed wave solution (Eq. (8)) in the form

$$\begin{aligned} F_n(t) &= (\phi_0 + b_n)e^{i\theta_n(t)+i\psi_n(t)} \\ &= (\phi_0 + b_n)(1 + i\psi_n)e^{i\theta_n(t)} \\ &= (\phi_0 + i\phi_0\psi_n + b_n)e^{i\theta_n(t)} \end{aligned} \tag{A1}$$

with $\theta_n(t) = (qn - \omega_0 t)$ such that $|\psi_n(t)| \ll |\theta_n(t)|$.

$$F_{n\pm1} = (\phi_0 + i\phi_0\psi_{n\pm1} + b_{n\pm1})e^{i\theta_n(t)}e^{\pm iq}. \tag{A2}$$

$$|F_n(t)|^2 F_n(t) = \phi_0^2(\phi_0 + b_n^* - i\phi_0\psi_n^* + 2b_n + 2i\phi_0\psi_n)e^{i\theta_n(t)}. \tag{A3}$$

$$\dot{F_n}(t) = \left(\dot{b_n} + i\phi_0\dot{\psi_n} - i\omega_0(\phi_0 + b_n + i\phi_0\psi_n)\right)e^{i\theta_n(t)}. \tag{A4}$$

We introduce equations A1, A2, and A3 into Eq. (5). After linearization, we separate the real and imaginary part and obtain the perturbed equations

$$\begin{aligned} &-\varepsilon\dot{b_n} - 2\omega_g\phi_0\dot{\psi_n} = -\alpha(b_{n+1} - 2b_n + b_{n-1})\cos(q) \\ &-\alpha(\psi_{n+1} - \psi_{n-1}) - 3a\omega_g^2\phi_0^2(b_n^* + b_n), \end{aligned} \tag{A5}$$

$$\begin{aligned} &2\omega_g\dot{b_n} - \varepsilon\phi_0\dot{\psi_n} = -\alpha\phi_0(\psi_{n+1} - 2\psi_n + \psi_{n-1})\cos(q) \\ &-\alpha(b_{n+1} - b_{n-1})\sin(q) - 3a\omega_g^2\phi_0^2(\psi_n - \psi_n^*) \end{aligned} \tag{A6}$$

Let us consider

$$\begin{aligned} Z_1 &= -\alpha(b_{n+1} - 2b_n + b_{n-1})\cos(q) \\ &\quad -\alpha(\psi_{n+1} - \psi_{n-1}) - 3a\omega_g^2\phi_0^2(b_n^* + b_n), \\ Z_2 &= -\alpha\phi_0(\psi_{n+1} - 2\psi_n + \psi_{n-1})\cos(q) \\ &\quad -\alpha(b_{n+1} - b_{n-1})\sin(q) - 3a\omega_g^2\phi_0^2(\psi_n - \psi_n^*). \end{aligned}$$

Equations (A5) and (A6) become:

$$-\varepsilon\dot{b_n} - 2\omega_g\phi_0\dot{\psi_n} = Z_1 \tag{A7}$$

$$2\omega_g\dot{b_n} - \varepsilon\phi_0\dot{\psi_n} = Z_2 \tag{A8}$$

The system formed by equations (A7) and (A8) is as follows:

$$\begin{cases} -\varepsilon\dot{b_n} - 2\omega_g\phi_0\dot{\psi_n} & = Z_1 \\ 2\omega_g\dot{b_n} - \varepsilon\phi_0\dot{\psi_n} & = Z_2. \end{cases} \tag{A9}$$

Solving (A9):

$$\dot{\psi_n} = -\frac{2\omega_g Z_1 + \varepsilon Z_2}{(4\omega_g^2 + \varepsilon^2)\phi_0^2}; \quad \dot{b_n} = \frac{-\varepsilon Z_1 + 2\omega_g Z_2}{(\varepsilon^2 + 4\omega_g^2)}. \tag{A10}$$

Eq. (A10) may be rewritten as

$$\begin{aligned} \dot{b_n} &= N_1\, b_n + N_2\,(b_{n+1} - 2b_n + b_{n-1}) \\ &\quad + N_3(\psi_{n+1} - 2\psi_n + \psi_{n-1}) + N_4\,(b_{n+1} - b_{n-1}) \\ &\quad + N_5\,(\psi_{n+1} - \psi_{n-1}) \end{aligned} \tag{A11}$$

$$\begin{aligned} \dot{\psi_n} &= P_1\, b_n + P_2\,(b_{n+1} - 2b_n + b_{n-1}) \\ &\quad + P_3(\psi_{n+1} - 2\psi_n + \psi_{n-1}) + P_4\,(b_{n+1} - b_{n-1}) \\ &\quad + P_5\,(\psi_{n+1} - \psi_{n-1}) \end{aligned} \tag{A12}$$

where the coefficients N_i, P_i are given by:

$$\begin{aligned} &D = \varepsilon^2 + 4\omega_g^2; \quad N_1 = \frac{6a\omega_g^2\varepsilon\phi_0^2}{D} \\ &N_2 = \frac{\alpha\varepsilon\cos(q)}{D}; \quad N_3 = -\frac{2\phi_0\omega_g\alpha\cos(q)}{D}; \\ &N_4 = -\frac{2\alpha\omega_g\sin(q)}{D}; \quad N_5 = \frac{\alpha\varepsilon\sin(q)}{D}. \\ &P_1 = \frac{12a\omega_g^3}{D}; \quad P_2 = \frac{2\omega_g\alpha\cos(q)}{D\phi_0^2} \\ &P_3 = \frac{\alpha\varepsilon\phi_0\cos(q)}{D\phi_0^2}; P_4 = \frac{\alpha\varepsilon\sin(q)}{D} \end{aligned}$$

$$P_5 = \frac{2\alpha\omega_g \sin(q)}{D\phi_0^2};$$

Appendix B

$$a_{11} = 2iN_4 \sin(Q) - 4N_2 \sin^2(Q/2) + N_1 \tag{B1}$$

$$a_{12} = -4N_3 \sin^2(Q/2) + 2iN_5 \sin(Q) \tag{B2}$$

$$a_{21} = 2iP_4 \sin(Q) - 4P_2 \sin^2(Q/2) + P_1 \tag{B3}$$

$$a_{22} = -4P_3 \sin^2(Q/2) + 2iP_5 \sin(Q) \tag{B4}$$

Appendix C

We consider Eq. (11) above

$$\begin{bmatrix} i\Omega + a_{11} & a_{12} \\ a_{21} & i\Omega + a_{22} \end{bmatrix} \begin{bmatrix} b_1 \\ \psi_1 \end{bmatrix} = \begin{bmatrix} 0 \\ 0 \end{bmatrix}.$$

The determinant of this matrix is:

$$\Omega^2 + A_1\,\Omega + A_0 = 0. \tag{C1}$$

Where the coefficients A_1, A_0 of Eq.(C_1) are given by

$$\begin{aligned} A_1 =& 4\,iN_2\,(\sin(Q/2))^2 + 4\,i(\sin(Q/2))^2 P_3 \\ & - iN_1 + 2\,N_4\,\sin(Q) + 2\,P_5\,\sin(Q) \end{aligned} \tag{C2}$$

$$\begin{aligned} A_0 =& 8\,iN_2\,\sin(Q)(\sin(Q/2))^2 P_5 - 16\,N_2\,(\sin(1/2\,Q))^4 P_3 \\ & - 8\,iN_3\,\sin(Q)(\sin(Q/2))^2 P_4 \\ & + 16\,N_3\,(\sin(Q/2))^4 P2 \\ & + 8\,iN_4\,\sin(Q)(\sin(Q/2))^2 P_3 \\ & - 8\,iN_5\,\sin(Q)(\sin(Q/2))^2 P_2 \\ & - 2\,iN_1\,\sin(Q)P_5 + 4\,N_1\,(\sin(Q/2))^2 P_3 \\ & - 4\,N_3\,(\sin(Q/2))^2 P_1 + 4\,N_4\,(\sin(Q))^2 P_5 \\ & + 2\,iN_5\,\sin(Q)P_1 - 4\,N_5\,(\sin(Q))^2 P_4. \end{aligned} \tag{C3}$$

References

1. A. Bershadsky, J. Vasiliev, *Cytoskeleton*. (Springer New York, New York, 1988).
2. B. Alberts, A. Johnson, J. Lewis, M. Raff, K. Roberts, P. Walter, (New-York and London: Garland Publishing, 2002).
3. C. Conde, A. Càceres, Nat. Rev. Neurosci. **10**, 319 (2009).
4. J. Howard, Sunderland, MA Sinaeur Assoc (2001).
5. M.V. Satarić, U. Kormidis-Luburić, L. Budinski-Petković, I. Loncarević, J. Comp. Theo. Nano. **6**, 721 (2009).
6. J. Yang, *Nonlinear Waves in Integrable and Nonintegrable Systems* (SIAM, Philadelphia, 2010).
7. M.L. Williams, R.F. Landel, J.D. Ferry, J. Am. Chem. Soc. **77**, 3701 (1955).
8. T. Yeung, B. Heit, V.G.D. Fairn, B. Chiu, R. Inman, A. Kapus, M. Swanson, S. Grinsten, Cell. Motil. **5**, 917 (2009).
9. K.R. Foster., J.W. Baish, J. Bio. Phys. **26**, 255 (2000).
10. S. Zdravković, M.V. Satarić, A. Maluckov, A. Balaž, Appl. Math. Comput. **237**, 227 (2014).
11. C.B. Tabi, E. Tankou, A. Mohamadou, Chaos Soliton Fract. **95**, 187 (2017).
12. M.C. Ekosso, A.J. Fotue, S.C. Kenfack, H. Fotsin, L.C. Fai, Mod. Phys. Lett. B **33**, 1950433 (2019).
13. S.E. Shirmovsky, D.V. Shulga, Physica A **534**, 122165 (2019).
14. A.T. Molines, J. Lemère, M. Gazzola, E.I. Steinmark, C.H. Edrington, C.T. Hsu, K. Suhling, G. Goshima, L.J. Holt, M. Thery, G.J. Brouhard, F. Chang, bioRxiv. (2020).
15. S. Zdravković, A.N. Bugay, G.F. Aru, A. Maluckov, Chaos **24**, 023139 (2014).
16. S. Zdravković, S. Zeković, A.N. Bugay, J. Petrović, Chaos, Soliton. Fractals. **152**, 111352 (2021).
17. Y. Kivshar, M. Peyrard, Phys. Rev. A **46**, 6 (1992).
18. I. Daumont, T. Dauxois, M. Peyrard, Nonlinearity **10**, 617 (1997).
19. W.D. Kuipou, D.B. Belobo, A. Mohamadou, Eur. Phys. J. Plus. **136**, 701 (2021).

20. D.B. Belobo, G. Ben-Bolie, T. Ekogo, C. Tiofack, T.C. Kofané, Int. J. Mod. Phys. B **26**, 1250164 (2012).
21. J. Pokorný, F. Jelinek, V. Trkal, I. Lamprecht, R. Hölzel, Astrophys. Space. Sci. **23**, 171 (1997).
22. J.E. Schoutens, J. Biol. Phys. **31**, 35 (2005).
23. J. Pokorný, J. Pokorný, J. Vrba, Int. J. Mol. Sci. **22**, 8215 (2021).
24. H.D. Wahlquis, F.B. Estabrook, J. Math. Phys. **31**, 1 (1975).
25. A. Pickering, J. Phys. A. **17**, 4395 (1993).
26. A.H. He, L.N. Zhang, Phys. Lett. A. **372**, 1044 (2008).
27. K. Nozaki, N. Bekki, Phys. Soc. Jpn. **53**, 1581 (1984).
28. A.V. Mikhailov, Integrability. (volume 767 of Lecture Notes in Physics, Springer Berlin Heidelberg, Berlin, Heidelberg 2009).
29. R.Y. Ondoua, J.C.M. Few, D.B. Belobo, C.B. Tabi, H.P.E. Fouda, Eur. Phys. J. Plus. **136**, 274 (2021).
30. S. Issa, C.B. Tabi, H.P. Ekobena Fouda, T.C. Kofané, Eur. Phys. J. Plus. **133**, 233 (2018).
31. H. Naher, F.A. Abdullah, App. Comput. Math. **3**, 1144 (2012).
32. J.R. Bogning, D.T.C. Djeumen, T.C. Kofane, Phys. Scr. **20**, 025013 (2013).
33. J.R. Bogning, D.T.C. Djeumen, T.C. Kofane, Far. East. J. Dyn. Syst. **20**, 101 (2013).
34. N.R. Watts, N. Cheng, W. West, A.C. Steven, D.L. Sacket, Biochemistry **41**, 12662 (2002).
35. L. Pimonow, Springer **9**, 24 (1954).
36. P. Minotti, V. Nocton, Mech. Mach. Theory. **31**, 91 (1996).
37. J. Le Bot, S.J. Le Montagner, Phys. Radium. **14**, 299 (1953).
38. J. Pouget, M. Remoissenet, J.M. Tamga, Phys. Rev. B. **47**, 14866 (1993).
39. A. Molines, (PhD Thesis, Universite Paris-SACLAY; 2016).
40. A. Kolman, Curr. Opin. Investig. Drugs. **5**, 657 (2004).
41. H. Wang, Z. Wang, S. Wang, M. Li, L. Nan, J.K. Rhie, J.M. Covey, R. Zhang, D.L. Hill, Cancer. Chemoth. Pharm. **56**, 255 (2005).
42. A. Guesdon, F. Bazil, R.M. Buey, R. Mohan, S. Monier, R.R. Garcìa, M. Angevin, C. Heichette, R. Wieneke, R. Tampé, L. Duchesne, A. Akhmanova, M.O. Steinmetz, D. Chrétien, Nat. Cell. Biol. **18**, 1102 (2016).

Commun Nonlinear Sci Numer Simulat 143 (2025) 108615

Contents lists available at ScienceDirect

Communications in Nonlinear Science and Numerical Simulation

journal homepage: www.elsevier.com/locate/cnsns

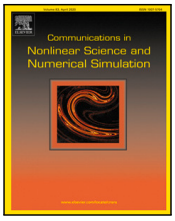

Research paper

Nonlinear dynamics effect of viscosity of cytosol into the microtubules and exact solutions

Tabapsi Kamdem Rostand [a,b,*], Belobo Belobo Didier [a,b,c], Bansi Kamdem Christel Delphin [a,b], Dang Koko Adamou [a,b,d], Tabi Conrad Bertrand [e], Kofané Timoléon Crépin [e,f]

[a] Laboratory of Biophysics, Department of Physics, Faculty of Science, University of Yaounde I, P.O. Box 812, Yaounde, Cameroon
[b] African Centre for Advanced Studies, P.O. Box 4477, Yaounde, Cameroon
[c] Department of Mathematics and Physical Sciences, National Advanced School of Engineering of Yaounde, University of Yaounde I, P.O. Box 8390, Yaounde, Cameroon
[d] Department of Maintenance, Higher Technical Teachers' Training College, University of Ebolowa, P.O. Box 886, Ebolowa, Cameroon
[e] Department of Physics and Astronomy, Botswana University of Science and Technology, Private Bag 16, Palapye, Botswana
[f] Laboratory of Mechanics, Department of Physics, Faculty of Science, University of Yaounde I, P.O. Box 812, Yaounde, Cameroon

ARTICLE INFO

Keywords:
Microtubules
Viscosity
Ginzburg–Landau equation
Solitary waves

ABSTRACT

The viscosity of the cytosol plays a crucial role in the biology of microtubules (MTs), affecting their architecture and dynamics function. Understanding the overall functionality of this parameter is essential. The effect of viscosity on MT dynamics is studied when modelling longitudinal and angular displacements. The rotating wave approximation is used to derive two uncoupled complex Ginzburg–Landau (CGL) equations for the longitudinal and angular displacements, respectively. Then, analytical two solitary wave solution types are constructed using the modified Hirota bilinear method. Its appears that the viscosity dampens the longitudinal displacements of MTs by significantly reducing the magnitude of longitudinal waves. In the case of angular displacements, the influence of viscosity is negligible, such that MTs angular displacements are transparent to viscosity. Our analytical predictions are confirmed by numerical solutions with pretty much high accuracy. The solutions obtained offer promising prospects for regulating the viscosity of the cytosol in order to control the assembly, disassembly and stability of MTs.

1. Introduction

Eukaryotic cells, which are characterized by a nucleus surrounded by a membrane, have distinctive features in the form of intricate networks of protein filaments also known as the cytoskeleton. At the core of this cytoskeleton are microtubules (MTs), the subject of this study. In conjunction with motor proteins, MTs play a central role in shaping and stabilizing cells, orchestrating cell division and monitoring various cellular cycling processes [1]. MTs have a cylindrical shape with outer and inner diameters of 15 nm and 25 nm, respectively [2]. They are mainly composed of protofilaments (PFs), 13 PFs arrange in parallel helically around an axis of rotation form a hollow cylinder. Each PF is made of a set of 8 nm long dimers, forming dipoles [2], the latter dimers are in turn composed of alpha and beta tubulin subunits with negative and positive charges, respectively. α, β tubulin binding sites for

* Corresponding author at: Laboratory of Biophysics, Department of Physics, Faculty of Science, University of Yaounde I, P.O. Box 812, Yaounde, Cameroon.
E-mail addresses: rostandtabapsi@gmail.com (T.K. Rostand), belobodidier@acas-yde.org (B.B. Didier), bansidelphin@yahoo.fr (B.K.C. Delphin), adamoudangk@acas-yde.org (D.K. Adamou), tabic@biust.ac.bw (T.C. Bertrand), tckofane@gmail.com (K.T. Crépin).

https://doi.org/10.1016/j.cnsns.2025.108615
Received 24 July 2024; Received in revised form 14 December 2024; Accepted 10 January 2025
Available online 17 January 2025

nucleotides are mainly the guanosine triphosphate (GTP) [3]. During MT assembly, β-tubulins link to the GTP bound to the plus end of the MT. During depolymerization, GTP hydrolyses into guanosine diphosphate (GDP), which weakens tubulin association and facilitates MT dissociation.

Research in cell biology has led to the introduction of many mathematical models whose analytical solutions are actively needed in various subfields. Among these subfields, MTs stands out with extensive studies aimed at modelling their complex properties. For example, a one-dimensional electrical model simulating MTs has been studied using a reductive perturbation approach [4], which explained that the evolution of ionic waves in MTs is governed by a NLS equation whose solutions help characterize possible biological implications of solitary wave like waves in MTs. Another mathematical description that leads to partial differential equations of MTs involved the analysis of conductive properties of MTs modelled as nonlinear electrical transmission lines [5]. In this work, we elaborate from a Hamiltonian that takes into account both kinetic and potential energies of MT dimers moving either longitudinally or radially to introduce via specific transformations presented below coupled CGL equations to model the dynamics of MTs. Solitary wave solutions of our derived CGL equations suggest possible biological information processing where stationary MTs may play the role of carpets on which rolls other proteins that may carry biological material or information. The study of the effect of cytoplasmic viscosity on MTs has opened up new perspectives for understanding future cellular processes. According to Betterton [6], an increase in viscosity is associated with a decrease in the rate of both MTs formation and disassembly. Shirmovsky et al. [7] have extensively studied the vibrational properties of MTs and highlighted the critical influence of viscosity on these processes, affecting the dissipation of vibrations and their energy management. This suggests a potential role in maintaining structural equilibrium or preventing damage. Molines et *al.* [8] shed light on a direct correlation between cytoplasmic concentration and the rates of MT polymerization and depolymerization, which are closely linked to fluctuations in cytoplasmic viscosity. This highlights the importance of viscosity in regulating MT dynamics, even in a normal cellular context. Using a discrete radial dislocation model, Tabapsi et al. [9] showed that viscosity alters modulation instability, expanding unstable regions and reducing their growth rates, in agreement with Molines et al. [8]. An investigation led by Latifah [10] delved into the influence of solvent viscosity on the dynamics of MTs, shedding light on its impact on assembly and disassembly processes. A result which implies that modulating solvent viscosity could constitute an effective strategy to expedite or modify cellular processes associated with MTs. MTs, in turn, respond to the electric field generated by the depolymerization of the neuronal membrane, as detailed in the study by Priya et *al.* [11]. In this context, the authors established a model with two degrees of freedom, namely longitudinal displacement U_n and an angular displacement ϕ_n. By deliberately neglecting cytosol viscosity in their work, they arrived at a third-order NLS equation. Examination of modulational instability led them to posit a possible localization of dipolar oscillations in the protofilament of neuronal MTs. The consideration of system viscosity holds paramount importance in biophysics [6–10]. Our approach aims to assess the impact of cytosol viscosity on the interaction of dimers in the presence of an electric field. In this work, we construct below exact solutions capable of elucidating the dynamics of MTs, taking into account cytosol viscosity, which influences MTs dynamics based on both longitudinal and angular degrees of freedom.

The structure of our work is outlined as follows: in Section 2, we delineate the Hamiltonian of the model and derive the uncoupled CGL equation, incorporating the effects of the double-potential well, the electric field, and viscosity using the Rotating Wave Approximation (RWA) [12]. Section 3 is dedicated to constructing exact solutions using the modified Hirota method [13]. Numerical investigations and discussions of the results will be conducted in Section 4. Section 5 will be devoted to summarizing the obtained findings.

2. Model

The Hamiltonian in [11] solves the movement of a single protofilament, affected by strong interactions between dimers that belong to the same protofilament. This model consists of two degrees of freedom, specifically the longitudinal displacement from the U_n model [14,15] and the angular displacement from the χ_n model [16]. We have chosen to introduce the moment of inertia, rather than simple mass, in the context of radial displacements. This decision is based on the fact that it offers a more thorough characterization of the behaviour of an object subjected to rotational forces, while providing a more robust foundation for calculations and analysis in rotational dynamics. The Hamiltonian combining both angular and longitudinal displacements [11] reads :

$$H = \sum_n \left[\frac{m}{2}\dot{U}_n^2 + \frac{I}{2}\dot{\chi}_n^2 + \frac{K_1}{2}(U_{n+1}-U_n)^2 + \frac{K_2}{2}(\chi_{n+1}-\chi_n)^2 - \frac{A}{2}U_n^2 + \frac{B}{4}U_n^4 - pE\cos(\chi_n) \right]. \tag{1}$$

In Eq. (1), the first couple of terms represents the kinetic energy related to the displacements U_n and χ_n, with m standing for the mass and $I = (m\,l^2)/12$, the moment of inertia of dimers, where $l = 8$ nm is the length of a single dimer. The dot implies the first derivative with respect to time t. The third and fourth terms emerge from the neighbouring dimers' restoring forces in the protofilament (PF), K_1 and K_2 account for inter-dimer stiffness parameters for the U_n and χ_n displacements, respectively. The fifth and sixth terms depict the double-potential well of U_n displacement [14,17,18], while the final term illustrates the dipole-dipole potential energy due to χ_n displacement. p denotes the electric dipole moment, and E is the intrinsic electric field of the dimers, whose order of magnitude is provided in [16,19] making sure that $p, E > 0$. A and B are positive parameters of the double-potential well. The aforementioned Hamiltonian integrates both radial and longitudinal aspects of the dimers which of course is a conservative system. In the context of eukaryotic cells, the cellular components are immersed in a fluid known as the cytosol, which is characterized by its viscosity. The viscosity of the cytosol acts as a dissipative term and may be incorporated into the dynamics using the following expressions: $F_v = -\gamma\dot{U}_n$ and $M_v = -\Gamma\dot{\chi}_n$. Here F_v and M_v denote the force and viscosity moment associated with longitudinal and

Table 1
Parameters network values.

Parameters	Values	References
γ	5.6×10^{-11} kg/s	[14,17,18]
A	1.8 eV	[20]
B	2.8 eV	[20]
K_1	0.5 N/m	[14]
K_2	0.1 eV	[21]
m	1.8×10^{-27} kg	[1,16,17]
Γ	43×10^{-30} Nms	[20]

angular displacements, respectively. Employing the Hamilton–Jacobi formalism, we derive the equations of motion that the dimer satisfies

$$\ddot{U}_n+\varepsilon_1\,\dot{U}_n=\alpha_1\,\left(U_{n+1}-2U_n+U_{n-1}\right)+\omega_{g_1}^2\,U_n-\tau\,U_n^3, \tag{2a}$$

$$\ddot{\chi}_n+\varepsilon_2\,\dot{\chi}_n=\alpha_2\,\left(\chi_{n+1}-2\chi_n+\chi_{n-1}\right)+\omega_{g_2}^2\,\left(a\,\chi_n^3-\chi_n\right), \tag{2b}$$

where $\varepsilon_1=\frac{\gamma}{m},\alpha_1=\frac{K_1}{m},\alpha_2=\frac{K_2}{I},a=\frac{1}{6},\omega_{g_2}^2=\frac{pE}{I},\tau=\frac{B}{m}$ and $\omega_{g_1}^2=\frac{A}{m}$. The value of ε_2 varies proportionally with Γ, since I is a constant, according to the relationship $\varepsilon_2=\frac{\Gamma}{I}$. Numerical values of the coefficients in Eqs. (2) are given in Table 1.

By exclusively considering the linear terms of Eqs. (2), we scrutinize its solutions in the form of plane waves, expressed in complex notation as $\underline{U}_n(t)\propto\exp i(q_1\,n-\omega_{g_1}\,t)$ and $\underline{\chi}_n(t)\propto\exp i(q_2\,n-\omega_{g_2}\,t)$. Here, q_1,q_2 are the wavenumber and angle, while $\omega_{g_1},\omega_{g_2}$ represent the longitudinal and angular frequencies, respectively. Inserting the above plane wave solutions into Eqs. (2) and neglecting frictional terms lead to the ensuing linear dispersion relations

$$\omega_1^2=-\omega_{g1}^2+\frac{4\,K_1}{m}\sin^2\left(\frac{q_1}{2}\right),\quad\text{with}\quad\omega_{g1}^2<\frac{4\,K_1}{m}, \tag{3a}$$

$$\omega_2^2=\omega_{g2}+\frac{4\,K_2}{I}\sin^2\left(\frac{q_2}{2}\right). \tag{3b}$$

By examining how a carrier wave with a frequency in the linear frequency range is modulated, we can insert the test solution into Eq. (2), in the form

$$U_n(t)=G_n(t)\,e^{-i\omega_{g_1}t}+G_n^*(t)\,e^{i\omega_{g_1}t}, \tag{4a}$$

$$\chi_n(t)=F_n(t)\,e^{-i\omega_{g_2}t}+F_n^*(t)\,e^{i\omega_{g_2}t}. \tag{4b}$$

First, we note that the functions $G_n(t),G_n^*(t),\ F_n(t),F_n^*(t)$ are complex functions that show slow variations over time compared to the main oscillations at frequencies $\omega_{g_1},\omega_{g_2}$. This is expressed as $\dot{U}_n\ll\omega_{g_1}\,U_n,\dot{\chi}_n\ll\omega_{g_2}\,\chi_n$. Substituting Eqs. (4) in Eqs. (2) and applying the RWA, i.e., keeping only terms proportional to $\exp(\pm i\omega_{g_1}t)$ and $\exp(\pm i\omega_{g_2}t)$, respectively, we derive the discrete CGL equations satisfied by $G_n(t),F_n(t)$

$$(\varepsilon_1-2\,i\,\omega_{g_1})\,\dot{G}_n-\alpha_1\,\left(G_{n+1}-2G_n+G_{n-1}\right)-\omega_{g1}^2\,G_n+3\,\tau\,|G_n|^2\,G_n-i\,\varepsilon_1\,\omega_{g_1}G_n=0, \tag{5a}$$

$$(\varepsilon_2-2\,i\,\omega_{g_2})\,\dot{F}_n-\alpha_2\,\left(F_{n+1}-2\,F_n+F_{n-1}\right)-3\,a\,\omega_{g_2}^2\,|F_n|^2\,F_n-i\,\varepsilon\,\omega_{g_2}\,F_n=0. \tag{5b}$$

Also, we assume that the function $G_n(t),G_n^*(t),\ F_n(t),F_n^*(t)$ varies slightly with time in the vicinity of the cut-off frequency. This means that G and F can be viewed as continuous functions of both space $x=nl$ and time t. As a result, after an appropriate Taylor series expansion, the discrete functions $G_n(t)$ and $F_n(t)$ in Eqs. (5) are replaced by their continuous counterparts $G(x,t)$ and $F(x,t)$, respectively, leading to

$$i\,G_t+P_1\,G_{xx}+Q_1\,|G|^2\,G-i\,\Lambda_1\,G=0, \tag{6a}$$

$$i\,F_t+P_2\,F_{xx}+Q_2\,|F|^2\,F-i\,\Lambda_2\,F=0. \tag{6b}$$

Eqs. (6) represents the continuous CGL equations, where P,Q and Γ are defined as follows

$$P_1=\begin{cases}P_{r_1}=\frac{\alpha_1\,l^2\,\varepsilon_1}{\varepsilon_1^2+4\,\omega_{g_1}^2}\\ P_{i_1}=\frac{2\,\alpha_1\,l^2\,\omega_{g_1}}{\varepsilon_1^2+4\,\omega_{g_1}^2},\end{cases}\quad P_2=\begin{cases}P_{r_2}=\frac{2\,\alpha\,l^2\,\omega_{g_2}}{4\,\omega_{g_2}^2+\varepsilon_2^2},\\ P_{i_2}=-\frac{\alpha\,l^2\,\varepsilon_2}{4\,\omega_{g_2}^2+\varepsilon_2^2},\end{cases}\quad Q_1=\begin{cases}Q_{r_1}=\frac{3\,\tau\,\varepsilon_1}{\varepsilon_1^2+4\,\omega_{g_1}^2},\\ Q_{i_1}=\frac{6\,\tau\,\omega_{g_1}}{\varepsilon_1^2+4\,\omega_{g_1}^2},\end{cases}$$

$$Q_2 = \begin{cases} Q_{r_2} = \frac{6\,a\,\omega_{g_2}^3}{4\,\omega_{g_2}^2+\varepsilon_2^2}, \\ Q_{i_2} = -\frac{3\,a\,\omega_{g_2}^2\,\varepsilon_2}{4\,\omega_{g_2}^2+\varepsilon^2}, \end{cases} \quad \Lambda_1 = \begin{cases} \Lambda_{r_1} = -\frac{3\,\omega_{g_1}\,\varepsilon_1}{\varepsilon_1^2+4\,\omega_{g_1}^2}, \\ \Lambda_{i_1} = \frac{-2\,\omega_{g_1}^3+\varepsilon_1^2\,\omega_{g_1}}{\varepsilon_1^2+4\,\omega_{g_1}^2}, \end{cases} \quad \Lambda_2 = \begin{cases} \Lambda_{r_2} = -\frac{2\,\omega_{g_2}^2\,\varepsilon_2}{4\,\omega_{g_2}^2+\varepsilon_2^2}, \\ \Lambda_{i_2} = \frac{\omega_{g_2}\,\varepsilon_2^2}{4\,\omega_{g_2}^2+\varepsilon_2^2}. \end{cases}$$

3. Exact solutions of nonlinear Ginzburg–Landau equation

Analytical solutions are essential for understanding the dynamics of biological systems and for validating numerical models. Several methods have been developed to solve nonlinear partial differential equations, including the modified bilinear Hirota method. Known for its precision and efficiency, the modified Hirota method uses a specific bilinear formulation to obtain exact solutions to nonlinear partial differential equations. The modified bilinear Hirota operator takes the form [13,22–25]

$$D_{\delta,t}^m\,D_{\delta,x}^n\,H\cdot T = \left(\frac{\partial}{\partial t'}-\delta\,\frac{\partial}{\partial t}\right)^m\left(\frac{\partial}{\partial x'}-\delta\,\frac{\partial}{\partial x}\right)^n H(x,t)T(x',t')|_{x'=x,t'=t}. \tag{8}$$

Setting

$$G(x,t) = \psi(x,t)\,e^{\Lambda_1 t}, \tag{9a}$$

$$F(x,t) = \phi(x,t)\,e^{\Lambda_2 t}, \tag{9b}$$

then substituting Eqs. (9) into Eqs. (6), we get

$$i\,\psi_t + P_1\,\psi_{xx} + Q_1\,|\psi|^2\,\psi\,e^{\Lambda_1 t} = 0, \tag{10a}$$

$$i\,\phi_t + P_2\,\phi_{xx} + Q_2\,|\phi|^2\,\phi\,e^{\Lambda_2 t} = 0. \tag{10b}$$

The two solitary wave solutions of Eqs. (10) are looked for in the form

$$\psi(x,t) = u_1(x,t) + u_2(x,t), \tag{11a}$$

$$\phi(x,t) = v_1(x,t) + v_2(x,t), \tag{11b}$$

with $u_1(x,t)\,u_2(x,t) = 0$ and $v_1(x,t)\,v_2(x,t) = 0$ corresponding to one solitary wave. Inserting Eqs. (11) into Eqs. (10), we get

$$i\,u_{1t} + P_1\,u_{1xx} + Q_1\,|u_1|^2\,u_1\,e^{\Lambda_1 t} + Q_1\,e^{\Lambda_1 t}\,\left(2\,u_2\,|u_1|^2 + u_2^*\,u_1^2\right) = 0, \tag{12a}$$

$$i\,u_{2t} + P_1\,u_{2xx} + Q_1\,|u_2|^2\,u_2\,e^{\Lambda_2 t} + Q_1\,e^{\Lambda_2 t}\,\left(2\,u_1\,|u_2|^2 + u_1^*\,u_2^2\right) = 0, \tag{12b}$$

$$i\,v_{1t} + P_2\,v_{1xx} + Q_2\,|v_1|^2\,v_1\,e^{\Lambda_1 t} + Q_2\,e^{\Lambda_1 t}\,\left(2\,v_2\,|v_1|^2 + v_2^*\,v_1^2\right) = 0, \tag{12c}$$

$$i\,v_{2t} + P_2\,v_{2xx} + Q_2\,|v_2|^2\,v_2\,e^{\Lambda_2 t} + Q_2\,e^{\Lambda_2 t}\,\left(2\,v_1\,|v_2|^2 + v_1^*\,v_2^2\right) = 0, \tag{12d}$$

where the asterisk (*) denotes the complex conjugate. We use the modified Hirota ansatz to construct solutions of Eqs. (12) as

$$u_1(x,t) = H(x,t)\,T_1^{-\delta_1}, u_2(x,t) = L(x,t)\,T_1^{-\delta_1}, \tag{13a}$$

$$v_1(x,t) = S(x,t)\,T_2^{-\delta_2}, v_2(x,t) = R(x,t)\,T^{-\delta_2}. \tag{13b}$$

In Eqs. (13), H, L, S, and R are complex functions, and T_1 and T_2 are real functions. The complex constant $\delta_j = 1 + i\,\delta_{ij}$ (where $j = 1, 2$) needs to be determined. Using Eq. (8) along with Eqs. (13) the bilinear form of Eqs. (12) are

$$\left(i\,D_{\delta_1,t} + P_1\,D_{\delta_1,x}^2\right)\,H\cdot T_1 = 0, \tag{14a}$$

$$\left(i\,D_{\delta_1,t} + P_1\,D_{\delta_1,x}^2\right)\,L\cdot T_1 = 0, \tag{14b}$$

$$D_x^2\,T_1\cdot T_1 = \frac{2\,Q_1\,e^{2\,\Lambda_1\,t}\,(|H|^2 + H\,L^* + 2\,L\,H^*)}{P_1\,\delta_1\,(\delta_1+1)\,T_1^{2\,\delta_1-2}}, \tag{14c}$$

$$D_x^2\,T_1\cdot T_1 = \frac{2\,Q_1\,e^{2\,\Lambda_1\,t}\,(|L|^2 + L\,H^* + 2\,H\,L^*)}{P_1\,\delta_1\,(\delta_1+1)\,T_1^{2\,\delta_1-2}}, \tag{14d}$$

$$\left(i\,D_{\delta_2,t} + P_2\,D_{\delta_2,x}^2\right)\,S\cdot T_2 = 0, \tag{14e}$$

$$\left(i\,D_{\delta_2,t} + P_2\,D_{\delta_2,x}^2\right)\,R\cdot T_2 = 0, \tag{14f}$$

$$D_x^2\,T_2\cdot T_2 = \frac{2\,Q_2\,e^{2\,\Lambda_2\,t}\,(|S|^2 + S\,R^* + 2\,R\,S^*)}{P_2\,\delta_2\,(\delta_2+1)T_2^{2\delta_2-2}}, \tag{14g}$$

$$D_x^2\,T_2\cdot T_2 = \frac{2\,Q_2\,e^{2\,\Lambda_2\,t}\,(|R|^2 + R\,S^* + 2\,S\,R^*)}{P_2\,\delta_2\,(\delta_2+1)T_2^{2\delta_2-2}}. \tag{14h}$$

Eqs. (14) are valid provided that the following conditions are satisfied $HL \neq 0, SR \neq 0, (H+L)(H^*-L^*)=0, (S+R)(S^*-R^*)=0, L=\epsilon H$ and $R=\epsilon S$, such that

$$\left(i\, D_{\delta_1,t} + P_1\, D^2_{\delta_1,x}\right) H \cdot T_1 = 0, \tag{15a}$$

$$\left(i\, D_{\delta_1,t} + P_1\, D^2_{\delta_1,x}\right) L \cdot T_1 = 0, \tag{15b}$$

$$D^2_x\, T_1 \cdot T_1 = \frac{2\, Q_1\, e^{2\,\Lambda_1\, t}(1+3\,\epsilon)}{P_1\, \delta_1\, (\delta_1+1) T_1^{2\,\delta_1-2}} |H|^2, \tag{15c}$$

$$D^2_x\, T_1 \cdot T_1 = \frac{2\, Q_1\, e^{2\,\Lambda_1\, t}(1+3\,\epsilon)}{P_1\, \delta_1\, (\delta_1+1) T_1^{2\,\delta_1-2}} |L|^2, \tag{15d}$$

$$\left(i\, D_{\delta,t} + P_2\, D^2_{\delta_2,x}\right) S \cdot T_2 = 0, \tag{15e}$$

$$\left(i\, D_{\delta,t} + P_2\, D^2_{\delta_2,x}\right) R \cdot T_2 = 0, \tag{15f}$$

$$D^2_x\, T_2 \cdot T_2 = \frac{2\, Q_2\, e^{2\,\Lambda_2\, t}(1+3\,\epsilon)}{P_2\, \delta_2\, (\delta_2+1) T_2^{2\,\delta_2-2}} |S|^2, \tag{15g}$$

$$D^2_x\, T_2 \cdot T_2 = \frac{2\, Q_2\, e^{2\,\Lambda_2\, t}(1+3\,\epsilon)}{P_2\, \delta_2\, (\delta_2+1) T_2^{2\,\delta_2-2}} |R|^2, \tag{15h}$$

with $\epsilon \in \{-1, 0, 1\}$. $\epsilon = 0$ corresponds to a one solitary wave. The left-hand sides of Eqs. (15c), (15d), (15f) and Eq. (15g) are real, so the right-hand side must be as well. The latter requirements impose real solutions to the following equations

$$\delta_{1i} = 0, \delta_{2i} = 0, \tag{16a}$$

$$\left(P_{1i}\, Q_{1r} - P_{1r}\, Q_{1i}\right) = \tan(2\,\Lambda_{1i}\, t)\, \left(P_{1i}\, Q_{1i} + P_{1r}\, Q_{1r}\right), \tag{16b}$$

$$\left(P_{2i}\, Q_{2r} - P_{2r}\, Q_{2i}\right) = \tan(2\,\Lambda_{2i}\, t)\, \left(P_{2i}\, Q_{2i} + P_{2r}\, Q_{2r}\right). \tag{16c}$$

Hence, Eqs. (15) can be rephrased as

$$\left(i\, D_{\delta_1,t} + P_1\, D^2_{\delta_1,x}\right) H \cdot T_1 = 0,$$
$$\left(i\, D_{\delta_1,t} + P_1\, D^2_{\delta_1,x}\right) L \cdot T_1 = 0, \tag{17a}$$

$$D^2_x\, T_1 \cdot T_1 = \frac{\left(P_{1i}\, Q_{1i} + P_{1r}\, Q_{1r}\right)\, e^{2\,\Lambda_{1r}\, t}(1+3\,\epsilon)}{\cos(2\,\Lambda_{1i}\, t)\, |P_1|^2} |H|^2,$$

$$D^2_x\, T_1 \cdot T_1 = \frac{\left(P_{1i}\, Q_{1i} + P_{1r}\, Q_{1r}\right)\, e^{2\,\Lambda_{1r}\, t}(1+3\,\epsilon)}{\cos(2\,\Lambda_{1i}\, t)\, |P_1|^2} |L|^2, \tag{17b}$$

$$\left(i\, D_{\delta,t} + P_2\, D^2_{\delta_2,x}\right) S \cdot T_2 = 0,$$
$$\left(i\, D_{\delta,t} + P_2\, D^2_{\delta_2,x}\right) R \cdot T_2 = 0, \tag{17c}$$

$$D^2_x\, T_2 \cdot T_2 = \frac{\left(P_{2i}\, Q_{2i} + P_{2r}\, Q_{2r}\right)\, e^{2\,\Lambda_{2r}\, t}(1+3\,\epsilon)}{\cos(2\,\Lambda_{2i}\, t)\, |P_2|^2} |S|^2,$$

$$D^2_x\, T_2 \cdot T_2 = \frac{\left(P_{2i}\, Q_{2i} + P_{2r}\, Q_{2r}\right)\, e^{2\,\Lambda_{2r}\, t}(1+3\,\epsilon)}{\cos(2\,\Lambda_{2i}\, t)\, |P_2|^2} |R|^2. \tag{17d}$$

Once the bilinear conditions and forms are available, the next step is to find the solitary wave solutions. Multiple solitary wave solutions are accessible, such as impulsive, frontal, and dark solutions [23]. The modified bilinear operators (8) frequently utilize these solutions. The impulsive solutions are of significant interest to us due to diverse applications in the signal processing and transportation of data in microtubular networks [5]. This is done by starting with an expansion written as

$$H = e^{\theta_1}, T_1 = 1 + N_1(t)\, e^{\theta_1+\theta_1^*} \tag{18a}$$
$$\text{where },\ \theta_1 = k_1\, x + h_1(t).$$

$$S = e^{\theta_2}, T_2 = 1 + N_2(t)\, e^{\theta_2+\theta_2^*}, \tag{18b}$$
$$\text{where }, \theta_2 = k_2\, x + h_2(t),\ \text{ with }\ k_1, k_2 \in \mathbb{R}.$$

h_1, h_2 and N_1, N_2 are time-dependent complex and real functions, respectively. By inserting Eqs. (18) into Eqs. (17), we obtain

$$\frac{dh_1}{dt} - i\, P_1\, k_1^2 = 0, \tag{19a}$$

$$\frac{dh_2}{dt} - i\, P_2\, k_2^2 = 0, \tag{19b}$$

$$\frac{1}{N_1(t)}\frac{dN_1}{dt} = 2\,P_{1i}\,k_1^2, \tag{19c}$$

$$\frac{1}{N_2(t)}\frac{dN_2}{dt} = 2\,P_{2i}\,k_1^2, \tag{19d}$$

$$N_1(t) = \frac{\left(P_{1i}\,Q_{1i} + P_{1r}\,Q_{1r}\right)\,e^{2\,\Lambda_{1r}\,t}(1+3\,\epsilon)}{2\,k_1^2\,|P_1|^2\,\cos(2\,\Lambda_{1i}\,t)}, \tag{19e}$$

$$N_2(t) = \frac{\left(P_{2i}\,Q_{2i} + P_{2r}\,Q_{2r}\right)\,e^{2\,\Lambda_{2r}\,t}(1+3\,\epsilon)}{2k_2^2\,|P_2|^2\,\cos(2\,\Lambda_{2i}\,t)}. \tag{19f}$$

After integration of Eqs. (19a)–(19d), we have

$$h_1(t) = i\,P_1\,k_1^2\,t, \tag{20a}$$

$$h_2(t) = i\,P_2\,k_2^2\,t, \tag{20b}$$

$$N_1(t) = N_{01}\,\exp\left(2\,k_1^2\,P_{1i}\,t\right), \tag{20c}$$

$$N_2(t) = N_{02}\,\exp\left(2\,k_2^2\,P_{2i}\,t\right). \tag{20d}$$

From Eqs. (19f), (19f) and Eqs. (20c), (20d), we obtain

$$N_{01} = \frac{\left(P_{1i}\,Q_{1i} + P_{1r}\,Q_{1r}\right)(1+3\,\epsilon)}{2\,k_1^2\,|P_1|^2}, \tag{21a}$$

$$N_{02} = \frac{\left(P_{2i}\,Q_{2i} + P_{2r}\,Q_{2r}\right)(1+3\,\epsilon)}{2\,k_2^2\,|P_2|^2}. \tag{21b}$$

Inserting Eqs. (21) and Eqs. (20) into Eqs. (9) and using the transformations Eqs. (11), the solitary wave solution associated with Eqs. (6) can be expressed in the form

$$G_1(x,t) = \frac{\exp\left(k_1\,x + \left(\Lambda_{1r} + i\,(\Lambda_{1i} + P_1\,k_1^2)\right)\,t\right)}{1 + N_{01}\,\exp\left(2\,k_1\,x\right)}, \tag{22a}$$

$$G(x,t) = (1+\epsilon)\,G_1(x,t), \tag{22b}$$

$$F_1(x,t) = \frac{\exp\left(k_2\,x + \left(\Lambda_{2r} + i\,(\Lambda_{2i} + P_2\,k_2^2)\right)\,t\right)}{1 + N_{02}\,\exp\left(2\,k_2\,x\right)}, \tag{22c}$$

$$F(x,t) = (1+\epsilon)\,F_1(x,t). \tag{22d}$$

Returning to the discrete system, Eqs. (22) transform as follows

$$G_1(n,t) = \frac{\exp\left(k_1\,n\,l + \left(\Lambda_{1r} + i\,(\Lambda_{1i} + P_1\,k_1^2)\right)\,t\right)}{1 + N_{01}\,\exp\left(2\,k_1\,nl\right)}, \tag{23a}$$

$$G(n,t) = (1+\epsilon)\,G_1(n,t), \tag{23b}$$

$$F_1(n,t) = \frac{\exp\left(k_2\,n\,l + \left(\Lambda_{2r} + i\,(\Lambda_{2i} + P_2\,k_2^2)\right)\,t\right)}{1 + N_{02}\,\exp\left(2\,k_2 n\,l\right)}, \tag{23c}$$

$$F(n,t) = (1+\epsilon)\,F_1(n,t). \tag{23d}$$

Employing Eqs. (13), (18), and Eqs. (20) within the context of Eqs. (4) facilitates the derivation of spatio-temporal solutions characterizing the longitudinal displacement U_n and the angular displacement χ_n. These solutions serve to elucidate the dynamics of energy propagation within the MT network, delineated by the formulation articulated in Eqs. (23). We obtain

$$U_n(t) = 2(1+\epsilon)\,\frac{\exp\left(n\,l - V_{u_n}\,t\right)}{\exp(-k_1) + N_{01}\,\exp(k_1\,n\,l)} \times \cos\{(k_1^2\,P_{1r} + \Lambda_{1i} - \omega_{g_1})\,t\}, \tag{24a}$$

$$\chi_n(t) = 2\,(1+\epsilon)\,\frac{\exp\left(n\,l - V_{\chi_n}\,t\right)}{\exp(-k_2) + N_{02}\,\exp(k_2\,n\,l)} \times \cos\{(k_2^2\,P_{2r} + \Lambda_{2i} - \omega_{g_2})\,t\}, \tag{24b}$$

with

$$V_{U_n} = \frac{\omega_{g_1}\left(2\,l^2\alpha_1 {k_1}^2 + 3\,\varepsilon_1\right)}{\left({\varepsilon_1}^2 + 4\,{\omega_{g_1}}^2\right)k_1}, \tag{25a}$$

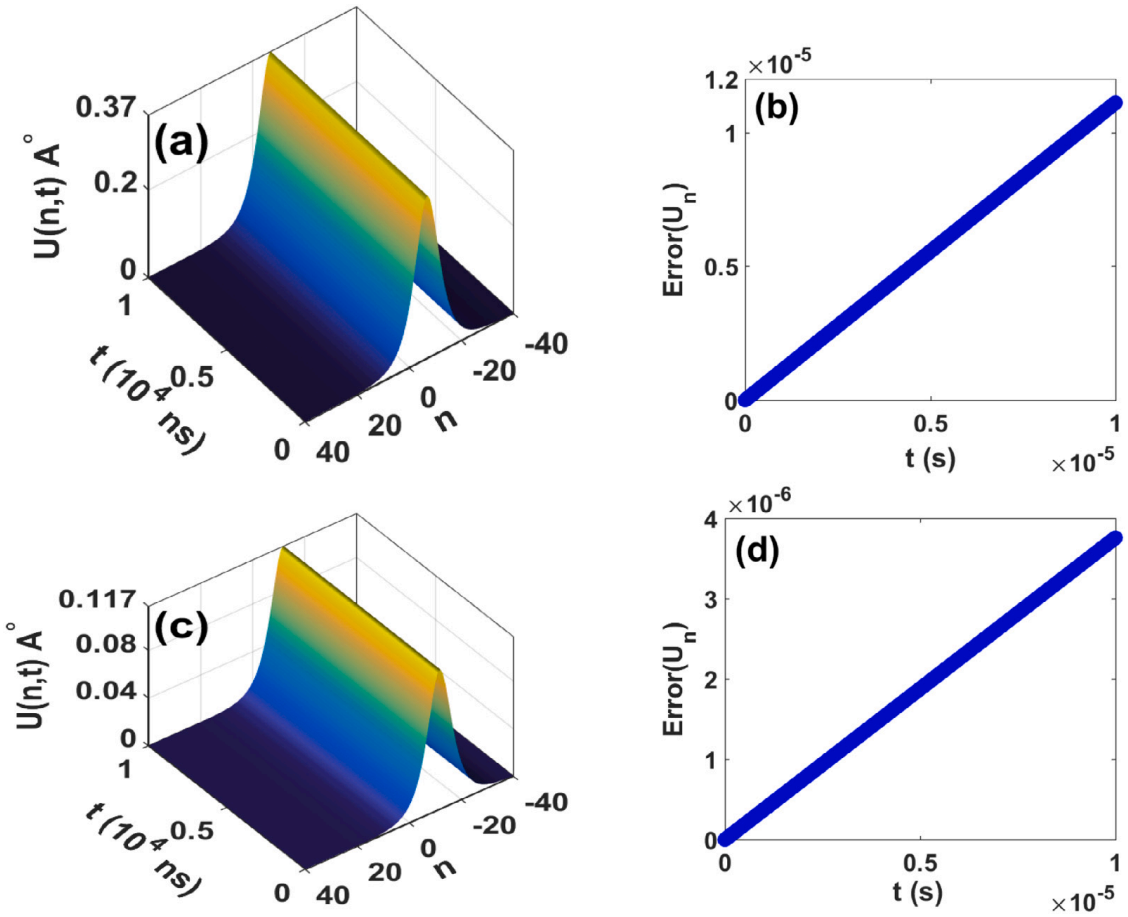

Fig. 1. Numerical spatiotemporal evolution of longitudinal displacement $\epsilon = 1$. For $\gamma = 0$, (a) bright solitary wave, (b) maximum of absolute error. For $\gamma = 5.6 \times 10^{-11}$, (c) bright solitary wave, (d) maximum of absolute error.

$$V_{\chi_n} = -\frac{2\,{\omega_{g_2}}^2 + \varepsilon_2\left(\alpha\, l^2 {k_2}^2\right)}{\left({\varepsilon_2}^2 + 4\,{\omega_{g_2}}^2\right) k_2}. \tag{25b}$$

Each solution of Eqs. (24) has one free parameter: k_1 for the longitudinal displacement and k_2 for the angular displacement. Eq. (24b) is valid for $0 < l, \varepsilon_2, \omega_{g_2}, \alpha_2 < \frac{2\omega_{g_2}^2}{l^2 k_2^2}$. This implies that $k_2^2 \in \left[0, \frac{2\omega_{g_2}^2}{\alpha_2 l^2}\right]$ such that $k_2 \in [0, 1.6719]$, and $\chi_{(n,t)} \leq \frac{\pi}{6}$ [26]. This leads us to choose the specific value $k_2 = 0.3$. The solution (24a) exists if $0 < l, \varepsilon_1, \omega_{g_1}, -\frac{3\varepsilon_1}{2l^2 k_1^2} < \alpha_1$. This imperative led to our preference for $k_1 = 0.3$. It is important to note that the solitary wave solutions resulting from Eqs. (23) differ significantly from previously derived kinks, breathers [16,27], and stationary bright solitary waves [9]. When $\epsilon = 1$, $G(x,t) = 2G_1(x,t)$ and $F(x,t) = 2F_1(x,t)$ which correspond to the two solitary wave solutions. The two solitary wave solutions differ from one solitary wave solutions ($\epsilon = 0, G(x,t) = G_1(x,t)$ and $F(x,t) = F_1(x,t)$) by a factor of two and by the expressions of the parameters N_{01} and N_{02}, which directly influence the functions $G_1(x,t)$ and $F_1(x,t)$. In contrast to the bright stationary solutions presented in [9] which are independent of viscosity and remain constant over time, the solutions described here are dynamic and depend explicitly on both time and the viscosity of the cytosol. Finally, for $\epsilon = -1$, Eqs. (6) yields a null solution. One solitary wave is a well-established solution found in various domains of physics. Unlike the one solitary wave solutions usely found, we propose in this work two solitary wave solutions to explain the dynamics of angular or longitudinal of MTs for the first time to the best of our knowledge.

4. Numerical experiments

Analytical methodologies are used to solve systems of ordinary and partial differential equations. These methods provide analytical solutions, which are often approximate and may not accurately reflect the reality of the studied systems. In contrast, numerical methods offer more suitable solutions that better align with real-world scenarios. Due to the nonlinear nature and complexity of many biological models, analytical solutions are often difficult to obtain. As a result, researchers must carefully select appropriate numerical techniques to solve and compare the results versus analytical solutions. In this part of the work, our objective is to numerical solve Eqs. (2) and compared the results against the analytical prediction found above. The fourth-order Runge–Kutta method was employed to conduct numerical simulations of Eqs. (2). The computations were performed on a spatial grid with 10^5

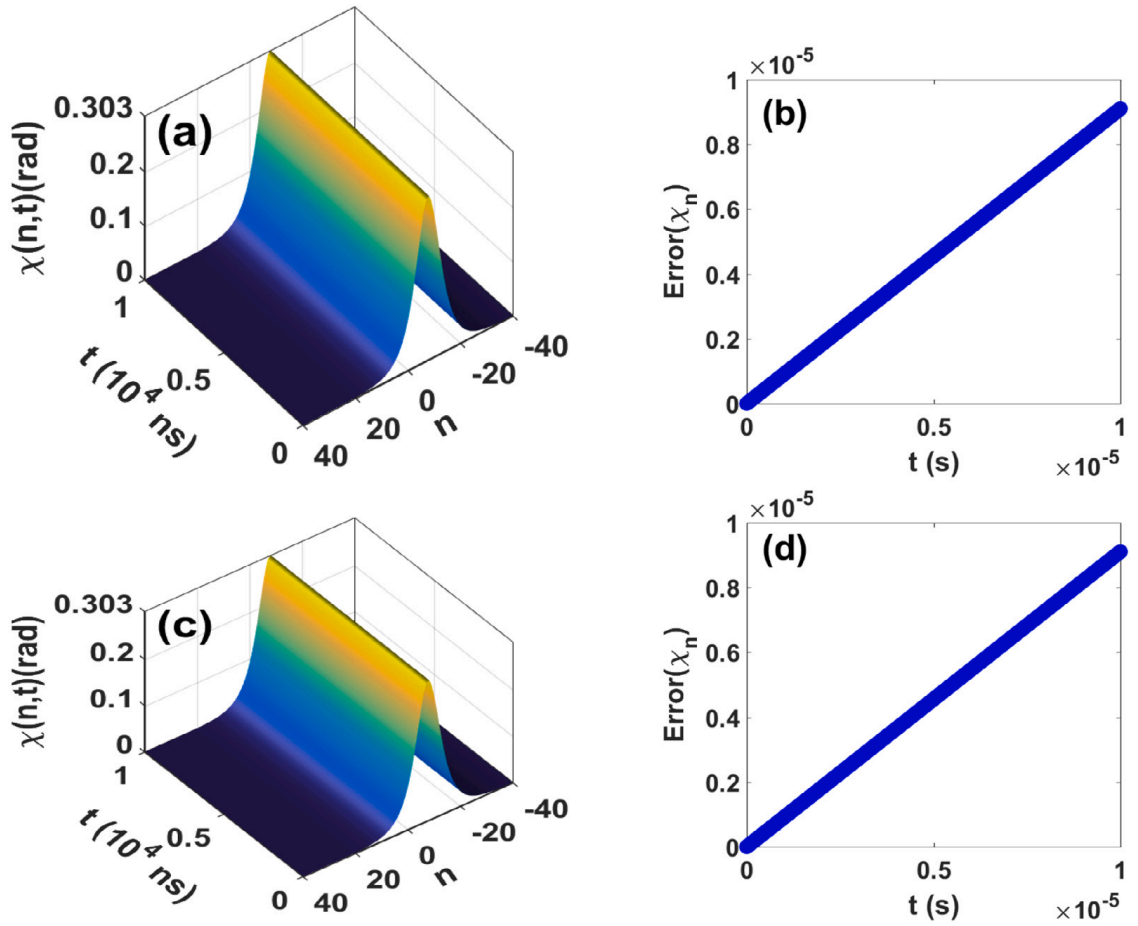

Fig. 2. Numerical spatiotemporal evolution of angular displacement $\epsilon = 1$. For $\varepsilon_2 = 0$, (a) bright solitary wave, (b) maximum of absolute error. For $\varepsilon_2 = 1.1\omega_{g_2}$, (c) bright solitary wave, (d) maximum of absolute error.

equally spaced points spanning the interval $[-40, 40]$ with periodic boundary conditions. The initial conditions at time $t = 0$ were derived from the corresponding analytical solutions (Eqs. (24)). Simulations run up to $t_{fin} = 10^4$ ns with the time step of $dt = 0.1$ ns.

In the absence of viscosity ($\gamma = 0, \varepsilon_2 = 0$), maxima of amplitudes remain constant at 0.37 Å in Fig. 1(a) for U_n but at 0.303 rad in Fig. 2(a) for χ_n. The initial conditions in Fig. 1(-a) and Fig. 2(a) evolves keeping their original shapes, without any disintegration, hence confirm that our analytical predictions may be considered as robust physical objects. Such results are also supported by very small discrepancies (of the same order of magnitude) between analytical and numerical solutions displayed in Fig. 1(b) for U_n and Fig. 2(b) for χ_n, respectively.

The presence of the viscosity for the angular displacement does not affect the dynamics of dimers as can seen by examining the numerical solution obtained for $\varepsilon_2 = 1.1\,\omega_{g_2}$ plotted in Fig. 2(c) and Fig. 2(a) where $\varepsilon_2 = 0$. Conversely, the viscosity significantly alters the dynamics of the longitudinal displacement U_n by drastically reducing the maximum amplitude from 0.37 Å ($\gamma = 0$, see Fig. 1(a)) to 0.117 Å displayed in Fig. 1(c). Similarly as above, our analytical solutions agree with the numerical ones with a rather good accuracy. The errors between analytical and numerical solutions exhibited in Fig. 1(d) for U_n and Fig. 2(d) for χ_n are bounded from above by 4×10^{-6} and 10^{-5}, respectively, definitely confirming the validity of our analytical solutions.

It is well known that the presence of viscosity in the medium influences the dynamics and functions of MTs in several ways. For instance, viscosity can affect the mobility of MTs by creating resistance to their movement, thus influencing the stability and processes of assembly and disassembly of MTs [6,8]. Authors in [9,10,27] suggested that an increase in viscosity acts as a damping factor for MT growth. Biologically, such a viscosity-induced resistance could be linked to an interaction between proteins associated with MTs, allowing the MT structure to remain stable. Regarding angular displacement, viscosity does not seem to influence the shape, amplitude, or propagation of the solution. This stability may be attributed to a stable configuration of MTs, including a curved conformation [28,29] or the presence of a GTP cap at their ends [30]. This stability could also result from the interaction of MTs with associated proteins such as dynein and kinesin, all contributing to MT stability. The latter arguments are consistent with those in [9]. The solutions obtained support potential important implications for regulating viscosity in the cytosol, the growth and division of cancer cells, as well as understanding and treating dysfunctions related to MTs. A better understanding of the correlation between cytosol viscosity and MTs could improve certain treatment modalities such as targeted therapies for specific pathologies, including cancer and neurodegenerative diseases [28,31].

5. Conclusion

In this work, we have constructed new types of solutions to deepen our understanding of MT dynamics including the influence of the cytosol viscosity on longitudinal and angular displacements. Assuming slow envelope variation of the waves, we employ the rotating wave approximation to derive discrete CGL equations satisfied by longitudinal and angular displacements of MT dimers. Then, we transformed the discrete equations into continuous ones using the semi-discrete approximation. The modified Hirota bilinear method enabled us to construct solitary wave solutions of our continuous CGL equations. An inverse operation helped us to recover the discrete solitary wave solutions that describe MT dynamics. We observed that for longitudinal displacements, the solution indicates a decrease in amplitude due to viscosity, while for angular displacements, viscosity seem to have no effect (at least for the total time of propagation considered in the current work). Hence, viscosity offers the possibility to effectively control the assembly, disassembly, and stability processes of MTs.

CRediT authorship contribution statement

Tabapsi Kamdem Rostand: Writing – review & editing, Writing – original draft, Visualization, Validation, Software, Methodology, Investigation, Formal analysis, Data curation, Conceptualization. **Belobo Belobo Didier:** Writing – review & editing, Writing – original draft, Visualization, Validation, Supervision, Methodology, Investigation, Formal analysis, Data curation, Conceptualization. **Bansi Kamdem Christel Delphin:** Writing – review & editing, Writing – original draft, Visualization, Formal analysis. **Dang Koko Adamou:** Writing – review & editing, Writing – original draft. **Tabi Conrad Bertrand:** Writing – review & editing, Writing – original draft. **Kofané Timoléon Crépin:** Writing – review & editing, Writing – original draft, Validation.

Declaration of competing interest

The authors declare that they have no conflict of interest.

Data availability

No data was used for the research described in the article.

References

[1] Zdravković S, Zeković S, Bugay AN, Petrović J. Chaos Solitons Fractals 2021;152.
[2] Zdravković S, Maluckov A, Crossed M, Signekić D, Kuzmanović S, Satarić MV. Appl Math Comput 2014;242:353.
[3] Carlier MF. Mol Cell Biochem 1982;47:97.
[4] Kengne E, Lakhssassi A. Chaos, Solitary Waves Fractals 2023;167:113094.
[5] Tankou E, Tabi CB, Kofané TC. Chaos, Solitary Waves Fractals 2022;162:112446.
[6] Betterton MD. Dev Cell 2022;57:419.
[7] Shirmovsky S, Shulga DV. Phys A Stat Mech Appl 2019;534:122165.
[8] Molines AT, Lemiere J, Gazzola M, Steinmark IE, Edrington CH, Hsu CT, et al. Dev Cell 2022;57:466.
[9] Tabapsi Kamdem R, Belobo Belobo D, Dang Koko A, Tabi CB, Kofané TC. Eur Phys J Plus 2023;138:433.
[10] Latifah S, Rohmah SF, Ramadhan IA, Dwiputra D, Hidayat W, Zen FP. J Phys Conf Ser 2019;1204:12015.
[11] Priya R, Kavitha L, Gopi D. Mater Today Proc 2019;26:3552.
[12] Kivshar YS, Peyrard M. Phys Rev A 1992;46:6.
[13] Kengne E, Vaillancourt R. Commun Nonlinear Sci Numer Simul 2009;14:3804.
[14] Zdravković S, Kavitha L, Satarić MV, Zeković S, Petrović J. Chaos, Solitary Waves Fractals 2012;45:1378.
[15] Zeković S, Muniyappan A, Zdravković S, Kavitha L. Chin Phys B 2014;23.
[16] Zdravković S, Satarić MV, Maluckov A, Balaž A. Appl Math Comput 2014;237:227.
[17] Zdravković S, Satarić MV, Zeković S. EPL 2013;102:38002.
[18] Satarić MV, Tuszyński JA, Akula RB. Phys Rev E 1993;48:589.
[19] Porkorný J, Porkorný J, Vrba J. Int J Mol Sci 2021;22:15.
[20] Zdravković S, Satarić MV, Sivčević V. Nonlinear Dynam 2018;92:479.
[21] Tabi CB, Tankou E, Mohamadou A. Chaos, Solitary Waves Fractals 2017;95:187.
[22] Nozaki K, Bekki N. Phys Soc Jpn 1984;53:5.
[23] Zakeri GA, Yomba E. J Phys Soc Japan 2013;82:1.
[24] Liu W, Yu W, Yang C, Liu M, Zhang Y, Lei M. Nonlinear Dynam 2017;89:2933.
[25] Yomba E, Kofané TC, Pelap FB. J Phys Soc Japan 1996;65:2337.
[26] Watts NR, Cheng N, West W, Steven AC, Sackett DL. Biochemistry 2002;41:12662.
[27] Zdravković S, Bugay AN, Aru GF, Maluckov A. Chaos 2014;24:2.
[28] Guesdon A, Bazile F, Buey RM, Mohan R, Monier S, Garca RR, et al. Nat Cell Biol 2016;18:1102.
[29] Hunyadi V, Chretien D, Janosi IM. J Mol Biol 2005;348:927.
[30] Desai A, Mitchison TJ. Annu Rev Cell Dev Biol 1997;13:83.
[31] Wang Z, Wang H, Rhie JK, Covey JM, Liang P, Wang S, et al. J Pharm Biomed Anal 2006;42:272.